DEPARTMENT OF ELECTRONIC & ELECTRICAL ENGINEERING

University of Strathclyde Engineering

Enhanced FRT Control Strategies for VSC-HVDC Connected Offshore Wind Farms

University of Strathclyde

Power Systems Research Group
Department of Electronic and Electrical Engineering
Institute for Energy and Environment

A thesis presented in fulfilment of the requirement for the degree of Doctor of Philosophy

February 2017

Declaration of author’s rights

This thesis is the result of the author’s original research. It has been composed by the author and has not been previously submitted for examination which has led to the award of a degree.

Signed:_____ Date: _____

Acknowledgements

I would like to thank my principal supervisor Dr. Olimpo Anaya-Lara who has provided guidance and useful comments throughout my PhD research. I also want to thanks to Dr Grain Philip Adam, without them my goal of submitting this thesis would not have been accomplished.

I would also like to thank my friends who have provided the support to accomplish this thesis and special thanks to every person who has contributed to accomplish this research.

Abstract

The EU has a binding target of 20% of energy to come from renewables by 2020, with an associated CO2 emissions reduction target of 20% (relative to 1990) and a 20% reduction in energy usage by the same date. This is the so-called 20/20/20 target. The UK target is for 15% of energy to be sourced from renewables by this date. For this target to be met, over 30% of electricity will need to be generated from renewables and it is anticipated that 31GW of this will come from wind power, with 13 GW onshore and 18GW offshore, by 2020. At present 6 GW of wind power have been installed onshore and 3.5+ GW offshore. To increase offshore capacity by at least a factor of five in 5 years, whilst minimising the cost of energy, presents very significant design, operational and logistical challenges. As the offshore infrastructure is established and connected big challenges are introduced such as the development of reliable and cost effective wind farm electrical collectors and offshore transmission systems, and the design and implementation of enhanced controls to enable wind farms to support power system operation and maintain system stability.

The objective of this thesis is to present, discuss and solve technical barriers for offshore grids. This research is based on simulation studies of control structures of Doubly-fed Induction Generator (DFIG) and Fully-Rated Converter (FRC) wind turbine generators, and VSC-HVDC offshore transmission systems. Simulation results validate the enhancements achieved in the control strategies of both wind turbine generators and VSC-HVDC. These enhanced controls enable the VSC-HVDC connected wind farms to comply with Grid Code requirements such as Fault Ride-Through and provision of voltage and frequency support. The thesis also discusses the pros and cons of installing modifications in the control system of the point-to-point HVDC converters. Furthermore, this research includes a mathematical analysis of the specific conditions of the VSC converters and the AC and DC transmission lines which need to be established in order to ensure the efficient performance of wind farms, and thus to comply with Grid Codes requirements. Matlab/Simulink software - specifically the SimPowerSystem tool for transient simulation - is used to model and examine a series of proposed scenarios. To achieve the objectives of this thesis and thus to investigate and provide an explanation of the operational system of the DFIG/FRC wind turbines, their interconnection to the offshore cluster substation (VSC converter) and the HVDC connection, basic models have been designed, analysed and tested. A variety of modifications in the control system of the power converters have been applied in

order to obtain a better dynamic response in each scenario (single point connection with basic point-to-point connection or more complex offshore scenarios which incorporate several offshore wind farms connected to one offshore cluster substation). These new models (wind turbines and VSC-HVDC) have been compared with the basic models to facilitate the analysis of both systems.

Table of Contents

List of Figures

List of Tables

Abbreviations

Abbreviations	Description
ASM	Ancillary Service Markets
BED	Break-Even Distance
CI	Customer interruptions
CML	Customer minutes lost
CAIDI	Customer average interruption duration index
CTAIDI	Customer total average interruption duration index
DFIG	Doubly-fed induction generator
EEPR	The European energy programme for recovery
EHV	Extra high voltage
Eirgrid	The Irish system operator
EMC	Electromagnetic compatibility
ENTSO-E	European Network of Transmission System Operators for Electricity
Energinet	The Denmark transmission system owner
ENA	Energy network association
FRT	Fault ride through
DNO	Distribution network operator
DFIG	Doubly fed induction generator
HVAC	High voltage alternating current
HVDC	High voltage direct current
IGBT	Insulated gate bipolar transistor
OWE	Offshore wind energy
LOLP	Loss of load probability
LOLE	Loss of load expectation
NERC	North American Electric Research council
NETS	National grid electricity transmission system
NGO	Non-governmental organization
NPC	Neutral point clamped or diode clamped
OWE	Offshore wind energy
OWF	Offshore wind farm
PLL	Phase locked loop
PMG	Permanent magnet generators
pf	Power factor
PCC	Point-of-common coupling
PWM	Pulse-width modulation
PCC	Point of common coupling
RES	Renewable energy source
R&D	Research and development
RMS	Root Mean Square
STATCOM	Static compensator
SVC	Static Var Compensator
STATNETT	Norwegian transmission system operator
SK	Skagerrak
UHV	Ultra-high voltage
SAIDI	System average interruption duration index
SAIFI	System average interruption frequency index
SCC	Self-commutated converters
SIL	Surge impedance loading
TSO	Transmission System Operator
THD	Total harmonic distortion
VSC	Voltage source converters
WFs	Wind farms
WTs	Wind turbines

Nomenclature

Symbol	Definition
A	The area swept by the rotor blades
C_{dc}	HVDC's Capacitor
dq	dq components
E_f	Synchronous generator field voltage
f	Frequency
f_o	Reference frequency
id^*	Active power reference signal (inner controller)
I_{d1}^*	Reference signal (in the offshore substation) for the inner controller
I_{q1}^*	Reference signal (in the offshore substation) for the outer controller
I_{d2}^*	Reference signal (in the offshore substation) for the inner controller
I_{q2}^*	Reference signal (in the offshore substation) for the outer controller
I_{dqr}	Rotor current in dq frame
I_{dqs}	Stator current in dq frame
I_{gd}	The generator current d-axis
I_{gq}	The generator current q-axis
I_{Ldc}	DC current of the LCC-HVC
I_{limit}	Pre-defined maximum reference signal of the active power
iq^*	Reactive power reference signal (outer controller)
I_{ds}	The stator current d-axis
I_{qs}	The stator current q-axis
I_s	The stator current
k	Constant
$k_{i1\text{-off}}$	Integral value "Power controller" offshore substation
$k_{i2\text{-off}}$	Integral value "Reactive power controller" offshore substation
$k_{i3\text{-dc}}$	Integral value "DC Power controller" onshore substation
$k_{i4\text{-on}}$	Integral value "Power controller" onshore substation
$k_{i5\text{-on}}$	Integral value "Reactive power controller" onshore substation
$k_{p1\text{-off}}$	Proportional value "Power controller" offshore substation
$k_{p2\text{-}}$	Proportional value "Reactive power controller" offshore substation

$k_{p3\text{-off}}$	Proportional value “DC Power controller” onshore substation
$k_{p4\text{-dc}}$	Proportional value “Power controller” onshore substation
$k_{p5\text{-on}}$	Proportional value “Reactive power controller” onshore substation
L_{dc}	DC cable inductance
k_{if}	Integral value of the frequency controller
k_{pf}	Proportional value of the frequency controller
M6	±150 kV symmetric base modules (ABB converter)
M9	±320 kV symmetric base modules (ABB converter)
m_a	Index modulation
p/f	Active/frequency
P/f	Power/frequency controller
P_{gdc}	FRC wind turbine dc power
P_{gen}	FRC wind turbine generator power
P_{ggr}	FRC wind turbine grid power
$P_{L\text{-id}}$	Power losses
P_{Lac}	Active power transferred in the LCC-HVDC
P_{Ldc}	DC power of the LCC-HVDC system
P_{out}	The power output
Q_{La}	Reactive power transferred in the LCC-HVDC
$R_{c\text{-c}}$	The “equivalent” commutating resistance.
R_{dc}	DC cable resistance
S_n	Power exported from the VSC converter
τ	Capacitor time constant
T_{em}	Electromagnetic torque applied to the rotor by the generator
$T_{m\text{-c}}$	Mechanical torque applied to rotor
$U_{ac}(t)$	“PWM” modulation signals
U_{tri}	“PWM” carrier signal
$V_{dc}^{*}{}_{\text{-angle}}$	Reference signal (in the onshore substation) for the inner controller
V_{dc}/f	DC voltage/frequency controller
V_{do}	Direct voltage (LCC System)

V_{dqr}	Rotor voltage in dq frame
V_{dq}	AC voltage (LCC System)
V_g	Terminal voltage of the generator
V_{Ldc}	DC voltage of the LCC-HVC
Vs_d	The ac system *d*-frame voltage component
Vs_q	The ac system *q*-frame voltage component
X_{gdq}	Generator self-inductance in the *dq* frame
ψ_{fq}	the field flux vector q-axis
ψ_s	the stator flux linkage vector
ω	The ac system angular frequency
ω_r	The rotor rotational speed
ζ	The damping ratio or damping factor

Chapter 1: Introduction

Advancements in offshore technology have started a new era in the wind energy sector. This new era has sharply increased the energy production from single wind turbines, and also facilitated the control and transmission of wind energy, principally using voltage sourced converters and HVDC transmission systems. The introduction of new power electronics devices - IGBTs self-commutating switches for power converter - has opened up the possibility of increasing the power output from single wind turbines and thus the possibility of developing bigger onshore and offshore wind farms, OWFs. Thus, the power electronics evolution has brought a new era for offshore wind energy. Principally, OWFs located in deep waters have become an attractive solution to help reduce CO_2 emissions and thus achieve the EU targets. The first generation of VSC converters have improved the power control, the transmission system and the quality of the obtained AC voltage - AC/DC conversion has thereby opened the opportunity to use an HVDC system for the transmission of energy. The maximum efficient length (underwater or underground) for high voltage AC cable transmission is about 50-100 km, [1]; due to the generation of reactive power. Nowadays, the average distance to shore (Break-Even Distance, BED) is between 35 to 60 km [2]. This BED depends on the voltage of the DC link and the diameter of the DC cable. Therefore, it has opened the opportunity for research and development of the new power electronic technology [3-6].

1.1 Introduction

Due to European CO_2 targets, the renewable energy sector has been growing strongly during the last three decades. As a result of this, the wind energy sector has become an important part of European growth; creating new jobs and high expectations for the future. Furthermore, it can potentially become the engine of economic changes in the imminent future along with heavy industry or the banking sector [5]. The best onshore wind resources are already taken and thereofore the future of the wind sector is in offshore waters [7]. Therefore, offshore wind energy is at the centre of future developments. The best offshore wind resources are in the middle of oceans. Due to high wind speeds and low or non-turbulence, factors which lead to steadier winds, allow wind turbines to produce a high quantity of energy. This sector has not been exploited yet (although there are a few exceptions), so expectations are extremely high [8], [9].

The report Wind in Power: 2015 European statistics (produced by the EWEA association) shows the wind power capacity installed in Europe, the UK and in the Baltic countries. The report, Figure 1-1, shows clearly that Germany and Spain have higher wind capacity installed than any other country in the EU, with 44,946.1 MW and 23,025.3 MW respectively; but it is also important to see that Denmark produces a higher percentage of its overall electricity from wind energy than these two countries, According to EWEA report, [10], by the end of 2012 Denmark consumes over 27% of its electricity produced by wind energy and by 2015, Denmark reaches 42% [11].

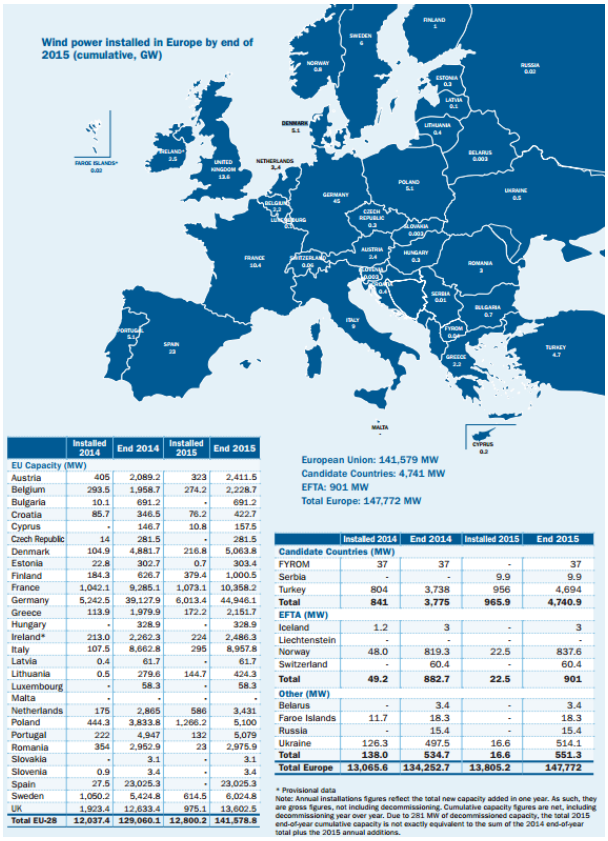

	Installed 2014	End 2014	Installed 2015	End 2015
EU Capacity (MW)				
Austria	405	2,089.2	323	2,411.5
Belgium	293.5	1,958.7	274.2	2,228.7
Bulgaria	10.1	691.2	-	691.2
Croatia	85.7	346.5	76.2	422.7
Cyprus	-	146.7	10.8	157.5
Czech Republic	14	281.5	-	281.5
Denmark	104.9	4,881.7	216.8	5,063.8
Estonia	22.8	302.7	0.7	303.4
Finland	184.3	626.7	379.4	1,000.5
France	1,042.1	9,285.1	1,073.1	10,358.2
Germany	5,242.5	39,127.9	6,013.4	44,946.1
Greece	113.9	1,979.9	172.2	2,151.7
Hungary	-	328.9	-	328.9
Ireland*	213.0	2,262.3	224	2,486.3
Italy	107.5	8,662.8	295	8,957.8
Latvia	0.4	61.7	-	61.7
Lithuania	0.5	279.6	144.7	424.3
Luxembourg	-	58.3	-	58.3
Malta	-	-	-	-
Netherlands	175	2,865	586	3,431
Poland	444.3	3,833.8	1,266.2	5,100
Portugal	222	4,947	132	5,079
Romania	354	2,952.9	23	2,975.9
Slovakia	-	3.1	-	3.1
Slovenia	0.9	3.4	-	3.4
Spain	27.5	23,025.3	-	23,025.3
Sweden	1,050.2	5,424.8	614.5	6,024.8
UK	1,923.4	12,633.4	975.1	13,602.5
Total EU-28	**12,037.4**	**129,060.1**	**12,800.2**	**141,578.8**

	Installed 2014	End 2014	Installed 2015	End 2015
Candidate Countries (MW)				
FYROM	37	37	-	37
Serbia	-	-	9.9	9.9
Turkey	804	3,738	956	4,694
Total	**841**	**3,775**	**965.9**	**4,740.9**
EFTA (MW)				
Iceland	1.2	3	-	3
Liechtenstein	-	-	-	-
Norway	48.0	819.3	22.5	837.6
Switzerland	-	60.4	-	60.4
Total	**49.2**	**882.7**	**22.5**	**901**
Other (MW)				
Belarus	-	3.4	-	3.4
Faroe Islands	11.7	18.3	-	18.3
Russia	-	15.4	-	15.4
Ukraine	126.3	497.5	16.6	514.1
Total	**138.0**	**534.7**	**16.6**	**551.3**
Total Europe	**13,065.6**	**134,252.7**	**13,805.2**	**147,772**

* Provisional data
Note: Annual installations figures reflect the total new capacity added in one year. As such, they are gross figures, not including decommissioning. Cumulative capacity figures are net, including decommissioning year over year. Due to 281 MW of decommissioned capacity, the total 2015 end-of-year cumulative capacity is not exactly equivalent to the sum of the 2014 end-of-year total plus the 2015 annual additions.

Figure 1-1 The wind energy capacity of the EU and the North Sea countries (Source: [11])

1.2 Background of the Research.

The expected increase on the use of renewable energies to produce power will have a significant impact on the electrical network. It is expected that offshore wind power will produce the biggest contribution of this renewable power, in the near future. It is certain that the UK will probably be one of the biggest offshore energy producers in Europe and also in the world; leading the offshore sector by installation of large OWFs, which could produce 14 GW by the end of 2020 and potentially 40 GW by the end of 2030. This exponential increase in the renewable power in the UK will cause significant technical issues in the onshore grid.

Therefore, with this expected high increment in the offshore power production, technical problems (i.e. power system integration) will arise regarding the control, operation and stability of the onshore grid [12-14]. This increase on offshore wind developments (UK marine renewable energy programme) in the UK is led by the Crown Estate and thus the offshore wind energy will play a major role in the Crown Estate strategy for offshore energy production. The Scottish Government, National Grid, Ofgem, and the Department for Energy and Climate Change (DECC; formerly BERR) are also involved in the Crown Estate strategy.

To lead this important increase in the production of offshore wind energy, the UK has projected three rounds of offshore wind expansion of which two so far have been undertaken. The purpose of these rounds is to reduce complexity and achieve CO_2 targets. Round 1 started in 2000 and was created in order to find the best seabed commercial areas and to begin to install small-scale wind turbines (no more than 30 turbines were installed with a total capacity of 1.1 GW). Round 2 started in 2003 and expanded the seabed commercial areas, incorporating 12 extra nautical miles. In this round, wind farms were larger than Round 1 and could be installed further from the shore, and thus Round 2 could produce a higher quantity of power, reaching a total generation capacity of 7.2 GW [15]. In 2010 was announced the extension of the geographical area of these wind farm locations, and thus Round 1 and 2 and extension (this extension should be operative on 2016 onwards) will increase their generating capacity to an extra 1.4 GW with a total power production of around 8.6 GW. Therefore, after the success of Rounds 1 and 2, the Crown Estate announced the development of Round 3. This Round had allocated up to 33GW of potential offshore wind capacity in UK offshore waters [15, 16].

One of the Crown Estate's development partners for Round 3 is the Supergen Wind Energy Technologies Consortium (SUPERGEN) was originally established by the EPSRC on 23rd March 2006 as part of its sustainable power generation and supply programme [17]. Supergen's research is focused on offshore wind operations. Specifically, it seeks to improve: energy production and wind turbine control, reliability and maintainability of the offshore schemes, offshore system connection, power transmission and finally the economic cost of offshore layouts. The research presented in this thesis is part of the Theme 3: Connection which in particular is concerned with the connection of the offshore grid to the onshore grid. The key points of the Theme 3: Connection are to develop an offshore substation which can control and transfer the offshore power to onshore and this thesis contributed to this aim. The second key point is to develop reinforcements for the onshore grid connections.

1.3 Research Aims and Objectives

This thesis research focuses on power control for large OWFs. This thesis research is focused also in transient stability and thus tries to enhance the overall dynamic interaction with the onshore power grid. The main objective is to demonstrate that the design coordinated power control of the offshore cluster substation and the improvements applied to the offshore and onshore converters have the ability, under most circumstance, to control and transfer power from offshore to onshore reliably. This research also aims to enhance the control system of the existing power converter of the DFIG and FRC wind turbines. Thus, this is set out to contribute efficiently to the recovery of the offshore system after a disturbance has occurred and thus enhances the entire offshore layout. In addition, the research will develop offshore AC and DC layouts which can be used in future offshore wind energy systems. In conclusion, the key factor in this research is the enhancement and appropriate control of the VSC converters for offshore applications and improve the dynamic behaviour of the offshore power system array. The VSC converters have a great potential applicability for control and transmission of power, especially when power systems are located offshore.

This research evaluates the benefits of the VSC-HVDC system for power management during large transients and thus attempts to address questions of offshore interconnection when a cluster substation system is controlling, managing and transferring the offshore power to onshore. Thus, in order to address the questions regarding the control of the VSC-HVDC system, the following tasks will be carried out:

a). To develop a realistic offshore power system which incorporates the two types of existing wind turbines (DFIG and FRC) to study the traditional power control system of the VSC converters and then implement innovative modifications. In order to obtain a reliable offshore layout, both controller systems (the control system of the offshore wind turbines and the control system of the offshore cluster substation) must have different control approach otherwise they can produce desynchronization. Thus, this thesis will investigate the relation between both control sources.

b). To develop an adequate coordinate power control for the OWFs. This control will also ensure the adequate behaviour of the wind farms and also ensure the correct power transmission.

c). To establish the appropriate transfer function for the VSC controllers and also to establish a further tuning methodology to calculate the values of the PI controllers which will help to understand the control effects of these parameters in the

performance of the network; this thesis will investigate a tuning criterion to determine the k_p and the k_i parameters of the inner and outter current controllers of the offshore and onshore substations.

d). To establish a more accurate control of the offshore layout, offshore cluster substation, the DFIG and FRC wind turbines and thus the wind farms; this thesis will investigate the impact of 1st and 2nd order filters, a more accurate control of the active and reactive power, a frequency controller, the third harmonic injection technique and DC voltage controller (only apply in the offshore and onshore substations).

e). The impact of a large transient in the offshore and onshore grids will be evaluated using transient stability analysis. The parameters of the control system of the offshore and onshore substations will be calculated using the modulus optimum criteria and the response of the power system evaluated.

f). An investigation of the steady-state and also transient conditions for the OWFs for the improvement of the fault ride-through capability of the power system will be analysed and the conclusion will be incorporated to improve the control system.

g). This research aims to demonstrate that an adequate coordinated power control which links the offshore system to the onshore grid through an HVDC link provides interchangeable and reliable solutions to ensure the security of the offshore power system, wind farms and offshore cluster substation, and power balance during large transients.

1.4 Research Methodology

To develop accurate scenarios for the VSC-HVDC and also for the wind turbines, the SimPowerSystem toolbox from the Matlab/Simulink software has been used. This toolbox allows simulating accurately the power system, its power flow and the transient. Furthermore, this toolbox also allows producing the modifications (1st and 2nd order filters, a more accurate control of the active and reactive power, a frequency controller, the third harmonic injection technique and DC voltage controller) in the control system of the VSC power converters. The modulus optimum criteria will be used to calculate the parameters (k_p and k_i) of the PI controllers of the offshore and onshore substations which lead this thesis to analyse and also to evaluate and finally to introduce the adequate parameters which will restore and also to achieve the fault ride-through capability of proposed power systems.

1.5 Thesis Contribution

The main objective of the thesis is to research the potential use of the VSC-HVDC control and transmission systems for high wind penetration when several large scale wind farms are connected to the offshore power system. Furthermore, to facilitate the understanding of the behaviour of the VSC-HVDC power system when large transients have been applied in the DFIG and FRC wind turbines or in the offshore cluster substation (different scenarios have been evaluated in this thesis) and thus through this, the research has developed a more reliable control system. Moreover, because the inadequacy of having in series two similar control systems in the same scenario - the control system of the wind turbines and the offshore cluster substation - which can lead the VSC-HVDC power system to collapse and therefore the power transferred from offshore to onshore to be stopped. This thesis has developed a coordinated power control for the offshore cluster substation which can be adapted to future wind farm developments (incorporation of different wind farms or existing offshore conventional power stations) with minor adjustments. Additionally, the analysis of different scenarios provided knowledge of the possibility of developing a complex offshore meshed grid. Furthermore, the control system modifications are used to enhance the controllers of the converter in both substations and therefore to enhance the power transmission for the HVDC system.

To improve the control system of the VSC converters, three main control system modifications have been studied and then have been implemented on it. Furthermore, this thesis has also studied passive filters (1^{st} and 2^{nd} order filters) which have been implemented into the converter control systems.

The modifications of the control system of the VSCHVDC power system are:

- The Third Harmonic Injection
- Frequency Controller
- Specific control for the DC Voltage

To conclude, this thesis enhances the ability of the control system to restore the power flow after the large transient is cleared and thus achieving the fault ride through capability - and therefore leading to greater understanding of the behaviour of the control system of the VSC-HVDC and the multi-terminal VSC-HVDC power system.

1.6 Publications

1.6.1 Chapter of a Book

1. Beddard, A., Barnes, M., Luque, A., Rudell, A., Anaya-Lara, O., Chapter 5: "Connection and transmission" in UK Wind Energy Technologies, Routledge, ISBN 1317399994, August 2016.

1.6.2 Journals

1. Antonio Luque, Olimpo Anaya-Lara, William E. Leithead and Grain P. Adam, "Enhanced FRT Control Strategies for VSC-HVDC Connected Offshore Wind Farms", in IEEE Power & Energy Society (PES), Submitted March 2016.

2. Antonio Luque, Olimpo Anaya-Lara, William E. Leithead and Grain P. Adam, "Coordinated control for DFIG wind farms and VSC-HVDC transmission to enhance FRT capability for offshore AC star layout" in European Wind Energy Association (EWEA), February 2013, Vienna, Austria.

1.6.3 Conference Paper

1. Antonio Luque, Olimpo Anaya-Lara, E. Leithead and Grain P. Adam, "Coordinated control for wind turbine and VSC-HVDC transmission to enhance FRT capability", in 10th Deep Sea Offshore Wind R&D Conference, Trondheim, Norway, January 2013, published Science Direct, Energy Procedia, Volume 35.

1.6.4 Supergen Wind Consortium

1. Antonio Luque, Olimpo Anaya-Lara, E. Leithead and Grain P. Adam. Report DY.3.2.2: Control strategies design and verification p.1-47, published in SuperWind Website. Available: https://community.dur.ac.uk/supergen.wind/index.html [2013].

1.6.5 Presentations

1.6.5.1 Supergen Wind Poster Presentations

1. Antonio Luque, Olimpo Anaya-Lara. Basic Offshore Networks Connection. Supergen Wind Consortium, general assembly meeting 1, Durham University, April 2011.
2. Antonio Luque, Olimpo Anaya-Lara. Offshore Networks Connection. Supergen Wind Consortium, general assembly meeting 2, Radisson Blu Hotel, Durham, March 2011
3. Antonio Luque, Olimpo Anaya-Lara. Control and Dynamic Performance of VSC-HVDC for Grid Integration of a Large Offshore Wind Farms. Supergen Wind Consortium, general assembly meeting 3, Bristol Marriott Royal Hotel, April 2013

1.6.5.2 University of Strathclyde: Presentation Day

Antonio Luque, Olimpo Anaya-Lara, FRT and Protection Assessment of Offshore Wind Energy Systems University of Strathclyde, Institute for Energy and Environment, July 2012.

Chapter 2: Offshore Power system

The European Union's energy consumption is still growing sharply. Consequently, the necessity to develop existing energy sources and also to create new energy resources is a primary concern of the EU. Thus, new power plants will be developed and will be built in the coming years. New nuclear, gas and coal power plants will be added to the EU (onshore) grid to supply part of the future energy demand. However, these power plants will supply part of the energy demand, the EU has also concerns of CO_2 emissions and with nuclear waste. Furthermore, the EU has a lack of these primary resources and they have to be imported from outside the EU. Therefore, the EU is trying to increase and also to develop the use of renewable energy sources such as onshore and offshore wind energy [7, 8]. The first wind energy scenario, in which the EU has already taken actions, is the increase of new onshore wind energy capacity. The second scenario is to develop the offshore wind sector; in this scenario, the offshore wind turbines will be installed in deep water or far from shore. An important role in this scenario is to create a European offshore grid which could connect large OWFs to the existing onshore grids (with power system operation benefits such as power balance enabled by pan-European interconnections) [7, 18]. Each energy scenario has its technological and logistical problems. For example: an important logistical obstacle to the increase of onshore wind power is that the best onshore renewable resources have already been taken and thus wind farms would be located in places where the average wind speed is lower or has more obstacles. A second obstacle to the proposed integrated onshore European grid (a large single European internal energy market, IEM [18]), is the fact that each country has different grid characteristics. Thus, new European Union countries need large reinforcements to accomplish the EU grid codes [16, 19, 20]. Thus, the main obstacle for developing the offshore grid is the grid codes characteristics but also the natural environment, sea waters. The salted water could be an important handicap for developing wind turbines which could affect their lifespan. It also could be a handicap the maintenance of these wind turbines. Nevertheless, the EU, North Sea and also Baltic countries are trying to build a unified offshore grid for the coming decade. The key to control and transfer the energy

produced by the OWFs to any position in the onshore grids is the development of offshore substations, cluster offshore substations. With the incorporation of these offshore cluster substations to this unified offshore grid; this could evolve from a point-to point offshore grid to a meshed grid in which, certainly, the power produced by future large OWFs could be transferred to any of these mentioned countries. Therefore, the offshore meshed scenario could be the appropriate solution for the creation of a large European unified grid. As mentioned, this offshore grid could connect North Sea countries, North Baltic countries, the UK and even Ireland (through the UK). Furthermore, the main component of the offshore substation is the VSC converter; this power converter can control and transfer the offshore power to the onshore grid with high reliability and also high efficiency. In addition, this power converter can start up or recover the steady state of the offshore VSC-HVDC power system without adding external equipment.

Figure 2-1 shows the proposed multi-terminal scenario, Chapter 6, which can represent a European grid connection similar to [3]. Furthermore, the EWEA has planned future offshore connections in the North Sea, Baltic Sea and the Celtic Sea in *the Ocean of Opportunities Report* 2009 [7].

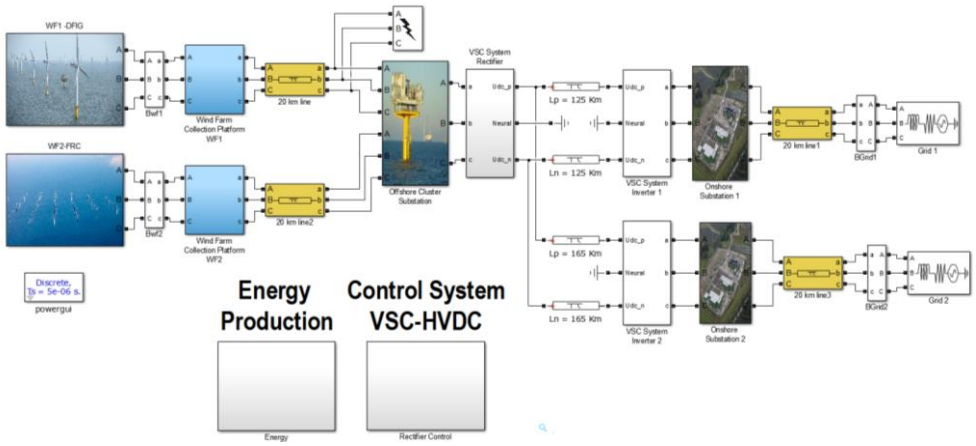

Figure 2-1: Multi-terminal offshore scenario

Even though the creation of an offshore meshed grid could bring large amounts of renewable power to the European grids, many uncertainties and challenges need to be answered. The challenges related to the development of and also the creation of reliable offshore grids are significantly high but the benefits of creating this offshore grid could benefit the future European Union and its economy. However, there are significant challenges to be overcome. In particular, it has become essential to research into methods to control the offshore power and also into the methods to transfer the offshore power to onshore grids, see Appendix A [18, 21, 22].

2.2 Transmission Systems

In the future, wind farms will be deployed far from shore and the power produced by these OWFs will be transferred into different points in the EU grid (meshed grid). The grid will move from a radial or point-to-point grid to a meshed or multi-terminal grid. Potentially, these offshore connections between North Sea countries could help to create a strong offshore grid with high flexibility and to generate renewable energy with high quality. Furthermore, the dynamics of this offshore network offers the possibility to transfer power at any time, offering voltage support in case of voltage or frequency fluctuation, helping to reduce or stop the cascade effect or recover the entire network after blackouts [12, 18, 23]. The primary tasks of a transmission system are to guarantee and maintain the power balance, to achieve system security, and then supply demand as economically as possible under any circumstance. However, the current pyramid transmission structure of the existing grid cannot match with the future connection of large scale wind farms. The main reason is that these wind farms will be connected to the power system at different transmission points in the transmission level or even in the distribution level. Figure 2-2 shows an example of a point to point offshore connection.

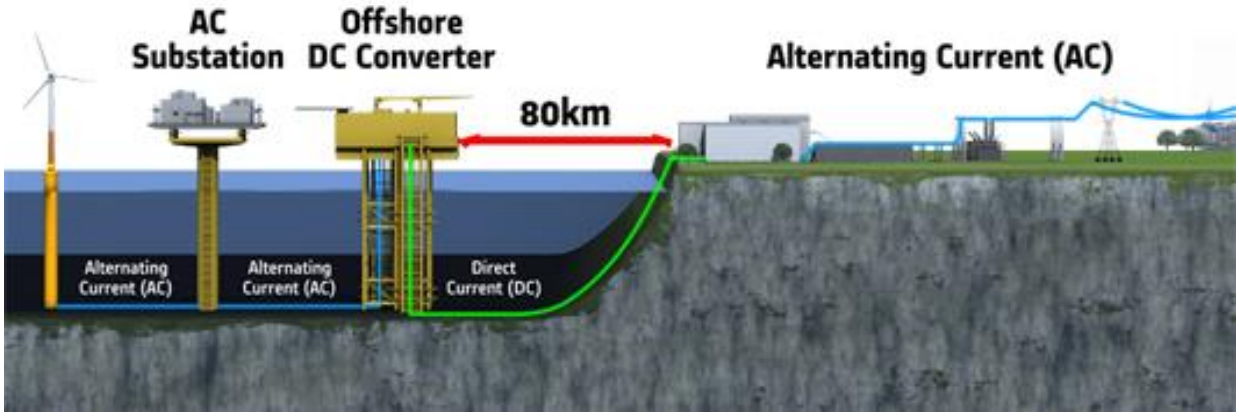

Figure 2-2: Example of possible future offshore structure (Source: Alstom UK)

With regards to wind farm locations in the North Sea, it is assumed that wind farms will be close to the biggest energy demand areas in the EU such as Germany, the UK, and France, or countries where renewable energy consumption is significant such as Denmark, Sweden or the Netherlands. Although, these OWFs will be installed close to big energy demand areas, they may be installed far from shore, and thus the HVAC system will be economically unprofitable [24, 25]. This happen because AC cable produces reactive power and also the power losses (over long distance). The submarine AC cable transmission can also produce others problems such as the high capacitive charging currents or problems with the proximity

of the cables. Consequent, these issues can generate problem with the AC voltage and frequency control and therefore problems with network stability. Therefore, for wind farms located far from shore, the HVDC system is the technology of choice to transfer the power to onshore. Furthermore, the HVDC technology could transfer higher amounts of power, through the same cable length and also cable diameter [26], and thus decreasing the power losses and improving the power quality.

2.3 Transmission System for Offshore Wind Farms

2.3.1 HVAC System

In cases where the OWFs are located in short distances from shore, the HVAC transmission has been used to connect them to shore [25]. Although the HVAC is the primary transmission system used to transfer offshore wind power over short distances, this transmission system still has serious drawbacks. The principal handicap is the fact that as the installation distance between OWFs and the shoreline increases, the power losses also increase. As a result of the power losses and also the increase in the reactive power flow, the electrical power system must compensate these constraints at both ends of the transmission lines. Therefore, and due to these, the overall cost of the installation also increases. Additionally, the transmission capacity of the HVAC cables is determined by the limits of its thermal capacity which in the future could influence any increment of the power transfer. The thermal limits of transmission lines are directly influenced by the power transfer and thus the AC current. A large AC current produces high power losses which are eliminated as heat. As a result, the transmission capacity may not be fully utilised. These limitations then restrict the implementation of an HVAC system for offshore applications involving long connection distances [27, 28].

Nowadays, the biggest advantage of the HVAC system is the knowledge that TSOs have of the system's power flow, and its controllability. TSOs also know how to effectively control and protect the entire electrical power system. In addition, this technology is also cheaper than HVDC technology, and hence preferred over short distances.

2.3.2 HVDC System

The HVDC system is able to transfer power at a higher power capacity over long distances. The HVDC technology can transfer a larger quantity of power through the same

cable diameter as HVAC and at the same power rating as HVAC. The DC technology has its biggest disadvantage (at least in the early days) in power losses associated with the converter switches. The conversion of energy, from AC to DC, produces high power losses [29-31]. The development of the self-commutating IGBT valves has decreased these power losses and thereby, has increased the competitiveness of the DC system but it still a handicap to overcome. Another reason for those lacks of development was the lack of reliable protection system for the HVDC. The protection of the HVDC need to control the AC side and therefore the entire HVDC system was disconnected. Finally, the most probably important reason to not use HVDC transmission systems (in the early days) is the overall high cost [32, 33], [34].

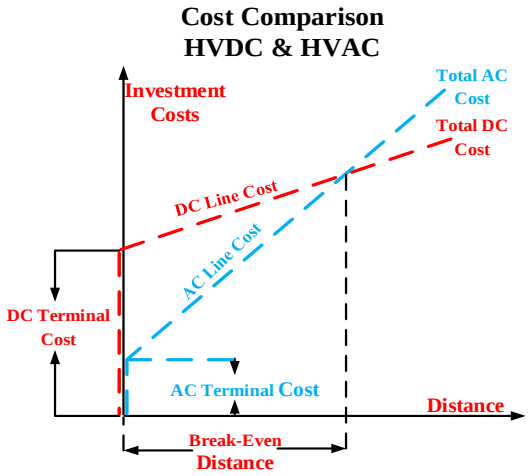

Figure 2-3: Cost comparison of HVDC & HVAC OHL (Source: [35, 36])

In terms of transferring power for long distances and also underwater, the HVDC system is more flexible than HVAC which needs to incorporate different electronic and electrical equipment to maintain voltage levels or reduce harmonics. The applications of HVDC include the following [37, 38]:

1. Underground and submarine cable
2. Long distance bulk power transmission
3. Interconnection of two different asynchronous power systems
4. Stabilization of power flows in integrated power systems
5. Mitigation of environmental concerns of the power transmission
6. Reduction of fault currents

2.3.2.2 Brief Comparison of HVAC and HVDC

The HVAC and the HVDC technologies for power transmission have to be compared with regards to two essential points: power transmission cost and benefits of the technology (technical aspects) [39].

Table 2-1: Comparison of HVAC and HVDC [3]

Issue	HVDC	HVAC
System Connection	Asynchronous	Must have same frequency and phase
Transmission System	High power transfer: two conductors	Lower power transfer: three conductors
Transmission distance	Limited (reactive power compensation)	Unlimited
Transmission System	High technological cost	Lower technological cost
Transmission System	Lower transmission losses	High transmission losses
Voltage conversion	Converter	Transformer
Losses	Lower injection of harmonics, no skin effect and no corona discharge	High harmonics injection, skin effect in cables and corona discharge
Space requirement	Lower Terminal footprint	Greater Terminal footprint
Converter technology	Converters need complex cooling system	No
System cost	Economical for long distances	Economical for short distances

Table 2-2: HVDC-HVAC Components performance

Components	HVDC	HVAC
Long-Haul OHL Bulk Transmission Capacity	High (> 1~2GW)	Limited
Long-Haul Transmission Stability	No Limit	Limited
Right-of-Way for Bulk Transmission OHL	Low	High
Long-Haul Transmission Loss	Low	High
Insulation / Clearance	Low	High
System Connection	Asynchronous	Synchronous
Power Flow Control	Easy and fast	Difficult
Multiple terminal (Tapping)	Difficult and costly	Simple and easy
Short Circuit Limitation	Effective	Not effective
Pollution Effect	More pronounced, higher insulation creep age is required	Relatively less

2.4 LCC-HVDC

Over long distances the OWFs are connected to shore by HVDC power transmission links [9]. There are two types of HVDC transmission technologies, Line-Commutated Converter, LCC, and Voltage Sourced Converter, VSC. The LCC-HVDC is known as the

classic or traditional HVDC system and has a mature control technology compared to VSC technology and thus its behaviour is better known. Furthermore, at this moment, the main advantage of the LCC-HVDC versus the VSC-HVDC system is the quantity of the power transferred through HVDC link. The LCC subsea cabling has a higher voltage rating than the VSC subsea cabling and thus this system can transfer a higher amount of power while also producing lower power losses [4, 40]. The LCC-HVDC also performs better during current fault. The fault current in the LCC-HVDC system is limited by large inductance or smoothing reactors. The drawback of the LCC-HVDC is the thyristor valves which need to absorb high quantities of reactive power that needs to be supplied by a strong grid. Furthermore, the LCC-HVDC power system cannot produce reactive power so this has to be supplied externally. Thus, this fact is a significant problem for offshore applications. Therefore, this becomes a handicap for offshore applications. In addition, when the active power and the reactive power are reversed in the classic HVDC system, the reactive power suffers an increment which can lead the system to suffer instabilities and can also lead to the injection of low-order harmonics [3, 34, 41].

The LCC-HVDC uses thyristor bridges which are connected in a 6-pulse or 12-pulse arrangement. For the 6-pulse bridge arrangement, the lowest order current harmonics are the 5^{th}, 7^{th} and the 11^{th} and for the 12-pulse arrangement are 11^{th} and 13^{th} (wye-wye, wye--delta isolation transformer) [42, 43]. The converter of the LCC-HVDC technology works with solid state semiconductor valves and they need a strong positive AC voltage to fire these valves. Without a strong grid at both ends of the HVDC system, the control system of the LCC converter cannot transfer power. The AC to DC and DC to AC conversion produces a large number of harmonics. To avoid these harmonics, filters need to be installed at both ends of the transmission system which increases the cost of LCC-HVDC transmission [4, 42, 44, 45]. The control system of the LCC converter determines the power transferred by the firing angle of the thyristor valves. This angle is used to regulate the DC voltage at both ends of the HVDC system because the LCC-HVDC is a bidirectional power system. Thus, the firing angle of the valves in the rectifier side has to be set to work within 0^0 to 90^0 and within 90^0 to 180^0 in the inverter side. Figure 2-4 shows an active-reactive power quadrant for the VSC-HVDC system (locus diagram of power transmission systems). The difference VSC-HVDC system allows transferring power through entire PQ locus diagram, 360 degrees, as is shown in the below figure. Figure 2-4 shows the active-reactive power quadrants for the VSC-HVDC [4, 46].

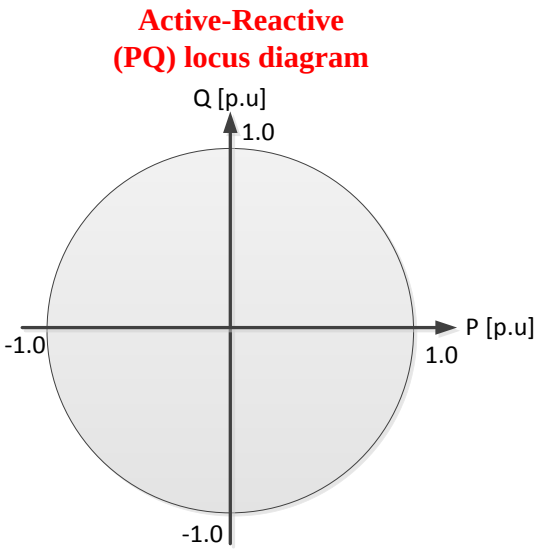

Figure 2-4: Active-Reactive (PQ) locus diagram of power transmission system [4, 46].

The valves need a positive ac voltage on the valves and a firing pulse to start the current flow in the HVDC system. The firing angle determines the direction of the power flow and therefore this direction can be changed by changing the firing angle of the thyristor valves which in turn changes the angle of the AC voltage [45, 47]. This change in the power direction, of the DC current, produces high stress in the HVDC system which could result in future damage to HVDC components [34, 40, 43, 48-51].

In general, a common method to control the LCC-HVDC system is to have constant power control in the rectifier side and the inverter working in constant angle control mode. This controlling method is called Maximum Available Power or MAP [40, 47]. A drawback of the LCC-HVDC system is that it consumes reactive power which may be up to 60% of the total active power being transmitted. Reactive power compensation is hence necessary to prevent drawing power from the grid and cause voltage issues. Another disadvantage is that changing the direction of the power flow is not possible. Some advantages are the for example higher power transfer capability and better performance during faults when compared with a VSC-HVDC systems.

2.5 VSC-HVDC

VSC-HVDC is based on voltage source converters (VSCs) which are controlled using vector control. This allows the independent control of active and reactive power. An important advantage of the VSC-HVDC technology with respect to the LCC technology for transferring power is the possibility of working in the four power quadrants (this converter is bidirectional). This is because of the valves used in the converter, IGBT switches, which

convert the AC power to DC power and allows the DC current to flow in both directions. Moreover, VSCs use the PWM techniques which allow the converter to operate at almost any phase angle or amplitude, and when suitable switching frequencies are employed the harmonic content in the output signals is considerably reduced [31, 52]. Figure 2-5 shows the MIXED scenario used in the case study 2.3.

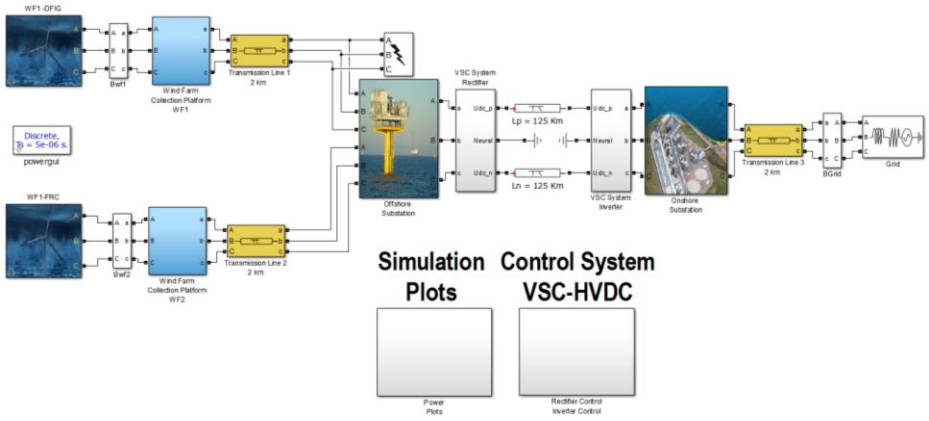

Figure 2-5: Point to point configuration for large scale offshore wind farms

The point to point system works with the idea of controlling the active power in the sending side (rectifier) and the DC power in the receiving side (inverter). For the installation of OWFs far from the shore, a key feature of the VSC-HVDC are the following and are briefly explained in the next section:

- The Black-Start Capability which allows the recovery of the power system without adding external equipment such as STATCOM or SVC.
- The fast communication between both converters which can rapidly adapt the VSC-HVDC system to any abnormal circumstances. Furthermore, the control system has high dynamic ability which adapt itself to the grid requirements.
- The VSC control system has high efficiency, in terms of, mixed power from different energy sources. The conversion of the AC power into DC power without causing mismatches in the power, high quantities of harmonics or altering normal operation of the grid.
- The VSC is a bi-directional system which works in the four power quadrants and thus can re-direct the active power to any position into the grid.

Table 2-3: Comparison of LCC-HVDC and VSC-HVDC systems [3]

Attribute	LCC-HVDC	VSC-HVDC
Converter Technology	Thyristor valve, grid commutation	Transistor valve (IGBT), self-commutation

Converter Technology	Bidirectional powers control: limited powers reversal	Four-quadrant power control: No limited powers reversal
Control of System	Only control the active power	Independently control power
Active Power Flow Control	Continuous ±0.1 Pr to ±Pr	Continuous 0 to ±Pr
Reactive Power Demand	Reactive demand = 60% of active power transfer	No reactive power demand
Reactive Power Compensation	SVC or STATCOM	Injection or withdrawal of reactive power unnecessary
Converter Protection	Due to system control delay with both converters	Instantaneous control of the system between both grids
Converter Technology	Difficult connection with weak grid. Requires strong grid in order to commutate both converters	Possible connection with weak or strong grids
Black Start Capability	No, special equipment needed	Yes
Typical System Losses	2.5 % - 4.5 % (decreasing)	4 % – 6 % (decreasing)
Scheduled Maintenance	Conversion losses around 0.5 %	Conversion losses around 1%
Multi- terminal configuration	Complex	Possible, some limitations

2.6 Features of the VSC-HVDC power system

2.6.3 Grid Codes

Grid connection codes define the requirements for the connection of generation and loads to an electrical network which ensure efficient, safe and economic operation of the transmission and/or distribution systems. Grid Codes specify the mandatory minimum technical requirements, that a power plant should fulfil and additional support that may be called on to maintain the second-by-second power balance and maintain the required level of quality and security of the system. The additional services that a power plant should provide are normally agreed between the transmission system operator and the power plant operator through market mechanisms. The connection codes normally focus on the point of connection between the Public Electricity System and the new generation. This is very important for wind farm connections, as the Grid Codes demand requirements at the point of connection of the wind farm not at the individual wind turbine generator terminals. The grid connection requirements differ from country to country and may differ from region to region. They have many common features but some of the requirements are subtly different, reflecting the characteristics of the individual grids. As a mandatory requirement the levels and time period of the output power of a generating plant that should be maintained within the specified values of grid frequency and grid voltage is specified in Grid Codes [53, 54]. Typically, this

requirement is defined as shown in Figure 2.6 where the values of voltage, V_1 to V_4, and frequency, f_1 tof_4, differ from country to country.

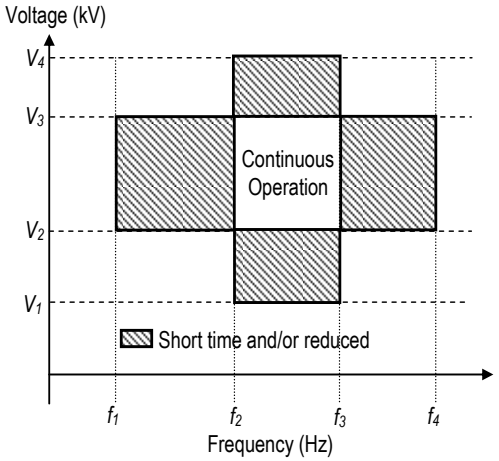

Figure 2-6: Typical shape of continuous and reduced output regions (after GB & Irish Grid Codes)

Grid Codes also specify the steady-state operational region of a power plant in terms of active and reactive power requirements. The definition of the operational region differs from country to country. For example, Figure 2-7 shows the operational regions as specified in the Great Britain and Ireland Grid Codes.

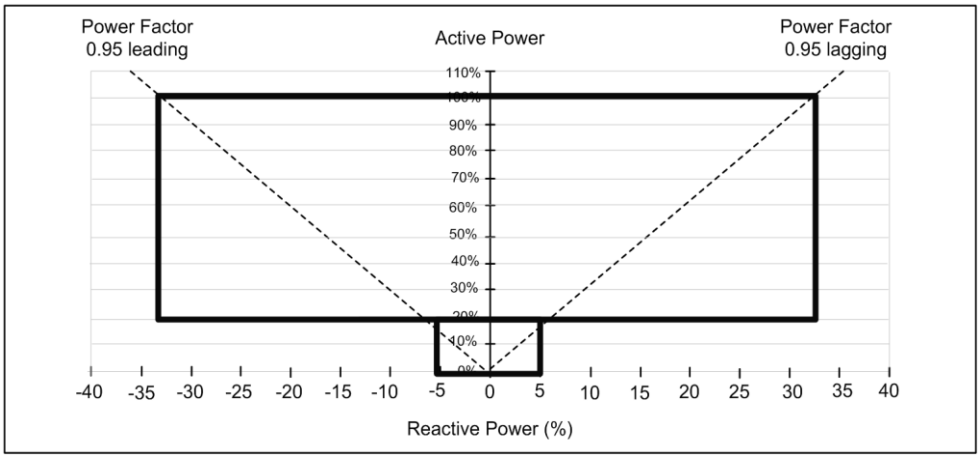

Figure 2-7: Typical steady state operating region (after GB & Irish Grid Codes)

Almost all Grid Codes now impose the requirement that wind farms should be able to provide primary frequency response. The capability profile typically specifies the minimum required level of response, the frequency deviation at which it should be activated and time to response. Traditionally wind turbine generators were tripped off once the voltage at their terminals reduced to less than 20% retained voltage. However, with the penetration of wind generation increasing, Grid Codes now generally demand Fault Ride Through capability for wind turbines connected to Transmission networks [53, 54]. Figure 2-8 shows a plot illustrating the general shape of voltage tolerance that most grid operators demand. When

reduced system voltage occurs following a network fault, generator tripping is only permitted when the voltage is sufficiently low and for a time that puts it in the shaded area indicated in Figure 2-8. Grid Codes are under continual review and as the level of wind power increases, are likely to become mode demanding.

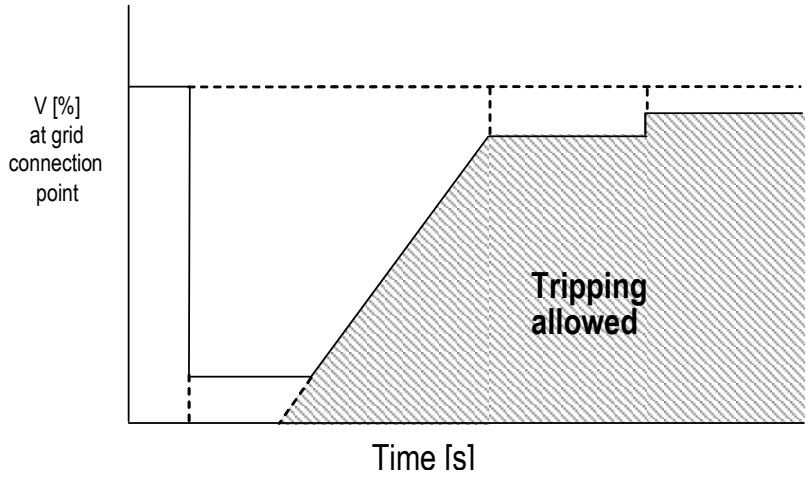

Figure 2-8: Typical shape of Fault Ride Through capability plot (after GB & Irish Grid Codes)

2.6.4 Capability chart of VSC -HVDC

Although the VSC converter improves the control of the active and reactive power of the system, it has its own limitations which influence the active and reactive power transfer capability [55]. The operational area for power transferred by VSC-HVDC systems is described in the *pq*-diagram or also known as the VSC capability chart. Perhaps the main factor that influences transfer capacity is the maximum current limitation of the IGBT valves. The second factor involves the HVDC DC capacitors which set the maximum DC voltage and the third factor is the maximum DC current which results in the maximum power transferred though the HVDC link [56, 57].

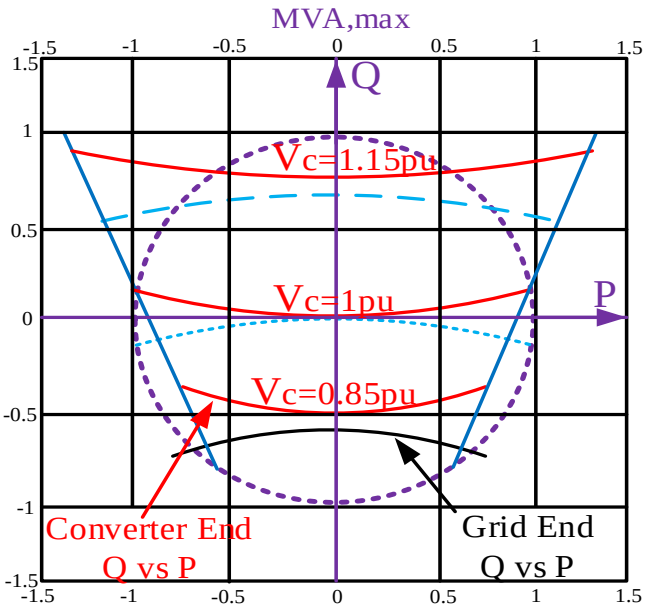

Figure 2-9: Four-quadrant operational chart capability of a VSC (Source: [49, 56, 57])

2.7 VSC System: Vector Control

VSC vector control or direct control is widely used in the control of the VSC converter. The vector control uses a basic idea of controlling the active and reactive power between two points connected through an inductance. Furthermore, this control system uses the decoupled voltages and currents to provide a voltage control signal which is used by the VSC converter to preserve/retain the voltage and frequency in the PCC at their reference values [43]. In addition, the vector control extracts the angle "θ" of the sinusoidal voltage waveforms and thus the control system can work with the numerical values (conversion of sinusoidal waveform "*abc*" to *dq* values) and so the power converter can work with frequency independence [43, 58, 59].

The key factors to control the VSC converter are [49, 60]:

- The Clark and Park transformations reduce the number of frames (three sinusoidal frames to *αβ*-frames and then to *dq*-frames).
- Instantaneous active and reactive power theory, the *pq* theory. This control system has an independent control over active and reactive power.
- The vector control extracts the angle "θ" of the sinusoidal voltage waveforms and thus can work with the numerical values and with frequency independence.

The VSC converter controls the amplitude of the AC voltage, and the phase shift (δ) of the output AC voltage; this in turn avoids synchronization issues produced by power unbalances [49, 60]. Figure 2-10 shows αβ and *dq*-frame coordinate systems and P/Q diagram.

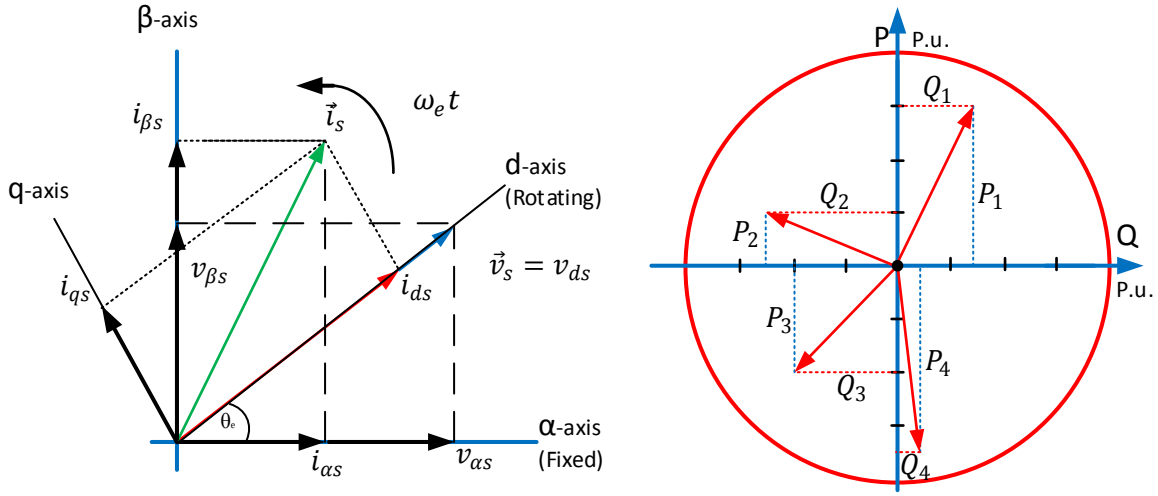

Figure 2-10: a) *αβ* and *dq*-frame coordinate systems[43], b) P/Q diagram for VSC converters [61]

The inductance which connected two power sources determinate the power (active and reactive powers) transfer through it. Thus, the difference between the angle in the PCC ($V_{c,o}$) and the angle in the converter side ($V_{s,\delta}$) influences the direction of this power, see Figure 2-11 [27, 62, 63].

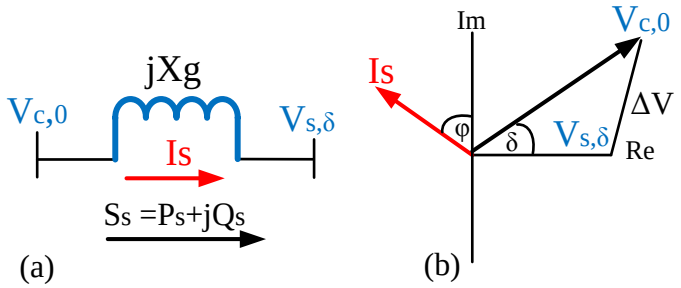

Figure 2-11: (a) Equivalent circuit of a VSC-HVDC transmission system (Xl=jωsl), equivalent circuit diagram and (b) phasor diagram [31, 43, 64]

By altering the phase angle between the converter voltage, $V_{c,0}$, and the grid voltage, $V_{s,\delta}$, the power flow of the VSC-HVDC system can be controlled. Therefore, the VSC-HVDC system can send power or can receive power from the grid [43, 64]. The control system applied to transfer the active and reactive power can be explain by [27, 62, 63] [65]:

$$S_s = \sqrt{P^2 + Q^2} \tag{2.1}$$

$$P_s = \frac{V_{c,o}V_{s,\delta}}{X_g}\sin X_g = \frac{V_{c,o}V_{s,\delta}}{X_g}\sin\delta \tag{2.2 a}$$

$$Q_s = \frac{V_{c,o}V_{s,\delta}}{X_g}\cos X_g - \frac{V_{c,0}^2}{X_g} = \frac{V_{c,o}V_{s,\delta}}{X_g}\cos\delta - \frac{V_{c,0}^2}{X_g} \tag{2.3 b}$$

In steady state and for a balanced system the basic relationship of the voltages and the AC currents across the VSC simple diagram, Figure 3-4, is expressed as follow [42, 52]:

$$V_{c,o} - V_{s,\delta} = L\frac{di_{abc}}{dt} + Rdi_{abc} \tag{2.4}$$

in the *dq0* synchronous reference frame can be described by [42, 52, 66]:

$$V_{cdq} - V_{sdq} = L\frac{di_{abc}}{dt} + Rdi_{abc} + j\omega Li_{dq} \tag{2.5}$$

Considering that the transmission system in a steady state, then $V_{cq} = 0$ and thus equation (2.4) can be expressed as:

$$\frac{d}{dt}\begin{bmatrix} i_d \\ i_q \end{bmatrix} = \begin{bmatrix} -R/l & \omega \\ -\omega & -R/l \end{bmatrix}\begin{bmatrix} i_d \\ i_q \end{bmatrix} + \frac{1}{l}\begin{bmatrix} V_{c,d} & -V_{s,d} \\ V_{c,q} & -V_{s,q} \end{bmatrix} \tag{2.6}$$

Thus, by using the load angle theory for power control and then using Clark and Park's transformations, the stationary values of the instantaneous voltage and current are transformed into numerical values [60, 62]. Therefore, first the system obtains the *abc* stationary axes, and sinusoidal values, then Clark's theory is applied to these parameters and thus they are transformed into algebraically three-orthogonal axes, (αβ0 axes). Then, Park's theory is applied to these coordinated αβ0 parameters and transforms them into coordinate parameters in the angular frame or the rotating frame, (ω), which allows the system to calculate the *dq0* parameters in the time-domain. The instantaneous apparent power is expressed as follows:

$$S(t) = [V_a(t)i_a(t) + V_b(t)i_b(t) + V_c(t)i_c(t)] \tag{2.7}$$

The instantaneous powers, in the time domain, can be expressed by the following equations [42, 52]:

$$P_s(t)_{ins} = \frac{3}{2}\left[V_{s,d}(t)i_d(t) + V_{s,q}(t)i_q(t)\right] \tag{2.8}$$

$$Q_s(t)_{ins} = \frac{3}{2}\left[-V_{s,d}(t)i_q(t) + V_{s,q}(t)i_d(t)\right] \tag{2.9}$$

As mentioned, the V_β and V_α are the components of the voltage in stationary two axis reference frames (Clark's), the $\frac{3}{2}$ is the peak value. The i_{dq} components can be considered

proportional if the $V_q$is equal to zero ($V_{dq} = V_d + j0$) [42, 52]. The angular position of the voltage vector (θ) is estimated by using the phase locked loop technique and is given by:

$$\theta = \tan^{-1}\frac{V_\beta}{V_\alpha} \tag{2.10}$$

The sending converter can be designed as an AC voltage source and the receiving converter can be designed as a DC voltage source. The control system of the VSC-HVDC system can obtain the amplitude, the phase of the AC voltage and the frequency of the network independently and thus, the active and reactive powers can be then controlled by controlling i_{dq} signals [60, 67, 68]. Therefore, the voltage converter output (obtained from the instantaneous active and reactive inputs) can be written as [60, 67, 68]:

$$\tilde{V} = {\tilde{V}_{dc}}/{2}\, m_a \sin(w_s t + \delta) + harmonics \tag{2.11}$$

The m_a is the modulation index and is defined as the process in which the AC and the DC voltage is used to control the VSC-HVDC system [52]. The relationship between the modulation index, DC voltage and decoupled AC voltage in time domain are given by [69]:

$$V_{ph} = {V_{dc}}/{2}\, m_a \sin(\omega t) \tag{2.12}$$

$$V_{s,d} = {V_{dc}}/{2}\, m_a \cos\delta \tag{2.13}$$

$$V_{s,q} = {V_{dc}}/{2}\, m_a \sin\delta \tag{2.14}$$

Thus, the modulation index equation in the *dq* frame is given by:

$$m_a = \frac{\sqrt{(V_{s,d}^2 + V_{s,q}^2)}}{{V_{dc}}/{2}} \tag{2.15}$$

The modulation index can also work in a range of $-1 \leq m_a \leq 1$. To avoid over modulation, the control system should keep it similar than 1. The VSC-HVDC system could enter in an over-modulation if $m_a > 1$ [52, 65].

2.7.1 Inner and Outer Current Controller: Operability

The VSC control systems control the power transfers through the HVDC system (AC voltage and AC current) by using a phase reactor (inductance) [52, 67]. According to the VSC converter control theory, the core of the control system of the VSC converter is the

inner and outer current controller. This controller uses a fast-tracking cascade control structure (with two control loops for the i_{dq} and V_{dq}) to provide a modulation signal. In addition, the control system of the VSC converter obtains the i_d signal from the active power and the i_q signal from the reactive power (this control system could be applied in the opposite way). Furthermore, in this thesis, the inner controller is used to track the error between active power reference and measured signals and the outer controller is used to track the error between reactive power reference and measured signals. The control system of the VSC converter can work as a power or voltage controller, depending on the controlled layouts. In this thesis, the offshore cluster substation works as a voltage source and the wind turbines control system as a power source [70, 71].

In conclusion, the function of the inner and outer controller is to provide power system stability by controlling the active and reactive power in the power system in real time and the function of the inner controller is to provide fast and accurate tracking control of the feed-forward signals (i_{dq}errors) [52, 67, 72].

The reference signals (i_{sd} and i_{sq}) can be calculated from equation 2.7 and 2.8.

$$i_{sd} = \frac{2}{3V_{s,d}} P_s(t) \tag{2.16}$$

$$i_{sq} = -\frac{2}{3V_{s,d}} Q_s(t) \tag{2.17}$$

Assuming that the examined scheme is in the steady state conditions, $V_{sq} = 0$. The feed forward signals (error of the system) are obtained through the PI controllers, then they are introduced in the inner and outer control algorithms [52, 73, 74]:

$$V_{s,d} = k_p(i_d^* - i_d) + k_i \int (i_d^* - i_d)\, dt \tag{2.18}$$

$$V_{s,q} = k_p\left(i_q^* - i_q\right) + k_i \int (i_q^* - i_q)\, dt \tag{2.19}$$

Where $k_p$and k_i are the proportional and integral gains of the current controller and the superscript * refers to reference values. Then, the system transfers (in cross-coupling terms) function of the VSC converter, in the offshore side, can be given by:

$$V_{cd,s} = V_{s,d} - (Ri_d + \omega Li_q) - L\frac{d}{dt}i_d \quad (2.20)$$

$$V_{cq,s} = V_{s,q} - (Ri_q - \omega Li_d) - L\frac{d}{dt}i_q \quad (2.21)$$

Both voltage equations are coupled due to the cross terms ωLi_q and ωLi_d (phase factor inductance). The cross-coupling terms are compensated by feed-forward signals which are switched from one axis to another, and thus both *dq* axes can be controlled independently. Figure 2-12 shows the core of the control system of the VSC converter.

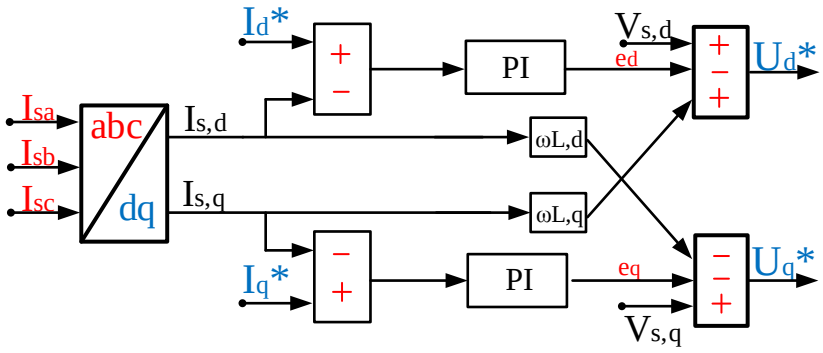

Figure 2-12: A block diagram of the inner and outer current controller for the offshore configuration (source: [52])

As mentioned, this control system works as a cascade controller where the reactive power (i_q) is introduced to the system after the active power [75, 76]. Due to the fact that the outer controller is slower, the i_q signal is fed into the inner current controller without causing instability in the VSC converter. Then, both reference signals are finally introduced into the generic control loop through a proportional-integral current controller (PI current controller). These errors are introduced in the control system with the objective of minimizing electrical power system issues during normal or abnormal power system operation and thus to stabilize the power system faster, and reach the steady state in better conditions [77]. The PI controller ensures that the tracking errors between control signals are correctly achieved and therefore, the appropriate tuning of PI parameters (k_p proportional and k_i integral) becomes essential for the control of the VSC-HVDC system.

2.7.2 Current Limiter

Due to the fact that high fault currents produce large transients, VSC converters can be damaged or their life span can be reduced. The VSC converter does not have any inherent overload capability "current limitation". The inner and the outer current controller cannot set the reference signals ($i_{dq}{}^*$) higher than the VSC current capability by itself and thus, to avoid high current values that could damage the IGBTs, a current limiter should be implemented

before control signals are integrated into the core block of the inner and outer current controller [78, 79]. The voltage amplitude of the VSC must also be limited, the produced reference voltage output of the VSC converter must be appropriately limited or it will also cause instability in the system. Therefore, during large transients, the active and reactive powers have to be limited. The current limit (i_{limit}) has to be calculated using the maximum power transferred through the HVDC and the AC voltage of the power system. Furthermore, when the current bypass the i_{limit}, the protection system limits the active and reactive power transferred. The maximum active and reactive power transferred (P_{max} , Q_{max}) could be estimated as are given by [78, 79]:

$$P_{max} = \sqrt{V_s^2 \ * i_{limit}^2 - Q_{max}^2} \tag{2.22}$$

$$Q_{max} = V_s * i_{limit} \tag{2.23}$$

The current limiting strategies depend on the connection of VSC-HVDC. For example, when the VSC converter is connected to a strong grid, the control system gives a high priority to the $i_{d,limit}$ and thus the active power could be increased and could also help to recover the AC voltage. When the VSC converter is connected to a weak grid, the control system gives a high priority to the $i_{q,limit}$ and thus the reactive power can be controlled and the reduction of the AC voltage can be maintained. A third current limit strategy is to maintain the angle of the AC voltage instead of the magnitude of the current [78, 79].

2.7.3 Pulse-Width Modulation (PWM)

The VSC uses a PWM technique to control the switching of the IGBT valves and synthesise the required output voltage signal. It is a widely used technique where a modulating signal is compared with a triangular signal or carrier signal ($V_{triangle}$) to produce the train of pulses to switch the IGBT [61, 68]. In addition, by changing the PWM pattern (the frequency of the carrier signal) the magnitude of the obtained voltage and phase angle can be modified almost instantaneously. Depending on the quality of the voltage output, the frequency of the carrier signal can be modified. Hence, the higher the frequency of the $V_{triangle}$, the higher the quality of the output power voltage but this higher frequency also leads to higher losses and higher THD. As the frequency of the PWM is lowered $V_{triangle}$, so is the quality of the output voltage, but this also leads to lower losses and low THD. Furthermore, the result of having a higher modulation index leads the system to have a smaller modulation index margin for dynamic response [61, 68].

Figure 2-13 shows a PWM system where a fundamental sinusoidal signal (black) and a signal obtained from the third harmonic injection technique (red). The carrier "$V_{triangle}$ " signal is in blue. In this equation, the k is a factor to increase the amplitude of the modulating waveform.

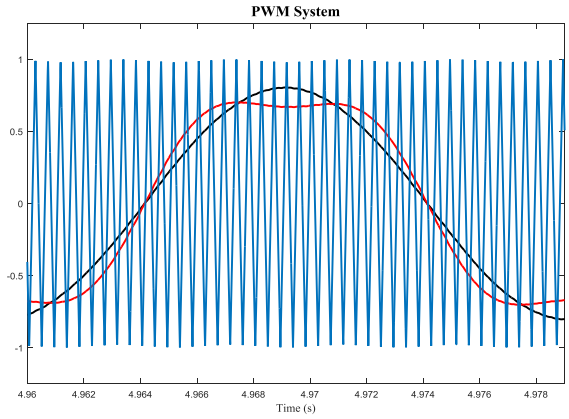

Figure 2-13: PWM modulation signals, this figure is taken from a thesis' simulation

$$\text{If } V_{ac}(t) > V_{triangle} \rightarrow S = 1$$

$$\text{If } V_{ac}(t) < V_{triangle} \rightarrow S = 0$$

2.7.4 Harmonics

The IEEE 1000 defines power quality (harmonics) as "*the concept of powering and grounding sensitive electronic equipment in a manner suitable for the equipment*" [80, 81]. The harmonic distortion can be divided into two groups:

- Voltage Harmonic Distortion (VHD):"*Voltage harmonic distortion is distortion caused by harmonic currents flowing through the system impedance. The utility power system has relatively low system impedance, and the VHD is very low. VHD on the distribution power system can be significant due to its relatively high system impedance*" [80, 82].
- Total Harmonic Distortion (THD):*"The square root of the sum of the square of all harmonic currents present in the load excluding the 50/60 Hz fundamental It is usually expressed as a percent of the fundamental*" [82].

Concerns regarding the incorporation of the offshore power to the onshore grid have increased the uncertainty over the quality of this power due to the use of power electronic converters. The Fourier transformation is used to carry out harmonic analysis. The Individual Harmonic Distortion, IHD, is the ratio between the RMS value of the individual harmonic analysed and the RMS value of the fundamental signal. This is measured at the Point of Interconnection (PCC) of the VSC-HVDC system [83, 84].

$$IHD_n = {\mathrm{In}_n}/{\mathrm{I}_1} \tag{2.24}$$

$$\mathrm{THD}(\%) = \sqrt{\sum_{\mathrm{n}} IHD_{\mathrm{n}}} = \sqrt{(\mathrm{IHD}_1^2 + \mathrm{IHD}_2^2 + \cdots \mathrm{IHD}_{\mathrm{n}}^2)} \approx 1.5 - 2.5\% \tag{2.25}$$

Evaluation formula of voltage THD

$$THD(\%)_{max} = max_{t,n,p}\left(\frac{\sqrt{\sum_{m=2}^{M} V_{mtnp}^2}}{V_{(fund)tnp}} * 100\right) \tag{2.26}$$

Where $V_{(fund)tnp}$ is the fundamental signal of the system.

2.8 Summary

HVAC and HVDC transmission systems have briefly been explained. The control system of the VSC and LCC converters have shortly been analysed. The VSC-HVDC has several advantages over the LCC-HVDC transmission system, especially for the integration of large OWFs far from shore, have also been explained. The characteristic of the VSC converter, the control system and beneficial features has also been introduced and analysed. As a consequence of the comparison of both technological systems, the research has shown that the VSC-HVDC is a better solution over the traditional LCC-HVDC system. In order to provide a deeper analysis of the technical characteristics of the components of the offshore/onshore substations, the chapter describes the VSC converter components and control system. In addition, this chapter describes the control system upgrades applied to improve the dynamic response of the system (VSC-HVDC).

Chapter 3: Operating Principles Control System of the VSC-HVDC

Chapter 3 introduces the operational principles for controlling the proposed offshore transmission schemes. The chapter focusses on the control of the VSC power converter and also the HVDC transmission link. Thus, the first part of the chapter introduces the theory and continues (Sections 3.2) with the description of the VSC substations components (including the theory and a mathematical analysis). Section 3.3 progresses with the explanation of the control strategies for the point-to-point converter substations including a detailed description of a basic control system. Section 3.3 contains the principal control technique for the power converter applied to the control of the offshore/onshore substations. Finally, Section 3.4 ends with an explanation and mathematical analysis of techniques which are used to improve the dynamic performance of the VSC power converter.

3.1 Introduction

The VSC-HVDC system can be connected to two different grids: an active AC grid (strong grid) or a passive AC grid (weak grid) [50, 66]. The difference between these two grids is that the strong grid is connected to a slack bus or a significant power generator which controls the AC voltage and the frequency of the entire electrical network. Therefore, the control of the entire system is carried out by a large generator at the slack bus and the VSC converter performs a minor role in the electrical power system. In addition, this large generator controls the voltage angle and the frequency of the electrical power system and thus, the VSC converter can partially affect the dynamic behaviour of the power system or influence its control. However, the influence of the VSC converter on the grid will depend on the power controlled [50, 85-87]. In a passive AC grid - for example an offshore grid - the VSC converter becomes the crucial part of the electrical power system. The role of the VSC system in such grids is to stabilize the electrical power system, and therefore the duty of the VSC is to stabilize the reference values for the AC voltage, voltage angle and the frequency of the entire power system. Thus, the VSC converter becomes the most important part of a passive grid and operates as a slack bus for it. As previously mentioned, an example of a passive grid is an offshore wind farm or collection of wind farms.

An HVDC system uses power converters to control the power transferred between the two substations (point to point). The control system of the VSC-HVDC is split into two substations: the sending and the receiving substations. Although, the HVDC link uses two different methods of controlling and thus transferring the power - active power control and DC power control - both control systems are simultaneously coordinated. In this research, the offshore substation has an active power controller (voltage controller) and the onshore substation controls the DC power. In order to coordinate both substations, and hence to regulate the power flow and also to avoid instabilities in both substations, both control systems have to control the AC voltage and current of both parts of each part of the electrical system. Furthermore, to achieve a reliable control system, the VSC converter also controls the reactive power in the sending and receiving substations. Figure 3-1 shows the VSC-HVDC transmission layout for a point to point connection; with an FRC wind farm connected to the offshore side and a grid connected to the onshore substation.

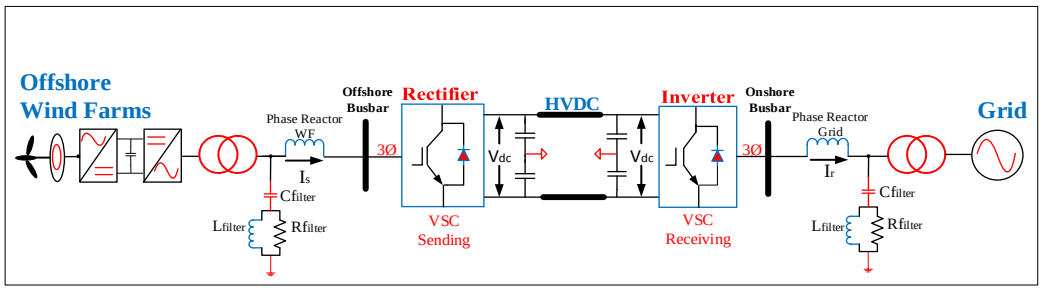

Figure 3-1: A basic configuration of VSC based HVDC transmission system

A typical AC voltage used to interconnect wind turbines and their wind farm substation is 33 kV. However, to reduce power losses, the voltage of these transmission lines could be increased to 66 kV [88, 89]. The transmission voltage from a wind farm platform to the cluster platform will probably remain at the same voltage level of 132kV but could be increased if the offshore system requirements change [88, 90]. Another factor which may influence the array is the number of offshore wind turbines, the power produced, and the number of offshore wind farm substations will dictate the offshore array for the underwater cables. The number of offshore wind farm substations and therefore the offshore cluster substations will depend on the power transferred.

3.2 Composition of the VSC Substation: Theory

An offshore cluster substation is composed by the following electrical and electronic components: VSC converter, transformers, phase reactors, AC filters, DC capacitors and finally the DC cables.

3.2.1 VSC Converter

As mentioned in the previous section, the converter is the key part of the HVDC transmission system. Its principal duty is to convert the power (AC/DC) or vice-versa. Depending on the characteristic of the power system, the role which it plays in the power system, the converter can be more or less significant. Thus, the converter can be part of the control of the network or can have entire control of the network. Furthermore, the characteristics of the VSC system provide the ability of working in 50 or 60 Hz with complete independence between both sides of the converter. There are two types of VSC converters operating in power transmission and one type is under development; the two-level, the three-level and the modular multilevel Converter (MMC). The two-level VSC converter is the simplest converter configuration but is widely used in numerous power system applications. A common type of the three-level converter is three-level neutral-point clamped, NPC, converter. This converter has a more complex structure than the two level but the power conversion is better achieved. Finally, MMC also uses three levels but with twelve pulse bridges in each level [42, 68, 79, 91].

As mentioned, the two-level converter is the oldest and simplest type of VSC converter. This converter is only capable of generating two voltage levels, $\pm \frac{1}{2}V_{dc}$. The benefits of this converter is its simple structure and its robust control system. A handicap of the converter is the quantity of harmonics created during the conversion of the power. This conversion produces a significant distortion of the obtained AC voltage which in turns needs to be filtered. To create this AC voltage, the IGBT switches have to be turned-on/off at specific times; this specific timing is achieved by pulse width modulation technique (used in this research) which compares a modulation signal, created by the control of the converter, and a triangular carrier signal. The benefits of this control strategy are that this active switching gives an accurate control of the obtained AC voltage phase and amplitude [42, 68, 79, 91, 92]. Figure 3-2 shows the evolution of VSC converters.

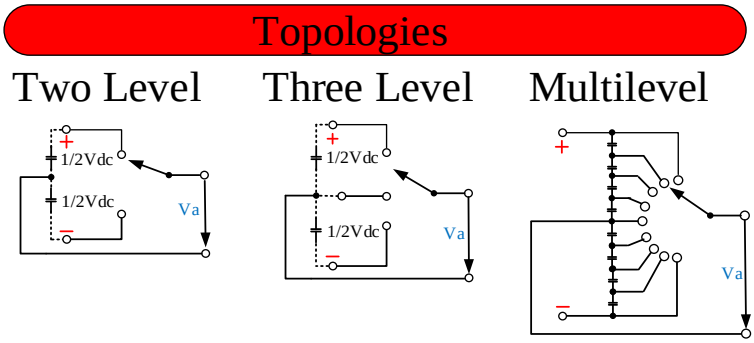

Figure 3-2: Evolution of VSC-HVDC converter [93, 94]

As mentioned, the three-level VSC converter is also widely used in power conversion and it is also considered a more efficient option than the two levels converter. Its structure allows the quantity of harmonics created during the power conversion to be reduced. Figure 3-3 shows a simplified circuit diagram of a Multi-level NPC converter [52].

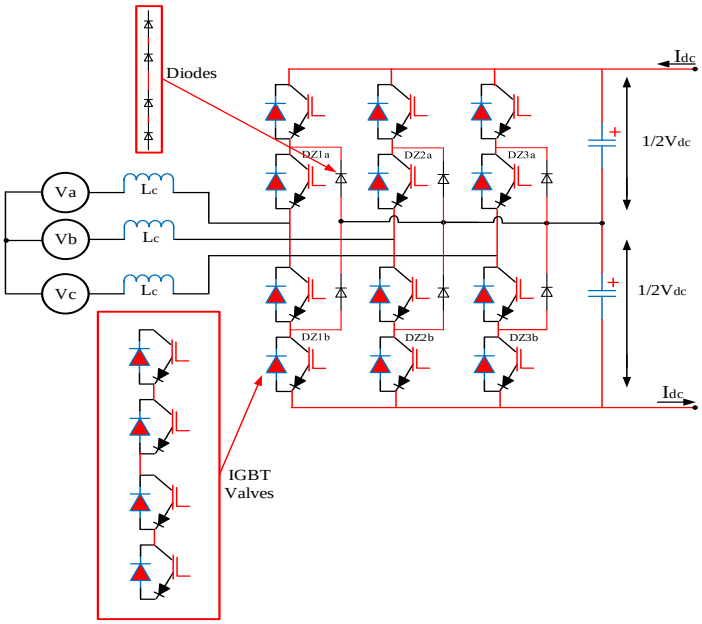

Figure 3-3: VSC Multi-level converter [93]

The Modular Multilevel Converter (MMC) is an evolved power converter. The design of this converter allows the control system to increase the number of voltage steps during the conversion of the DC into AC power. By increasing the number of voltage steps allows the control system to reduce the number of harmonics in the output signal, the stress and the EMC of the power system. Moreover, the improvement in the fundamental signal leads to a reduction in the size of the harmonic filters in the VSC-HVDC system (if the MMC converters are controlling the offshore VSC-HVDC system, filters can be eliminated [92, 95]) and thus the cost is also reduced [96-98]. As the three level converter, the IGBT switches work at the fundamental switching frequency or high switching frequency and therefore the power losses produced in the converter can be reduced [42, 68, 79, 91]. The MMC converter

can also work, as the two or three level converter does, at medium and high voltage power ratings. Thus, this converter can be widely applied to many power system applications. In contrast with the improvement of the power conversion and power losses, the MMC converter has an important drawback which unfortunately increases the price of the converter. Its particular design which introduces a higher number of IGBT valves in its structure makes it more expensive than other converter designs. Another disadvantage is that the large number of semiconductor switches can introduce voltage imbalances for real power "*conversion without sacrificing output voltage performance*" [94]. Another disadvantage of this type of converter is the impossibility of blocking fault currents during a DC pole to pole fault. In recent years, there has been a substantial increased interest in MMC and it seems that in a few years this converter will begin to replace the three-level VSC converter and therefore these problems should be fixed [94, 99, 100].

3.2.2 AC Transformer

Transformers level up or down the AC voltage. In the VSC-HVDC system, the transformer is set to suit the AC voltage level of the system to a correct value for the VSC converter. The VSC converter is connected to the AC grid through a phase reactor and then to the transformer. To achieve a maximum power transmission, the transformer is designed to have a very high magnetizing inductance but very low winding resistance. As a result of this the VSC system has lower power losses and the distortion of the AC voltage is also lower. The impedance values of the transformers must be calculated based on the power transferred, so the rating of the transformer (MVA rating). This thesis uses a three-phase transformer with two windings taken from the SimPowerSystems™ toolbox.

3.2.3 Phase Reactor

The principal functions of the phase reactor are to help to decouple and control the active and the reactive powers. Thus, by controlling the current which pass through the phase reactor the VSC converter controls the power and thus the power transferred from offshore to onshore or vice-versa is regulated [64, 101]. The inductance is also used as an AC filter and therefore, is used to reduce the high frequency harmonics. In addition, the phase reactor is also used to limit the fault current in case of a transient. The reactors are usually about 0.15 pu [61, 64, 101]. The choice of the size of the phase reactor depends on the switching frequency of the VSC converter and its control algorithm. The value of the phase reactor is

directly influenced by the converter saturation and thus it should be adapted to the scale of converter. The delay time of the phase reactor can be calculated by [64, 68, 102]:

$$\Delta_t = \frac{0.9\, L_{reactor}}{\omega_s (V_{acmax} - V_{ac})} 0.612 V_{dc} \quad (3.1)$$

Where the minimum reference current tracking time (Δt) is less than the time constant of the converter current controller. V_{ac} is the voltage line to line and V_{acmax} is the maximum line to line voltage. The V_{acmax} is calculated by the following formula:

$$V_{acmax} = \frac{\sqrt{3} m_a V_{dc}}{2\sqrt{2}} \approx 0.612 V_{dc} \quad (3.2)$$

3.2.4 AC Filters

In general, the VSC-HVDC link has AC filters installed in both substations installed between the transformer and the phase reactor. These filters are an essential part of the VSC scheme and are installed in order to reduce the high number of harmonics produced by the transmission and also by the conversion of the energy [103]. The design of passive filters only allows installation of passive components such as resistors, inductors and capacitors; these components allow certain frequencies to pass while rejecting others [103]. The AC filter typically installed in the VSC scheme is a passive high-order low-pass filter such as the RLC or LCL filters, but in offshore schemes more complex active filters may be installed. Although these active filters are much more expensive, they can guarantee proper harmonics filtering. Due to their design, these filters can adapt themselves to the active and reactive power transmitted and therefore result in less stress for the VSC-HVDC power system [83, 104]. Furthermore, to level up the voltage level in the transmission line, a capacitor bank has been installed in the offshore substation.

3.2.5 DC Capacitors

In terms of transmission a large capacitance with a small time constant will decrease the ripple of the DC voltage but will affect the reaction time of capacitors during disturbances. Conversely, a small capacitance with a large time constant can produce a large current which reduces the charging time and also reduces the recovery time of the capacitor. However, this high current can significantly reduce the lifespan of the capacitor (in this thesis the time constant is calculated in Chapter 5) [68, 79, 87]. The instantaneous DC current can be calculated using the follow equation:

$$i_c = C_{dc} \frac{dV_{dc}}{dt} \quad (3.3)$$

The following equation is used to calculate the size of the DC capacitors:

$$C_{dc} = \frac{\tau * 2S_n}{V_{dc}^2} \quad (3.4)$$

Where τ is the time constant, S_n is the power transferred and V_{dc} is the voltage line of the HVDC link. The intention of having a small time constant is that the recovery time of the VSC-HVDC system can be reduced and therefore the VSC-HVDC system can reach the steady state faster[1].

Table 3-1: DC link parameter for a case study of two wind farms connected to VSC-HVDC link

Description	Value	Unit
V_{dc}	±150	kV
S_n	600[2]	MW
Capacitor	2.5e-9	Farad (F)

In cases of large HVDC transmission systems which carry large quantities of power, the recovery time of the VSC-HVDC power system becomes essential, and therefore the capacitors' design is decided based on this. Thus, the time constant (τ) of the DC capacitors is chosen to have a high value. In contrast, in wind turbines the key factor is the DC voltage ripple and thus a capacitor must be designed in order to ensure a low DC voltage ripple or a constant value. So, in such cases, the τ has a low value (between 2ms and 5ms). This low value of the τ is possible because of the low quantity of power transferred between both converters [68, 79, 87].

3.3 Design and Control Strategies: Offshore and Onshore Substations

This section explains the control strategies applied to enhance the performance of power converters for both point to point substations including a description and mathematical analysis of the VSC power converters. Furthermore, Section 3.3 presents the principal control theory and techniques for the power converter, including: schematic diagram of the control systems, mathematical analysis of the *dq* theory, active and reactive power controller systems, the AC voltage controller, the inner and outer current control technique. Furthermore, as mentioned they are part of the main contribution of this thesis.

[1] The power transfer through the HVDC link changes depending on the case study
[2] Case study 3 has two wind farms rated at 300MW

3.3.1 Offshore Substation: Rectifier Converter

The main objective of the rectifier converter is to maintain the AC voltage amplitude, phase angle and frequency of the entire offshore layout. Thus, the principal control idea of the offshore converter is to work as a power source and thus to control the system from its connection point, the slack bus, and also to regulate the exchange power to the onshore grid [50, 79, 105, 106]. Figure 3-4 shows a VSC connected to an AC power system.

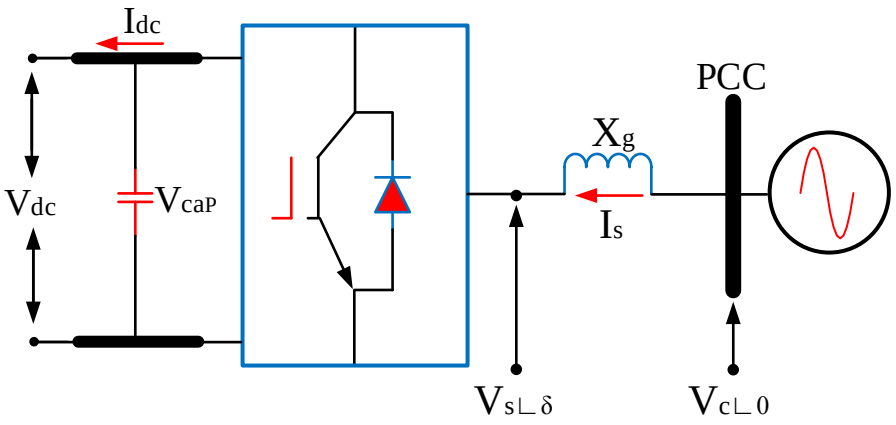

Figure 3-4: VSC basic diagram used for an integration system [43, 85]

Figure 3-5 shows the vector diagram of the offshore substation where the active power is controlled by controlling voltage angle and the reactive power can be controlled by controlling the amplitude of the voltage in the converter side.

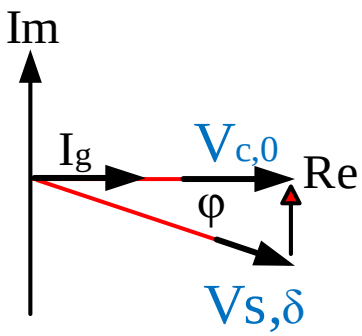

Figure 3-5: Vector diagram: Representation of a sending substation (rectifier) [85, 86, 107]

To achieve the right power transferring of the offshore electrical network, the $V_{c,0}$ is higher than the $V_{s,\delta}$, and thus the converter can send power through the HVDC link to the onshore grid. On the other hand, if the onshore grid needs to send power to offshore, the $V_{c,0}$ will be lower than the $V_{s,\delta}$, and therefore the offshore converter will receive power from the grid [85, 86]. A basic active and reactive controller can be seen in Figure 3-6.

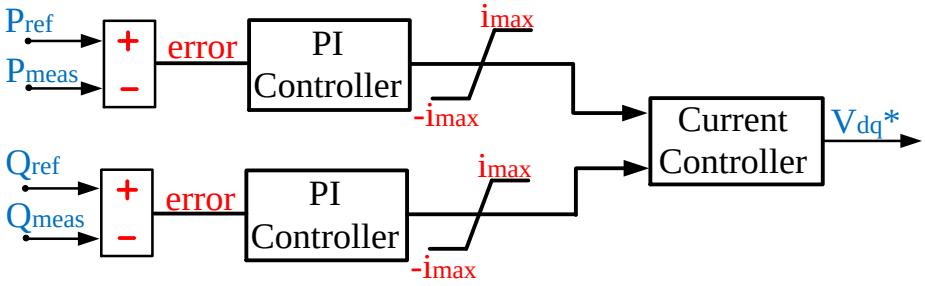

Figure 3-6: Control loop diagram of the active and reactive power use to control the offshore converter

In order to limit fault current and therefore to prevent damage to the control system, the output between the reference and the measured signals, the error, is limited [42, 50, 68]. The imposed limits for errors of the active power are set as 1.1 and -1.1 and for the reactive power are set 1.1 and -1.1.

3.3.2 Onshore Substation: Inverter Converter

The onshore substation does not have a significant influence on the AC voltage, current or frequency [85, 86]. Therefore, the main objective of the inverter VSC converter "substation" is to control the DC power and balance this power with the onshore grid. Furthermore, the VSC control system must also achieve the grid requirements.

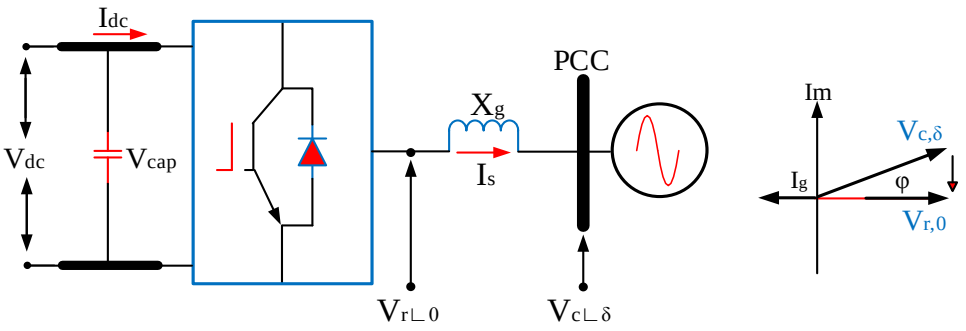

Figure 3-7: VSC basic diagram and a vector diagram of a receiving substation (Inverter) [43, 85, 86, 107]

Figure 3-8 shows a basic control system of the onshore substation, where the DC voltage is used to obtain the $i_{d,r}{}^{*}$ and the reactive power is used to obtain the $i_{q,r}{}^{*}$ [42, 49, 50].

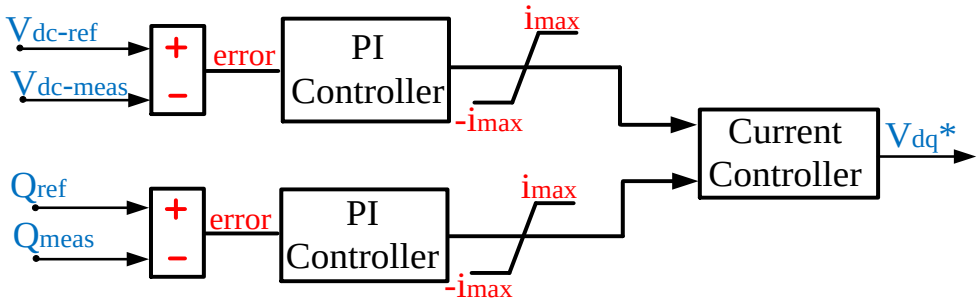

Figure 3-8: Control loop diagram DC voltage and reactive power regulators use to control the onshore converter

For the offshore controller, limits were set 1.1 and -1.1 and for the reactive power are set 1.1 and -1.1 [42, 50, 68]. The power balance relationship between the AC input and the DC power transferred through the HVDC is given as [52, 85, 86]:

$$P_r = \frac{3}{2} P_{dc} + P_{cap} \tag{3.5}$$

$$P_r = \frac{3}{2}\left(V_d * i_d + V_q * i_q\right) \tag{3.6}$$

Where the P_r is the power send from offshore to onshore. Furthermore, in steady state, $P_{dc} = V_{dc} * i_{dc}$ is the output of the VSC converter. The i_{dc} and i_{cc} are the DC bus current and the capacitor current respectively, and the 3/2 factor comes from Park's transformation. The same current in terms of voltage across the capacitor is given by:

$$i_{dc} = C\, {dV_{dc}}/{dt} + icc \tag{3.7}$$

In a steady state case, the current which passes through the capacitor is equal to zero, $i_{cap} = 0$, and therefore the $i_{dc} = I_{cc}$. The output equation of the inner and outer current controller in the onshore substation is described by [52, 85, 86]:

$$V_{cd,r} = V_d - R i_d + \omega L i_q - L \frac{d}{dt} i_d \tag{3.8}$$

$$V_{cq,r} = V_q - R i_q - \omega L i_d - L \frac{d}{dt} i_q \tag{3.9}$$

The reference signals, i^*_{dq}, can be calculated as follow [52, 85, 86]:

$$i^*_{d,r} = k_{p3}\,(V^*_{dc} - V_{dc}) + k_{i3} \int (V^*_{dc} - V_{dc})dt \tag{3.10a}$$

$$i^*_{q,r} = k_{p4}\,(V^*_{ac} - V_{ac}) + k_{i4} \int (V^*_{ac} - V_{ac})dt \tag{3.11b}$$

Parameters k_{p3}, k_{i3}, k_{p4}, k_{i4} are the proportional and integral gains of the DC voltage and AC voltage controllers respectively.

3.3.3 Active Power Controller.

The active power controller ensures the normal operation of the system during any disturbance or any variation of the DC power in the HVDC link (this is achieved by fast tracking of the AC power). In addition, to ensure this fast tracking of the disturbances, the active power is decoupled to obtain the i_d signal. This is compared with a reference signal and then the error is fed into the control system of the VSC converter. As mentioned, the key factor for the active power control is the PI controller value (i_{dq}) which produces these fast tracking errors of the active and reactive power. Thus, to obtain a reliable control system, the error between the expected power and the obtained power should be similar to zero. A basic equation which can describe the control system of the active power in the VSC-HVDC is given by [42, 50, 68, 105]:

$$i_d = \frac{3}{2}\frac{P_{ref}}{V_d} \tag{3.12}$$

Figure 3-9 shows the active power control loop topology which has been chosen to control the active power in the offshore scheme. Furthermore, this $P_{cal,s}$ is calculated using the total power transferred through the HVDC link. Thus, the P_{meas} is the power measured in the PCC point and the P_{cal} is obtained by using the conversion of the AC power into DC power. To simplify the scheme; it is assumed that there is no power losses in the conversion and therefore P_{cal} can be calculated as $P_{cal,s} = P_{dc}$, more information see (3.14-3.17).

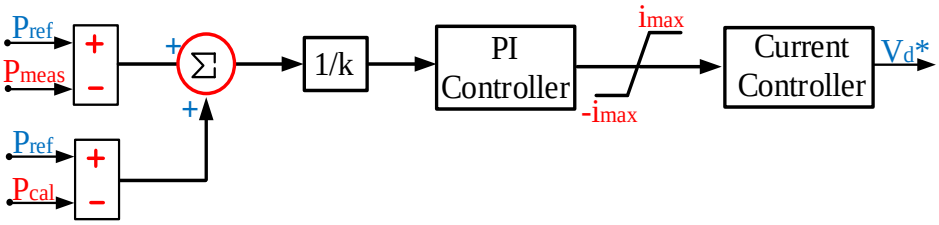

Figure 3-9: Control block diagram of the active power controller

In order to limit fault current and therefore to prevent damage to the control system, the output between the reference and the measured power signals, the error, is limited by the upper and the lower saturation limit of the PI controller.

3.3.3.1 Offshore Cluster Substation: Control System

Wind farm platforms which are adjacent to the offshore cluster substation have to level up the AC voltage to 132 kV and this power is then sent to the offshore cluster substation. The total power collected in the cluster substation at the PCC point is the combined power

sent from all wind farm platforms. Thus, the total power at PCC in the cluster platform has also been defined as P_{meas} and Q_{meas} or $P_{cluster}$ and $Q_{cluster}$. Equations to define the power/voltage in the cluster substation are as follows:

$$\sum P_{wfs} = P_{meas} \tag{3. 13}$$

$$\sum Q_{wfs} = Q_{meas} \tag{3.14}$$

Figure 3-10 shows the research cluster substation control system, where the power/voltage controllers are implemented along with a frequency control.

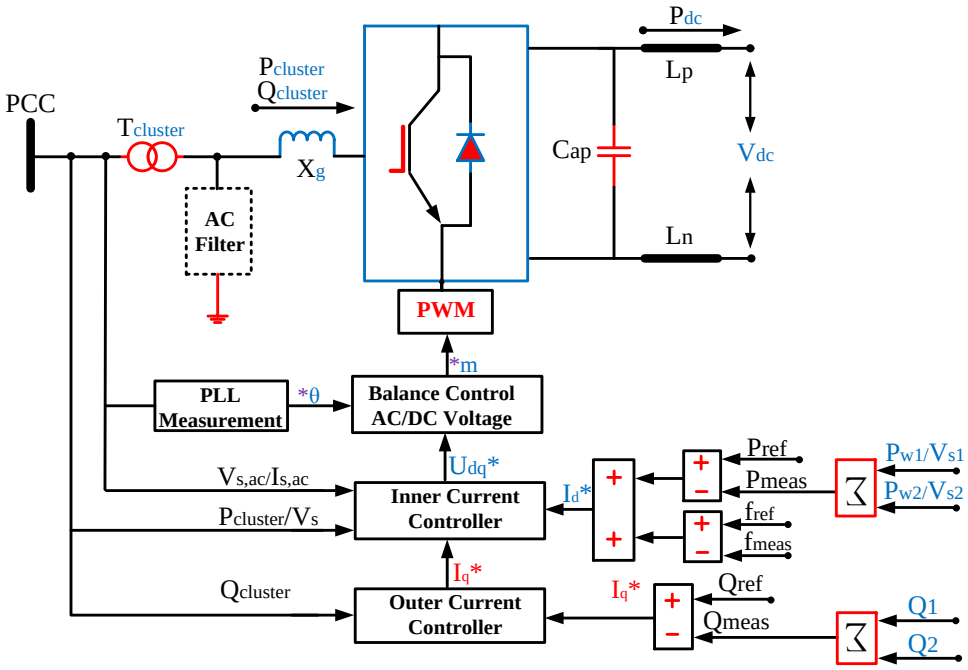

Figure 3-10: The block diagram of the multi power control for three WFs connected to a VSC converter

As mentioned, the P_{meas} is the power collected in the cluster substation at the PCC. This collected power involves the power sent from each offshore wind farm substations. As mentioned, assuming that there are no losses in the conversion of the energy (AC/DC), the $P_{cal,s} = \frac{3}{2} P_{dc}$. The dc side of the VSC system (considering the power-balancing theory) can be expressed as follow by [42, 50, 68, 105]:

$$P_{cal,s} = \frac{3}{2} P_{dc} \tag{3.15}$$

$$V_{ac,s} * i_{ac,s} = \frac{3}{2} V_{dc} * i_{dc} \tag{3.16}$$

The $P_{cal,s}$ is power send from offshore to shore, more information sees Section 2.7. The obtain control value, $i^*_{d,s,}$ is calculated as follow:

$$V_{dq,s} * i_{dq,s} = \frac{3}{2} V_{dc} * i_{dc} \tag{3.17}$$

$$i^*_{d,s} = \frac{3}{2} \frac{V_{dc} * i_{dc}}{V_{dq}} \tag{3.18}$$

The obtained reference signals, $i^*_{d,s}$, is compared with the obtained i_d signal from equation (3.19). The result is adapted to the control signal and then it is introduced in the inner and outer current control system. Furthermore, considering that the power system is in steady state can be considering that the reactive power is similar than zero and therefore can be considered that $V_{q,s}$ and $i_{q,s}$ are similar to zero; the final equations for the $V_{d,s}$ and $i_{d,s}$ are:

$$V_{d,s} = \frac{3}{2} \frac{V_{dc} * i_{dc}}{i^*_d} \tag{3.20}$$

$$i^*_{d,s} = \frac{3}{2} \frac{V_{dc} * i_{dc}}{V_d} \tag{3.21}$$

3.3.4 Reactive Power Controller

The implementation of the reactive power controller and therefore the calculation of the PI values are similar to the active power controller. Therefore, a basic equation which can describe the control system of the reactive power in the VSC-HVDC transmission system is given as [42, 50, 68, 105]:

$$i_{q,s} = -\frac{3}{2} \frac{Q_{ref}}{V_d} \tag{3.22}$$

In general, the reactive power should be equal to zero, but depending on the grid requirements for reactive power compensation, this signal may not be zero. Therefore, the reactive power controller has to adapt the reference controlled signal, $i^*_{q,s}$, to obtain an error signal similar to zero and Figure 3-11 shows the reactive power control loop. Finally, an equation to describe the reactive power controller is given by:

$$Q_{ref} \cong Q_{meas} \tag{3.23}$$

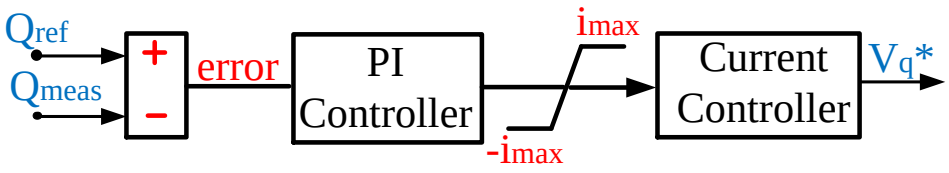

Figure 3-11: Control loop diagram of the reactive power controller with a PI

The above topology with the loop controller has been chosen to control reactive power in the offshore scheme.

3.3.5 AC Voltage Controller

Due to the incompatibility of having two equal control systems (power control in the wind turbines and a power control in the offshore cluster substation), the control system in the cluster offshore substation must be a voltage controller. Wind turbines have already incorporated a power control in their grid converter and therefore the cluster substation has to have an AC voltage controller, otherwise problems could arise with the stability of the VSC-HVDC system. Therefore, both control systems (wind turbines and the offshore cluster substation) cannot act as a power source, one converter needs to act as a power source and the other converter needs to act as a voltage source [50, 86]. Furthermore, the offshore substation has to take control of AC voltage and, as a consequence, of the entire offshore layout [50, 86]. In addition, this AC voltage controller has to have a similar purpose to the power source control system: to control and maintain the AC voltage and frequency at rated values. This AC voltage controller has the same control method as the active power controller. The AC voltage controller will take control of the power system by using a phase reactor. Thus, the alteration of the AC voltage (Δv) is the key to ensure an accurate control of the power transferred through the HVDC [42, 50, 68, 105]. To obtain a reliable DC voltage control, the measured voltage has to be equal to the reference voltage.

$$V_{ac-ref} \cong V_{ac-meas} \tag{3.24}$$

$$V_{d-mes} = \Delta V - (L_{Phrec-pu} * i_d + R_{Phrec-pu} * i_d) \tag{3.25}$$

In this thesis, the $R_{Phrec-pu} * i_d$ is equal to zero. Figure 3-12 shows a control system of the AC voltage at the PCC.

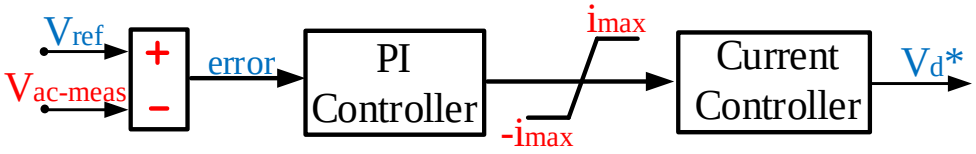

Figure 3-12: Control loop diagram of the AC voltage controller with a PI Controller

In this thesis control system is applied to the offshore cluster substation.

3.3.6 V_{dc} Voltage Controller

The main objective of the DC controller is to regulate the DC voltage in the HVDC transmission link and thus allows the DC power to be transferred. Therefore, the DC voltage controller has to detect DC voltage alteration in any DC capacitors. When DC voltage is

altered, the DC controller requests extra active power, this power request is sent through the VSC converter and the request stays on until both capacitors are balanced [64, 75, 108]. The DC voltage controller is set in the onshore substation, while the AC voltage controller is implemented in the offshore substation, and is also set to have a similar control strategy to the active power controller. The DC voltage controller is set to be the reference signal ($i_{d,r}^{*}$) for the inner and outer current controller while the reactive power controller is used to control the $i_{q,r}^{*}$. The reference signals are also compared with the measured signals from the onshore current obtained in the grid PCC point. Furthermore, the signal obtained from the comparison of both signals is fed into a PI controller which will provide a fast tracking error of the power system. Finally, these are introduced into the inner and outer current controllers. The DC controller ensures fast tracks of the DC power during any onshore disturbances or any variation of the offshore DC power [42, 50, 68, 105, 108]. As can be seen in Figure 3-13, to obtain a reliable DC voltage control, the measured voltage has to be equal to the reference voltage:

$$V_{dc-ref} \cong V_{dc-meas} \tag{3.26}$$

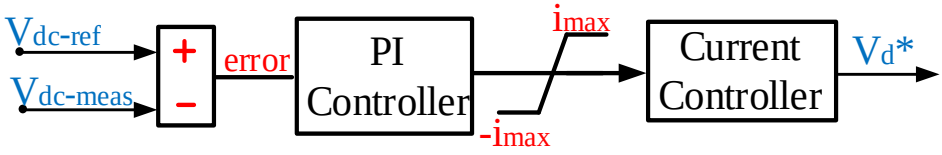

Figure 3-13: Control loop diagram of the DC voltage controller with PI

Figure 3-14 shows the DC control system with the incorporation of the frequency controller.

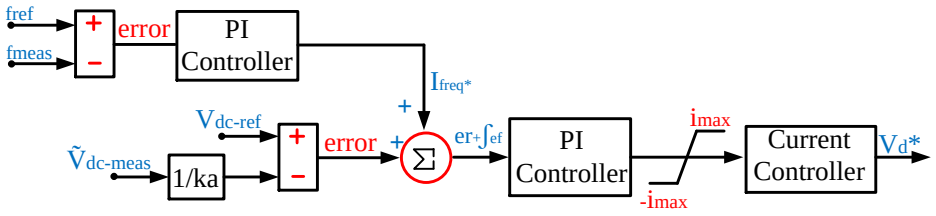

Figure 3-14: Control loop diagram of the dc voltage controller with the introduction of the frequency controller

To obtain reference signal for this DC control system $i_{d,r}^{*}$; the DC voltage has to be converted in per unit. Thus, the k_a depends on the rated voltage of the HVDC transmission system (in this thesis is 300kV). Therefore, k_a is proportional to the DC voltage in the HVDC transmission line and therefore it is equal to the total value of the DC capacitors. Furthermore, in order to design the inner and outer current controller of the onshore substation, the DC voltage and AC voltage controllers have to produce the set-points for the active and reactive current components [42, 50, 73]. In addition, the relationship of the

modulation index in the onshore substation DC link voltage and the *dq* components of the AC voltage are given by [42, 50, 73]:

$$V_{cd,r} = \frac{1}{2} M V_{dc} \cos \delta \tag{3.27}$$

$$V_{cq,r} = \frac{1}{2} M V_{dc} \sin \delta \tag{3.28}$$

Furthermore, using the square roots of the $V_{cd,r}$ and $V_{cq,r}$, the modulation index is calculated, more information sees Figure 3-7.

3.4 Technical Features of the Control System

The following section introduces the control strategies applied to enhance the power performance during large transients. These techniques are introduced into the control system to improve the dynamic response of the VSC power converter. The section shows diagrams and also mathematical analysis for each feature introduced into the control system of the power converter. Thus, plots and diagrams show the proposed benefits of these techniques i.e. the third harmonic injection technique plot displays the inflection that this technique applied to the modulation signal. The schematic diagram of the frequency controller presents the final control system diagram applied to the control of the offshore substation. In addition, the optimum tuning criteria technique shows the mathematical analysis used to define the k_p and k_i parameters.

3.4.1 Third Harmonic Injection

The idea of the third harmonic injection technique is to inject the third harmonic component into the modulation signal, which is compared with a carrier "triangular" signal in the PWM block. The purpose of this technique is to rectify the modulation waveform signal at maximum and minimum positive and negative peaks. Thus, this technique increases the modulation region of the VSC converter by 15% [92, 109, 110]. The introduction of the third harmonic injection technique reduces the amplitude of the modulation signal of the PWM without affecting the normal operation of the VSC converter. This reduction in the waveform of the modulation signal influences the harmonics reduction and also reduces the stress of the converter [34, 91]. Moreover, the incorporation of this control technique can decrease the DC bus voltage by about 13% with respect to the amplitude of the AC voltage [52].

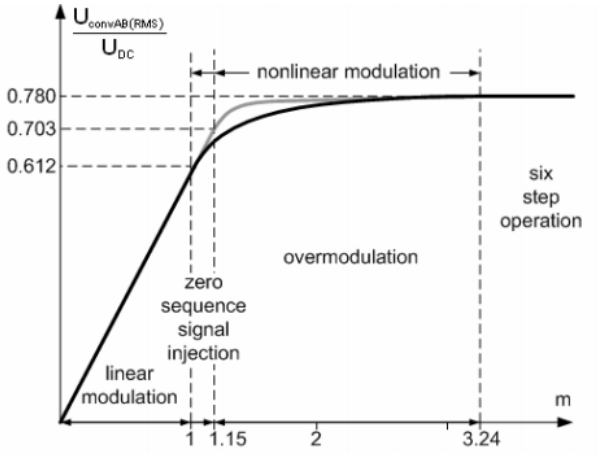

Figure 3-15: Modulation index range [111]

Figure 3-15 shows the modulation index performance during linear and nonlinear range. Between the range 0 to 1, the VSC converter performs in linear modulation and between 1 to 1.15, the third harmonic injection technique helps to add this to the linear modulation range and thus the VSC converter continues to operate normally. After this point the converter enters over-modulation (the over-modulation results in an increment of the low order harmonics introduced in the resultant output of the converter).

3.4.2 Frequency Controller

The control of the network power is based on the idea of a balance between supply and demand; the power supply must always meet the power demand under any circumstances. The frequency of the electrical network directly depends on this fact. The frequency will increase if power generation is higher than the power demand and decrease in the reverse situation [43]. As mentioned, when the VSC-HVDC system is connected to a passive grid, the VSC converter can be considered as a synchronous generator or a big power plant, and hence the power production of the scheme is fully controllable by the VSC converter. Therefore, considering the nature of the offshore VSC-HVDC system - a passive grid controlled by a VSC converter - it has been decided to introduce a frequency controller into the VSC control system to improve the performance of the HVDC transmission system. Along with the active power and the DC power controllers, the introduction of an additional frequency controller in both substations, offshore and onshore, is intended to ensure the fast response of the power system to any changes in the frequency. To obtain reliable control of the converter, the frequency controller has to have a slower response than the applied controller (active power/voltage). Otherwise, this signal could create problems in the power system [34, 79, 112]. Figure 3-16 shows a basic frequency controller.

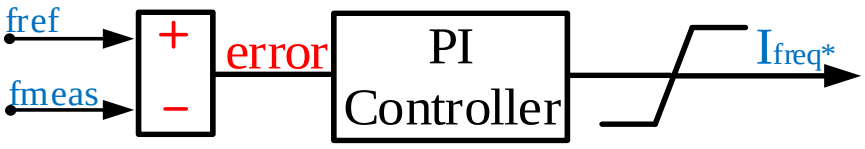

Figure 3-16: Control loop diagram of the frequency controller with PI

The error limit in the PI controller is set to 0.25 and -0.25.

As mentioned, the implemented frequency control loop to the power control loop has to provide faster control during abnormal situations and thus improve the behaviour of the power system. Figure 3-17 shows a power control loop with the introduction of the frequency controller.

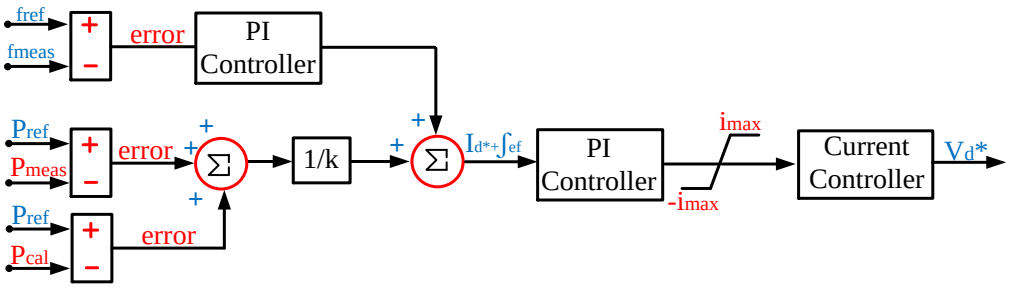

Figure 3-17: Control loop diagram of the active power controller with the incorporation of the frequency controller

The 1/k is a correction factor applied to control system created by this thesis.

The operation of the frequency controller can be described by:

$$f - f_o = k(P - P_o) \tag{3.29}$$

Any changes in the frequency have to be controlled by the open control loop. The control loop has to be open otherwise it will produce alteration in the overall control system of the VSC converter. Furthermore, the error between the ideal frequency and the frequency measured produces a correction signal (e_f), before this error is introduced into the VSC control system through a PI compensator. This PI compensator fulfils the same function as the previously mentioned PI compensator. The frequency controller can be described as [73]:

$$e_f = k_{pi} \int (f - f_o)\, dt \tag{3.30}$$

$$e_f = k_{pf}(f^* - f_{meas}) + k_{if} \int (f^* - f_{meas})\, dt \tag{3.31}$$

Finally, the control signal of the frequency controller is added to the inner and outer current controller, through the reference signal i_d^*, and thus the final expression of the new reference signal for the active power or DC power controllers can be written as:

$$i_d^* = \int e_f + i_d \, dt \tag{3.32}$$

3.4.3 Numerical Control for the DC Voltage

The results of applying a numerical control over the V_{dc} voltage gives a more accurate control method to the DC voltage in the offshore and onshore substations. Thus, the actual DC voltages in both capacitors of the DC link are converted to pu values. Then the sum of the positive and the negative DC voltages are introduced into the control system to be multiplied with the V_{dq}^*. This control modification of the V_{dc} allows a faster response of the VSC converter under any circumstances. It also reduces the stress of the V_{dc} system during transients or high dynamic disturbances.

3.4.4 Phase-Locked Loop

The function of this PLL is to ensure that the input signal stays at the specific frequency of the system and that the output signal can be used to modulate other signals without causing a mismatch. The synchronization of the VSC converter with respect to the offshore/onshore grid is highly important to the performance of the PWM system. Therefore, the role of PLL becomes essential in the control of the VSC converter and thus in the control of the grid. The aim of the PLL controller is to provide the phase synchronous angle "θ" for the conversion of the obtained signals (V_{dq} signals). Accordingly, this conversion can be placed from an abc sinusoidal system to the *dq* coordinate system or vice-versa (abc ↔ dq). Furthermore, the PLL maintains the output signal of the AC voltage in synchronization with an input signal of the PWM, in frequency and angle. Furthermore, it also minimizes the possible error in the phase of the angle and the frequency of the input signal of the PWM and thus can provide a fast response to any disturbances. There are a few methods which can generate sinusoidal signals for the PWM controller and which can also obtain the desirable frequency of the system, and thereby obtain the desirable control of the PLL: the zero crossing detection, the filtering of grid voltages and the voltage controlled oscillator technique (VCO) [55, 79]. Figure 3-18 shows a basic PLL control loop.

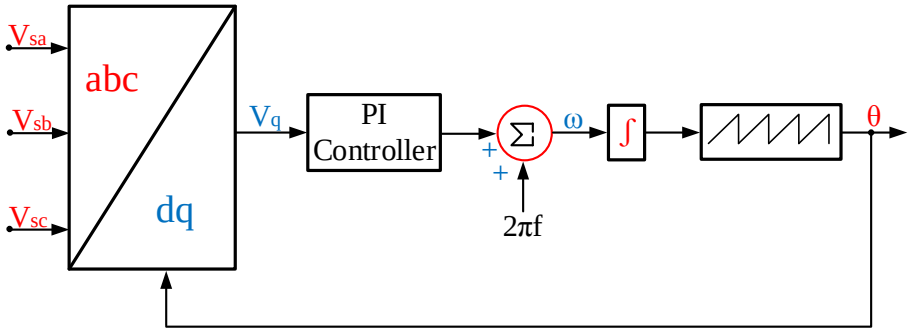

Figure 3-18: Block diagram of PLL taken from [86, 113]

The PLL technique is based on the *dq* decoupling technique, where the control system tracks the V_q (in the reference frame). The PI controller is set to control the variability of the input signal (V_q) with respect to the frequency of the system (ω). After integrating the output of the PI controller; the signal is combined with the voltage angle "in radians" which varies between 0 and 2π (ωt). The design requirements for the damping factor are equal to $\zeta = \frac{1}{\sqrt{2}}$. The damping is equal to ζ=0.707 and the T_s is set to 0.04 seconds. [86, 113]. The natural frequency, ω_n, can be calculated as given:

$$\omega_n = \frac{4.6}{\zeta T_s} \tag{3.33}$$

3.4.5 Tuning of the PI Controllers

The PI controllers have to provide fast tracking signals and therefore they have to be correctly defined and tuned. Furthermore, the combination of proportional and integral terms increases the response of the controller signal and also the PI controller to eliminate the steady state error. The key factors in tuning the controller are the cut-off frequency being set "as high as possible", the proper control of damping oscillations, and ensuring a small overshoot. However, these key factors are applied to the system according to the total power transfer and the value of the parameters of transmission lines (AC or DC), they have to be integrated to the control system depending on the transfer function of the PI control loop. Thus, the error of the system should be proportional to the k_p and the k_i is set to eliminate the offset of the error of the system which produces the instability. The k_i is a large integral gain and works at low frequencies. As a result of the tuning of the k_p and the k_i the offset and load disturbances are controlled and then eliminated from the power system [49, 52, 70, 76, 114, 115]. Furthermore, in a steady state the k_p and k_i can be calculated by [49, 52, 70, 76, 114, 115]:

$$k_p = 2\zeta\omega_n L - R \tag{3.34}$$

$$K_i = \omega_n^2 L \tag{3.35}$$

$$T_s \approx \frac{4}{\zeta\omega_n} \tag{3.36}$$

Where
k_p is the Proportional gain
k_i is the integral gain
ζ is the Damping factor
ω_n is the undamped frequency.

The proportional gain and the integral gain can be calculated in real time using the output equations of the inner and outer current controller for the onshore substion. In addition, considering that the power system is at steady state, a further tuning method is the modulus optimum criteria which uses the steady state parameter to calculate the k_p and the k_i [49, 52, 70, 76, 114, 115]:

$$k_p = \omega_c T_i \sqrt{1 + T_a^2 \omega_c^2} \tag{3.37}$$

Where, ω_c is the cut-of frequency T_i is the integration time and T_a is the time delay of the converter.

The PI controller parameters for the inner current loop are determined by the optimization criterion of the power system and the transmission of the energy and thus the proportional and integral gains are given by [49, 52, 70, 76, 114, 115]:

$$k_p = \frac{\tau_{pu}\, r_{pu}}{2T_a} \tag{3.38}$$

$$k_i = \frac{k_p}{T_i} \tag{3.39}$$

$$T_i = \tau_{pu} = \frac{L_{pu}}{r_{pu} * \omega_b} \tag{3.40}$$

$$\tau_{pu} = \frac{L_{pu}}{r_{pu} * \omega_b} \tag{3.41}$$

Where, τ_{pu} is the delay time provided by each component of the power system. These parameters are different from the T_s or settling time which is the time that an input signal needs to reach the steady state within 2% (in some cases this is 5%) of the final value. The integration time is considered the largest time constant of the examined system [49, 52, 70, 76, 114, 115].

$$T_a = \frac{T_{switch}}{2} = \frac{1}{f_{switch}} \quad (3.42)$$

Where T_a is the first-order time delay of the VSC converters. L_{pu} and r_{pu} are the p.u. inductance and resistance between the converter and grid. The base frequency is the ω_b= 314.16 and f_{switch} is the frequency of the converter switches. The transfer function of the DC controller parameter is given as follows [49, 52, 70, 76, 114, 115]:

$$G_{dc} = k_p\left(1 + \frac{1}{T_i s}\right) \quad (3.43)$$

$$k_p = \frac{4C_{dc}}{9*a*V_{d,dc}T_i} \quad (3.44)$$

$$k_i = \frac{k_p}{T_i} \quad (3.45)$$

The V_{dc} is the steady state value for the DC voltage in the *dq* theory. The integration time is equal to $T_i = a^2 * T_{eq}$and according to this criterion the phase margin "theta angle" is imposed at 45°, the parameter "a". T_{ed} is set at $4T_a$[3] and the T_i "the integration time" is given as [49, 52, 70, 76, 114, 115]:

$$T_i = a^2 * T_{eq} \quad (3.46)$$

$$a = \frac{1+\cos\varphi}{\sin\varphi} \quad (3.47)$$

$$T_{eq} = 4 * T_a \quad (3.48)$$

The damping factor and the natural damping (the undamped frequency) of the system can be calculated by using the following equations [49, 52, 70, 76, 114, 115]:

$$\zeta = \frac{1}{2}\sqrt{\frac{T_i*r_{pu}}{k_p*T_a}} \quad (3.49)$$

$$\omega_n = \sqrt{\frac{k_p}{T_i*r_{pu}T_a}} \quad (3.50)$$

[3] Thesis: Control of Offshore Passive Platform System Voltage and Frequency through Control of Onshore point to point Voltage Source Converters

3.5 Summary

In this chapter, the VSC converter topologies and the control systems and also each component of the sending and receiving substations have been mathematically analysed and studied. The chapter has explained and has also analysed the functionality of each component of both substations, their dynamic in steady state. Thus, the chapter has also explained and has also analysed the principal factor of the control system of both VSC substations with a significant emphasis on the VSC converter. In addition, in order to benefit the system dynamic of the electrical power system, it also has detailed implementations applied to the control system of both substations.

Chapter 4 Wind Turbines

This chapter presents the most used wind turbine topologies in the energy market for offshore applications. In this thesis, the two most common wind turbines have been studied, the power control has been improved and then they have been introduced in the VSC-HVDC power system. This chapter introduces the control systems of the power converter of the double fed induction generator (DFIG) and fully rated converter (FRC) wind turbines. The intention of this is to study the conventional power control system of both established wind turbines and then compare them with a control system which has applied different modifications in the power control system of the power converter (Chapter 5). Thus, this chapter has been divided into two major sections; the primary section introduces the wind turbines and thus explains the types of generators (topologies) and also their control systems. The second major section introduces the control system modifications implemented into the control system of both wind turbines. Section 4.1 has a short introduction of the wind turbine sector. Section 4.2 and 4.3 describe the conventional power control system for both wind turbines topologies and are explained detailed. Then, Section 4.4 explains the fault ride-through capabilities and the grid codes for these wind turbines are described. Finally, Section 4.5 describes the implementation applied into the control system of both wind turbines.

4.1 Introduction

Wind has been used as a source of power since early human history. Windmills have been used for a variety of different purposes including pump water and grind grain. The incorporation of power engineering into the design of windmills have resulted in the evolution and thus in the creation of the modern wind turbines which can produce energy. With the incorporation of power electronics, wind turbines have become, in recent years, one of the most mature and reliable technologies for energy production in the renewable energy sector. Furthermore, with the sharp increase in size, the power generated by these wind turbines have also sharply increased. Nowadays modern wind turbines are widely used for energy production and wind farms have become a clear potential alternative to conventional power stations. Despite a few earlier attempts to develop wind windmills as an energy generator; it was not until the early 1970's in Denmark where their traditional windmills were developed into modern wind turbines which could produce energy. The first of these modern wind turbines were called fixed wind turbines or fixed speed wind turbines, because their rotational speed changed only slight when wind speed increased or decreased (the operating slip variation was less than 1%). Thus, the rotational speed of the generator does not change significantly. In contrast to the most advanced wind turbines in which the rotational speed of the generator changes significantly when the wind speed increases or decreases. These are considered variable wind turbines because the rotational speed of the generator changes significantly however the control system of the wind turbine maintain an optimal tip speed ratio (λ) for the prevailing wind speed [34, 116, 117]. The main advantages of fixed wind turbines are that they are more reliable and also robust than variable wind turbines. Due to their fixed-speed, wind turbines have a simpler design and use less electrical and electronic components. Furthermore, this WTs have less component failures and therefore, the number of electrical and electronic failures are less significant. Even though fixed turbines can last longer and also require less maintenance, a singular fixed wind turbine produces significantly less output power than a variable turbine and therefore makes fixed turbines the less commercially attractive. Another significant technical drawback of fixed wind turbines is the reactive power. Thus, this type of wind turbine consumes reactive power. To compensate it, a bank capacitor has to be added to the system. Fixed wind turbines are economically less profitable, and technically and economically inappropriate in offshore applications [34, 116, 118]. Wind turbines have become a predominant aim to be investigated in the offshore layout

and therefore they have been incorporated into this research. Figure 4-1 shows the variable wind turbines evolution since 1985.

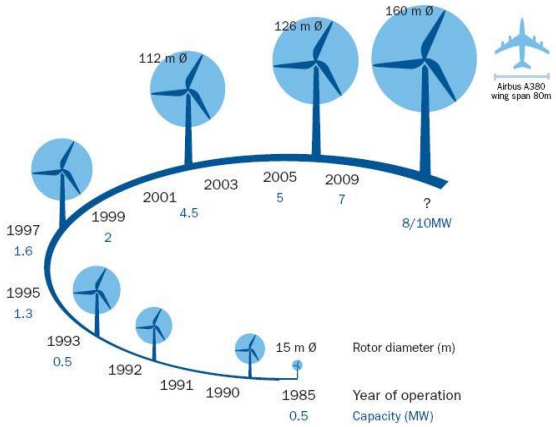

Figure 4-1: Wind turbine size evolution

The evolution of the fixed wind turbines into variable-speed wind turbines was achieved by the use of power electronics. The development of power electronics and their incorporation into the wind energy sector has increased the energy production from a singular wind turbine. Thus, these type of wind turbines have become the dominant generators for onshore and offshore applications. These wind turbines are designed to be at the maximum aerodynamic efficiency at each wind speed. Furthermore, the incorporation of power electronics has improved their reactive power production and control. The accurate control of the reactive power improves the power factor of the power produced which is also adapted by itself to the grid requirements. Moreover, the quality of the power produced is also improved and thus the variable wind turbine can better accomplish grid codes [27, 92, 119]. On the other hand, the overall cost of these wind turbines is higher than fixed WTs; the power electronics equipment has a high cost and the failure rate of the components is higher than fixed wind turbines. Thus, it results in higher maintenance costs.

Presently, there are two main types of variable wind turbines. The main difference between DFIG and FRC wind turbines is their controllability. The DFIG system is partially controlled and thus the generator is controlled by the rotor side converter but it is also connected to grid. The FRC is totally decoupled from the grid and there is no contact between the generator and the grid. Furthermore, the DFIG wind turbines are used for almost 50% of all operational generators and thus have become the market leading generator technology for onshore/offshore [34, 116, 117].

4.2 DFIG Wind Turbine Technology

The introduction of power electronics in the control wind turbines has improved their power performance, increasing the active power production and decreasing the reactive power. The wind turbine developers have introduced back-to-back VSC converters with self-commuted IGBTs switches. A typical configuration of a DFIG uses a wound rotor, IG. The control system can inject a current into or out of the rotor windings through the generator slip rings which allow an accurate control of the generator torque, Figure 4-2 [117]. By injecting a controllable voltage into the rotor at a desirable slip frequency through the control system of the generator's converter, the magnitude and phase of the AC voltage can also be controlled over the speed range of the induction generator; the wind turbine can inject power into the grid (from the stator or from the converter). Furthermore, the characteristic of the wind turbine allows the rotor to absorb power [54, 117]. The DFIG wind turbine can operate in two modes or "states" super-synchronous, $\omega_r > \omega_s$, and sub-synchronous, $\omega_r < \omega_s$ (where ω_s is the synchronous speed and ω_r is the rotor speed). In the super-synchronous state, the power output is supplied from the rotor through the converters to the network. When the DFIG wind turbine operates in the sub-synchronous state, the rotor will absorb power from the network through the converters [54]. To achieve maximum power extraction from a singular wind turbine the speed rotation must vary as the wind speed increases or decreases, allowing C_p to be kept at its maximum value (peak power tracking) [117]. Moreover, the DFIG wind turbine's converters are rated at around 30% of the wind turbine rating [117, 120]. A basic configuration of a DFIG wind turbine is shown in Figure 4-2.

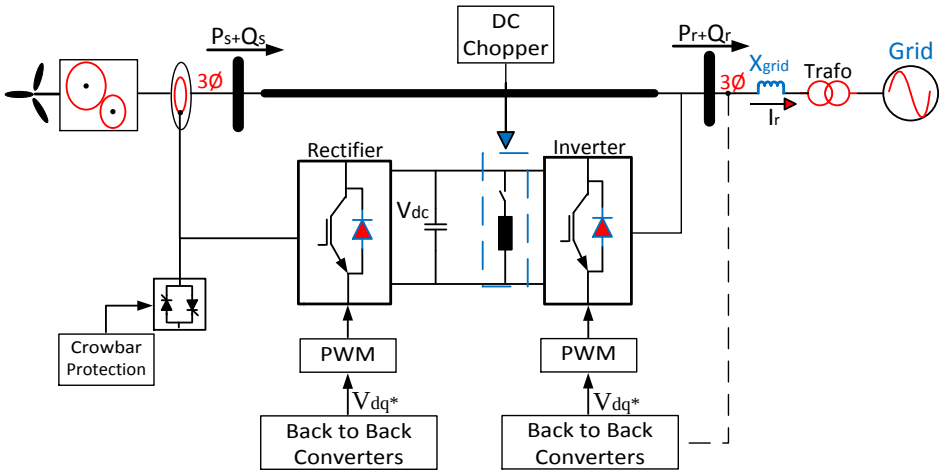

Figure 4-2: DFIG wind turbine configuration

As previously mentioned, a variable-speed wind turbine can track each wind speed, hence WTs output can be increased or decreased by changing the applied voltage to the rotor

windings via the rotor-side converter [120]. By changing the rotor speed, the slip is increased or decreased and the wind turbine is adapted to each wind speed. This allows the torque to be adapted and working at the desirable mode [121, 122]. As can be seen in Figure 4-2 the rotor and the stator are fed through a VSC converter and the grid requirements are partially obtained through the grid side converter. Furthermore, the generator and converters are protected by voltage limits and from over-current by a crowbar. Another advantage of this wind turbine is that it does not need a soft starter system to limit current peak during the start-up of the system. The DFIG wind turbine is partially controlled and thus the cost of wind turbine is less than FRC converters. The power converters are rated between ±25-30 percent of the total power output of the generator while the FRC is fully controlled and the power converter are rated at maximum power output. The partial control of the converter decreases the cost of the DFIG wind turbine but leads to a lower degree of control of the asynchronous generators. As a consequence of this, the converters have a lower control of the wind turbine output. Figure 4-3 shows the curve of maximum power output from a variable-speed wind turbine and the characteristics of the generator torque speed [120].

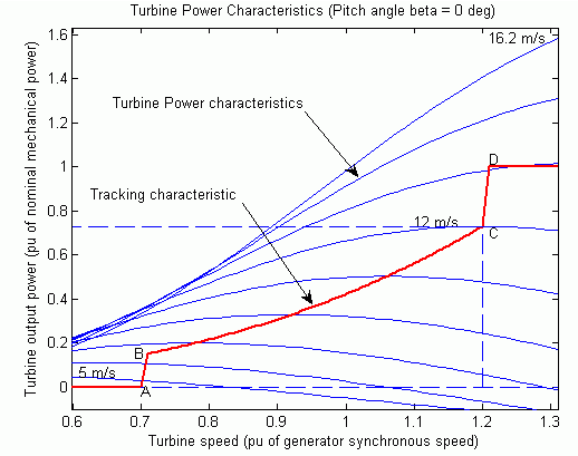

Figure 4-3: Sourced (Matlab/Simulink), Wind Turbine DFIG (Phasor Type)

4.2.1 DFIG Control Systems

4.2.1.1 DFIG Torque control

The basic purpose of the torque control system is to adapt the electromagnetic torque of the DFIG WT to wind speed changes, hence WTs should always work at the reference operating point, and thus they will always supply their maximum output power. The actual power output of the turbine is defined as:

$$P = {}^{1}/_{2}\,\rho C_p A V^3 \tag{4.1}$$

Where the $C_p$is the coefficient for the maximum power extraction of the wind turbines. A is the swept area of the turbine and is equal to πR^2. The R^2 is the squared radius of the wind turbine blades and V^3 is the wind speed [27, 54]. In steady state, the mechanical power delivered to the generator, rotor electrical power and stator electrical power (the rotor losses are considered neglect) relationship is taken from [27, 54]:

$$P_{air\ gap} = P_m - P_r \tag{4.2}$$

Where $P_{air\ gap}$ is the power at the generator air gap is, P_m is the mechanical power delivered to the generator and P_r is the power delivered by the rotor. If the stator losses are neglected, the power delivered by the stator should be equal to the $P_{air\ gap}$.

$$P_{air\ gap} = P_s \tag{4.3}$$

The power delivered by the stator can be expressed by:

$$P_s = P_m - P_r \tag{4.4}$$

The above equation can be also described as a function of the generator torque:

$$T\omega_s = T\omega_r - P_r \tag{4.5}$$

Thus, the power generated by the stator is equal to $P_s = T\omega_s$, the power generated by the rotor is equal to $P_r = T\omega_r$. Where the power generated by the rotor can also be described as:

$$P_r = -T(\omega_s - \omega_r) \tag{4.6}$$

Furthermore, the power generated by the stator and rotor can be also related to the slip, s, $(s = (\omega_s - \omega_r)/\omega_s)$.

$$sT\omega_s = -P_r \tag{4.7}$$

Finally, the power delivered by the wind turbine to the grid can be written as:

$$P_g = P_s + P_r \tag{4.8}$$

The efficiency of an induction generator is given by $(1 - s)$.

$$\eta = \frac{(1-s)P_r}{P_r} = (1 - s) \tag{4.9}$$

4.2.2 Vector Control Theory

The vector control theory corresponds to the control of the system (DFIG wind turbine) using *pq* theory, the decoupled voltage, current and rotor and stator fluxes are converted into

the *dq* frame. The DFIG wind turbine control system uses the *q* components of the current to regulate the torque and *d* components to regulate the power factor of the system or the voltage at the terminal [27]. The torque of the system, which is altered by the rotor current, is adapted to the wind speed variations, thus adapting the wind turbines to the required operational point reference to achieve the maximum power output. Despite the fact that the rotor flux controls the voltage magnitude (V_{qr}), this parameter also depends directly upon the stator capacity and current of the rotor (i_{qr}). Furthermore, " *in a sub-synchronous mode V_r is approximately in-phase with the internal voltage vector, in a super-synchronous mode, the two voltage vectors are approximately in anti-phase*" [117, 120].

The acquisition of the electromagnetic torque provides the rotor V_{qr} and i_{qr} measure signals and through the flux of the stator, the V_{qs} and i_{qs} measured signals are obtained. These measures are adapted to the requirements of the WT by using PI controllers and these compensators have to minimise the cross-coupling between torque and voltage loops [120, 123, 124]. Figure 4-4 shows an equivalent circuit of a) equivalent circuit with injected rotor voltage, and b) equivalent circuit with injected rotor voltage of the DFIG wind turbines [54].

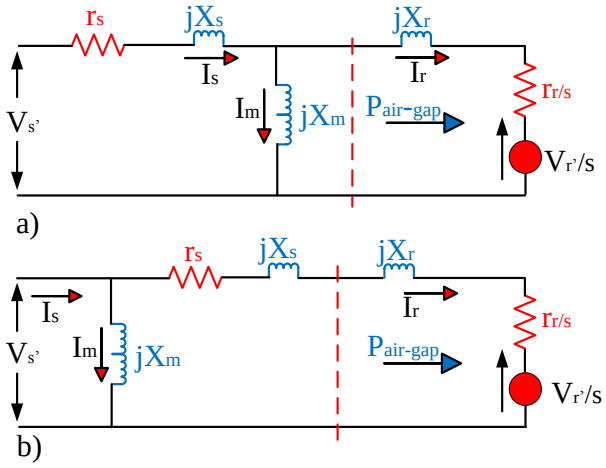

Figure 4-4: DFIG equivalent circuit with injected rotor voltage and DFIG equivalent circuit with injected rotor voltage

$\boldsymbol{V_s}$:	the stator voltage	$\boldsymbol{jX_s}$:	stator self-reactance
$\boldsymbol{V_r}$:	the rotor voltage	jX_r :	rotor self-reactance
$\boldsymbol{i_s}$:	the stator currents	r_s :	*the stator resistance (per phase)*
$\boldsymbol{i_r}$:	the rotor current	r_r:	*the rotor resistances (per phase)*

1. For a positive V_r, the slip increases and the rotor speed is reduced: sub-synchronous operation [27, 117].
2. For a negative V_r, the slip becomes negative and the rotor speed increases: super-synchronous operation [27, 117].

Where the rotor current given by [27, 54]:

$$I_r = \frac{V_s' - \left(V_r'/s\right)}{\left(r_s + \left(r_r/s\right)\right) + j(X_s + X_r)} \tag{4.10}$$

The equivalent power through the stator to the rotor gap equates to the electrical torque and is given by [27, 54]

$$T_e = \left(I_r{}^2 * \left(r_r/s\right)\right) + \frac{P_r}{s} \tag{4.11}$$

As mentioned, the equivalent power across rotor and the stator gap is equal to T_e and the P_r is the rotor active power and this can be calculated as followed:

$$P_r = \frac{V_r}{s} I_r \cos\delta \tag{4.12}$$

This rotor active power is absorbed or delivered by the controllable voltage, depending on the operational modes, sub-synchronous or super-synchronous operation.

4.2.1.1 Rotor Side Converter: Current Controller (PV_{dq})

To deliver the maximum power, the torque of the generator has to be adapted to an operating point reference with respects to the different wind speeds. This technique is set to adapt the electromagnetic of the generator to this wind speed variations [27, 54]. The electromagnetic torque which is a function of rotor current and stator flux linkages can be also calculated using the *dq* decoupled vectors and is given by:

$$T_e = l_m\left(i_{dr} i_{qs} - i_{qr} i_{ds}\right) \tag{4.13}$$

The V_{ds}: is given by:

$$V_{ds} = -\omega_s\left(-X_s i_{qs} + X_m i_{qr}\right) \tag{4.14}$$

Thus, $i_{qs,}\, V_{ds}$ and i_{ds} are calculated by:

$$i_{qs} = \frac{1}{\omega_s X_s} V_{ds} + \frac{X_m}{X_s} i_{qr} \tag{4.15}$$

$$V_{qs} = \omega_s(-X_s i_{ds} + X_m i_{dr}) \tag{4.16}$$

$$i_{ds} = \frac{1}{\omega_s X_s} V_{qs} + \frac{X_m}{X_s} i_{dr} \tag{4.17}$$

Table 4-1: Induction machine equations in *dq* coordinates (in per unit) [120]

Voltage Equations	**Flux equations**
$\boldsymbol{V_{ds} = -r_s i_{ds} - \omega_s + \frac{1}{\omega_b}\frac{d}{dt}\psi_{ds}}$	$\psi_{ds} = X_s i_{ds} + X_m i_{dr}$

$V_{qs} = -r_s i_{qs} + \omega_s + \frac{1}{\omega_b}\frac{d}{dt}\psi_{qs}$	$\psi_{ds} = X_s i_{qs} + X_m i_{dr}$
$V_{dr} = r_r i_{dr} - s\omega_s \psi_{qr} + \frac{1}{\omega_b}\frac{d}{dt}\psi_{dr}$	$\psi_{dr} = X_r i_{dr} + X_m i_{ds}$
$V_{qr} = r_r i_{qr} + s\omega_s \psi_{dr} + \frac{1}{\omega_b}\frac{d}{dt}\psi_{qr}$	$\psi_{qr} = X_r i_{qr} + X_m i_{qs}$

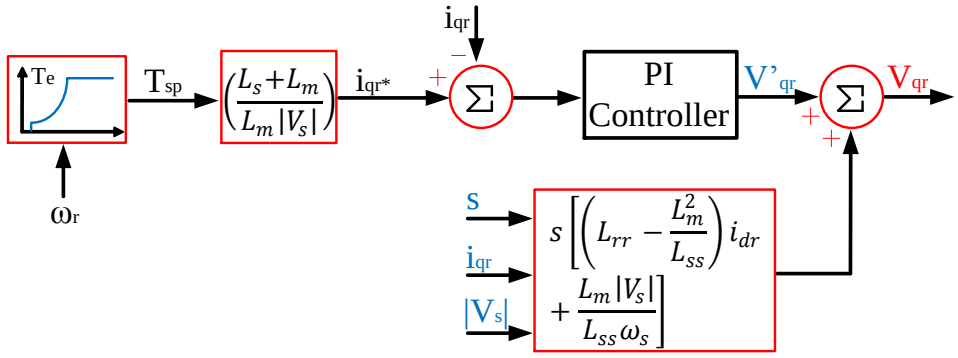

Figure 4-5: DFIG torque control strategy, [120]

Where T_{sp} is the optimal torque set point from the torque-speed characteristic for maximum power extraction. The error between the i_{qr}^{*} reference signal and the obtained i_{qr} signal is then uses to obtained the reference V_{qr}^{*}.

4.2.1.2 Rotor Side Converter: Voltage Control System

The voltage control system is generally used as a reference voltage controller or the reference power factor of the rotor converter. It also provides an accurate control of the reactive power. The reactive power controller has to accomplish the following basic requirements [117, 120, 125]:

1. The generator magnetizing current has to adapt the reactive power produced by the DFIG generator.
2. The component of the generator‘s current which controls the reactive power has to be adapted to the terminal voltage of the converter, if the value of the voltage is higher or lower.

$$Q_s = Q_{grid} = V_{qs} I_{ds} - V_{ds} I_{qs} \tag{4.18}$$

The voltage control system can be expressed through the following diagram. The gain K_{vc} is inserted into the system to improve terminal voltage or the power factor performance.

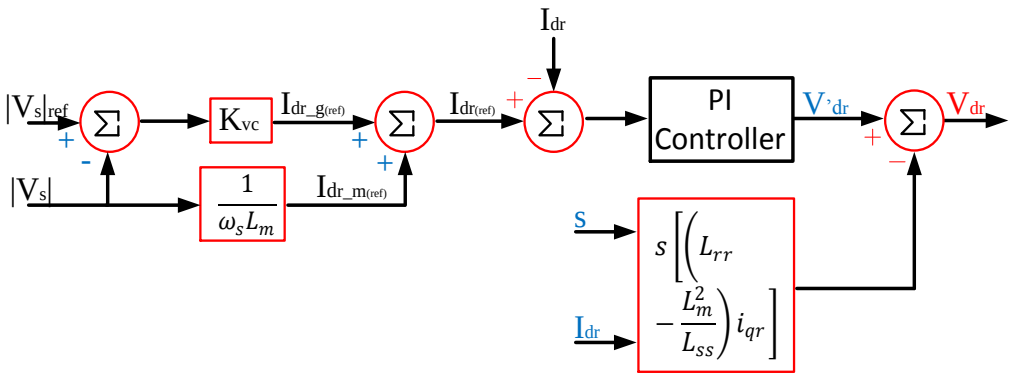

Figure 4-6: DFIG terminal voltage control strategy (the control gain Kvc is adjusted to improve terminal voltage or power factor performance), [120]

4.2.1.2 Flux Oriented Control

The authors of [126] have said that "*stator flux vector as d-axis and the q-axis component of the rotor current controls either the generator torque or the stator side active power of the DFIG. On the other hand, regulating the rotor d-axis current component controls directly the stator-side reactive power*".

4.3 FRC Wind Turbine Technology

The FRC is fully decoupled and thus the generator converter has full control of the rotor and the stator while the grid side converter accomplishes the grid requirements for the wind turbines. Furthermore, the generator side converter is used to control and regulate the electromagnetic torque of the generator and the grid side converter is designed to regulate the active and reactive power output which depends on the grid requirements. Thus, for example, the controllability of the reactive power is better achieved than in the DFIG wind turbines**.** In addition, another advantage of this type of WT is that as the power flow passes through both converters, the electrical generator is totally isolated from the grid and thus disturbances rarely affect its operation. Due to this, the generator is much less sensitive to grid disturbances [27, 117, 127-129]. Moreover, the decoupled control of the voltage and current of the rotor and stator gives the RSC a higher degree of control over the generator and thereby improve the generator efficiency. However, the power converter has to be equal to the total power generated by the wind turbine (plus switching losses) and therefore this wind turbine is much more expensive than the DFIG wind turbine.

The fully rated converter wind turbines use, generally, three types of generator: wound rotor synchronous generators (WRSG), permanent magnet synchronous generators (PMSG) and squirrel-cage induction generators (SCIG). The FRC wind turbine does not need a

reactive magnetising current because this wind turbine can create it by conventional field winding or by using permanent magnets. Thus, this type of generator (PMSG) has a simple structure and therefore it is widely used for the construction of FRC WTs. In addition, it also has higher efficiency than the other SG [118, 120, 130]. Another advantage of these generators (PMSG) is that they can be used without a gearbox, using a direct-drive technique, if there are a suitable number of the poles in the generator. Due to the increased number of generator poles the gearbox can be therefore removed from the WT. The direct drive technique allows for a low speed operation of the FRC wind turbines. Therefore, the relationship between the frequency of the system, the number of poles of the generator and n_{sync} in rpm is described in the following equation.

$$n_{sync} = \frac{120 f_s}{p} \tag{4.19}$$

The electrical frequency is equal to f_s. Additionally, if it is necessary to decrease the rotational speed of the generator, the number of poles has to be increased and if it is necessary to increase the rotational speed of the generator, the numbers of poles has to be decreased. In both cases the frequency must be kept constant. The direct-driven of the FRC wind turbine has a simple structure which leads to low maintenance cost, high conversion efficiency and high reliability compared with other FRC generators [27, 127, 131]. A structure of a direct-driven PMSG WT system is shown in Figure 4-7.

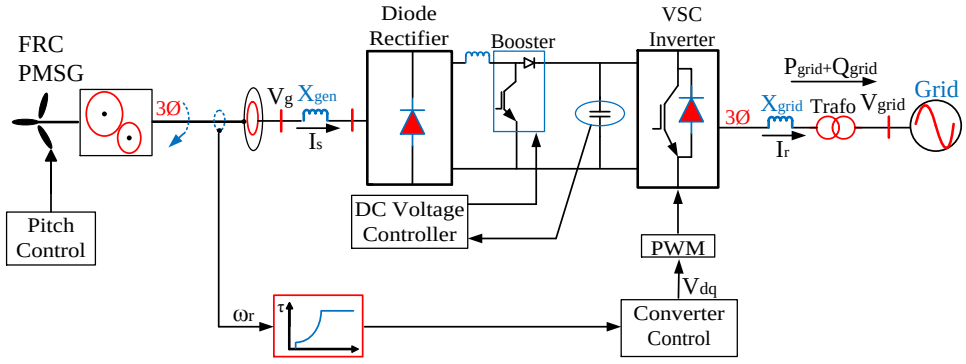

Figure 4-7: Permanent magnet synchronous generator with two back to back voltage source converters, [120]

Figure 4-7 shows the configuration of the wind turbine used in this thesis. The uncontrolled diode rectifier is set to convert the AC power into DC power and the booster controller is set to maintain the DC voltage in the link at a set value. The VSC converter is set to converter and then to transfer the power generated by the wind turbine to the grid [54].

4.3.1 FRC Control Systems

The full control of the FRC wind turbine has to be achieved through the back to back VSC converters by using a load angle control or "vector control", which is a more accurate control technique. In the past, the grid-side converter was normally controlled by using the load angle control technique and the grid converter was controlled by the vector control. However, the load angle control could be inaccurate during transients. Therefore, presently, both VSC converters use the vector technique and PWM technique [117, 120]. The primary objectives of the control system of the back to back converters of the FRC wind turbines are to control the magnetisation of the generator and to avoid frequency problems with the grid. Thus, the control system of the converters has to synchronize the rotation of the generator versus the grid's synchronization.

4.3.1.1 Rotor Side Converter (RSC): Wind Turbine Control System

As mentioned, the diode rectifier converts the generated AC power into DC power. The booster controller is implemented to set the DC voltage link to a set value. Therefore, the booster controller is set to maintain the DC voltage at the specific value and thus to ensure the appropriate power transfer from the generator to the grid converter [132].

4.3.1.2 Grid Side Converter (GSC): Wind Turbine Control System

The principal objective of the GSC control system is to convert and then to transfer the generated power into the grid. This is achieved when the DC voltage of the capacitor starts to increase, the control system has to begin to transfer the power to the grid. The control system of the GSC has also to ensure that the reactive power meets grid specifications [27, 120]. Furthermore, the power transferred has to be equal to the DC power and the power injected into the grid, the following equations are taken from [27, 120].

$$P_{gen} = P_{dc} \tag{4.20}$$

$$P_{dc} = P_{grid} \tag{4.21}$$

To obtain accurate control of the GRC, the control system evaluates the system as GRC is the sending source and the grid is the receiving source. The voltage angle of the grid is equal (referential voltage and angle) to zero and thus the phase angle δ of the GRC converter can be considered positive. To decouple the active and reactive power an inductance coupling is installed between these two sources. Therefore, to control the DC power of the back to back

link, it is necessary to control the power across the capacitor and thus the control system is given by:

$$P_{dc} = V_{dc} * I_{gdc} = V_{dc} * C \frac{dV_{dc}}{dt} \tag{4.22}$$

The DC voltage is determinate by:

$$P_{dc} = V_{dc} * C \frac{dV_{gdc}}{dt} = \frac{C}{2} * 2 * V_{dc} \frac{dV_{dc}}{dt} = {}^{C}/_{2} \frac{V_{dc}^2}{dt} \tag{4.23}$$

To calculate the V_{dc} the voltage is integrated on both sides of the equation

$$V_{dc}^2 = \frac{2}{C} \int P_{dc}\, dt \tag{4.24}$$

$$V_{dc} = \sqrt{\frac{2}{C} \int P_{dc} dt} = \sqrt{\left(P_{gen} - P_{grid}\right) dt} \tag{4.25}$$

As mentioned before, the P_{gen} is the generator output power and P_{grid} is the power sent to the network.

4.5 Wind Turbines Control System Modifications

The DFIG and the FRC wind turbines are important in the overall control of the VSC-HVDC transmission system and thus it has become a primordial task to study their performance (during steady state and during transients). Then, to improve their performance and finally to implement these in the offshore grid. To improve the performance of theses wind turbines and thus to improve the behaviour of the active and reactive power of the offshore grid several changes have been introduced in the power control system of the VSC converter.

4.5.1 Introduction of Wind Turbines Control Strategies

After the control system of the DFIG/FRC wind turbines (Matlab/Simulink demos) were careful analysed (in this thesis, these wind turbines were introduced in the offshore layout). It had appeared the necessity of improving the control parameter of the power converters. The V_{dqr}, V_{dqs}, i_{dqs} and i_{dqr} control signals were performing below expectations and thus the observed response of the RSC and GSC converters were slow. The improvement of these control signals will improve the dynamic response of the control systems of the wind turbines, DFIG and FRC. To improve these mentioned signals, the first modification implemented in the control system of VSC converters was with the incorporation of the 1st and 2nd order filters. These filters were principally implemented to reduce the harmonics

produced by power conversion (AC/DC) and thus to improve the conversion from the sinusoidal waveforms into *dq* parameters. The introduction of these filters in the control system had improved the dynamic behaviour of the wind turbine. Nevertheless, the overall performance of these wind turbines were below expectations and therefore, it had been decided to introduce a more accurate control for the V_{dqr}/V_{dqs} signals. This control system was established with similar control ideas of [120, 121]. However, the implementation of a more accurate control structure of the V_{dqr}/V_{dqs} signals (in both wind types of wind turbines) allow VSC converters to have high control of the wind turbines during disturbances and therefore this control system continues to improve the dynamics of the wind turbines, though it was below expectations [34, 50, 73, 133].

In terms of continues improving the wind turbines control, a frequency controller has also been implemented in the RSC converter and in the GSC converters of the DFIG wind turbine and also in the GSC converter of the FRC. The benefits of this specific controller introduced in both converters is that it helps to regulate the frequency of the IGBT valves, for more information sees Chapter 3 [34, 50, 73, 133]. Furthermore, the third harmonic injection technique has also been implemented in the control system. This control technique benefits principally on the dynamic behaviour of the reactive power and secondly on the dynamic behaviour of the active power. Thus, it helps to reduce the power peaks and also fluctuations during transients and it therefore helps to improve the overall performance of the grid.

4.5.2 1st and 2on order Filters

The 1st and 2nd order filters were introduced in the wind turbines control system to improve the active and reactive power delivered and thus improve the AC voltages and currents behaviour of the wind turbines and also of the offshore scheme. Thus, 1st and 2nd order filters have been used to improve the conversion from the sinusoidal waveforms to *dq* parameters inside the control system of the wind turbines and consequently the performance of wind turbines and also the VSC-HVDC link. The quality factor Q_f of the filter is designed to obtain the best characteristic over the required frequency band. This type of filter does not have an optimal Q_f with tuned filters. Figure 4-8 plot shows the basic structure of a second order filter.

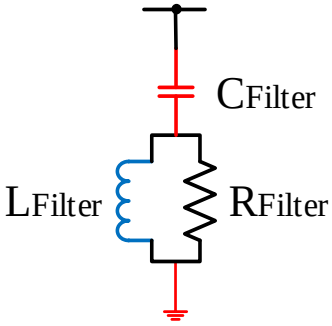

Figure 4-8: Passive second order high pass filter

The typical value of the quality factor Q_f is between 0.5% and 5%. The AC filter rating (Q_{filter}) and the harmonic order h are used as design parameters. Thus, the filter parameters are calculated based on the following equations (the resistance R_{filter}, capacitor C_{filter}, inductances L_{filter}) [68].

$$C_{filter} = \frac{(h^2-1)Q_{filter}}{h^2 \omega_s V_{ac}} \tag{4.26}$$

$$L_{filter} = \frac{1}{C_{filter} h^2 {\omega_s}^2} \tag{4.27}$$

$$R_{filter} = Q_f \sqrt{\frac{L_{filter}}{C_{filter}}} \tag{4.28}$$

Considering a basic VSC-HVDC scheme, the value of Q_{filter}= 15% of the converter rating, and Q_f= 3% and h=35 are used as design inputs. It should be remarked that these values depend on the harmonic requirements of the specific system under study [68].

4.5.3 V_{dqr}/V_{dqs} Controllers

As mentioned, the primary function of the control system of both wind turbines is to control and transfer the active power produced to the offshore cluster substation. The offshore substation is taking control of AC voltage of the entire offshore layout and thus acts as a voltage source [50, 86]. The purpose of improving the control of the V_{ds} is to enhance the power produced by the generator. Then, the obtained control signal is then introduced in the control system of the rotor side converter [134]. Figure 4-9 shows the applied stator voltage control loop.

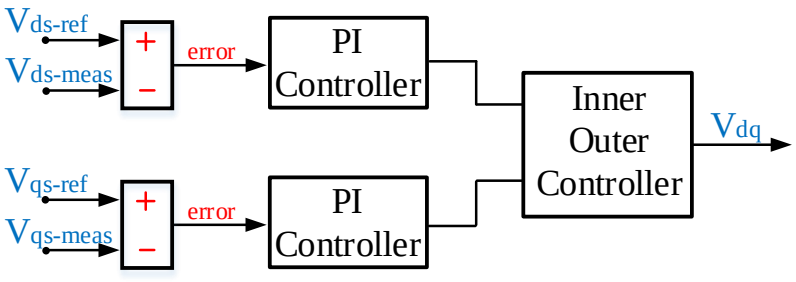

Figure 4-9: Control loop diagram of the V_d with a PI controller

The implementation of the V_{dqs} controller is fundamental to the control of the active power and the reactive power generator by the wind turbine. The PI controller has to have high flexibility and thus the dynamic of the obtained signals are better controlled. These signals are also introduced in the inner and outer current controller of the grid side converter. Therefore, the dynamics of the power system is improved. In addition, the reactive power should be equal to zero, but depending on the grid requirements, i.e. for reactive power compensation.

4.5.4 Frequency Controller

The wind turbine frequency controller is based on the idea of helping power converters to recover faster from abnormal circumstances. The VSC converters are basically formed by IGBT valves and its control system which has to be synchronized along with the frequency of the power system and therefore they are highly influenced in the power control dynamics when the frequency is altered [34, 50, 73, 133]. Considering the nature of the offshore VSC-HVDC system - a passive grid controlled by a VSC converter - the introduction of the frequency controller into the wind turbines converter (VSC converters) should help the wind turbines and also the entire power system to recover the steady state faster, for more information see Chapter 3, Section 3.42.

4.5.5 Third Harmonic Injection Technique

The idea of the third harmonic injection technique is to inject the third harmonics component into the modulation signal obtained from the inner and outer current controller. This harmonic injection technique helps to reduce the amplitude of the positive and negative peaks of the sinusoidal waveform which is compared with a triangular signal in the PWM block. The reduction on the sinusoidal peaks increases the modulation region of the VSC converter by 15% [92, 109, 110]. Thus, this control technique improves the behaviour of the VSC converter during abnormal circumstances. Furthermore, it also decreases the reactive

power peaks and troughs and also helps to reach the steady state of the power system faster, for more information see Chapter 3, Section 3.4.1.

4.6 Summary

The purpose of this chapter has been to outline the principal characteristics of the existing wind turbines topologies. Thus, in this chapter, a short introduction of the variable wind turbine topologies and their control strategies have been introduced. Furthermore, to explain the converter control of the DFIG and the FRC wind turbines, the generic equations of the control system of both wind turbines has been introduced. In addition, it has also explained the concepts of synchronous and asynchronous generators and also the fault ride-though capability characteristics for both topologies. Finally, it has also introduced a brief explanation of the improvements which had been applied into the control system of the power converters of the wind turbines and thus it has explained a 1st and 2nd order filter, V_{dqs} controllers, frequency controller and third harmonics injection technique (to have a more in-depth view of the aforementioned improvements applied into the control system of the VSC converters can be seen in the previous chapter, Chapter 3).

Chapter 5: Simulation and Results

This chapter presents simulation results demonstrating the efficiency of the different modifications in the control system of the VSC converters, DFIG/FRC wind turbines and principally on the VSC-HVDC control systems. Furthermore, the chapter also includes a mathematical analysis for the calculations of the PI controllers of the VSC converters and also a mathematical analysis for the calculations for the power losses of the offshore and onshore schemes. Section 5.1 begins with a short introduction of the offshore wind farm and the system stability of the VSC-HVDC system and the objectives of the simulation related to the thesis' objectives. Then, Section 5.2 introduces basic case studies of the DFIG and FRC wind turbines and also the VSC-HVDC power system (how this research has organized simulations of the mentioned cases). Sections 5.3 presents the simulation of the wind turbines (DFIG and FRC) and also a basic scenario for the VSC-HVDC power system. In this section a mathematical analysis is also introduced for key parameters of the wind turbines and VSC converters. Then, Section 5.4 presents the most complex scenarios evaluated for the control of the VSC-HVDC power system and an extra modification introduced in the coordinated control of the VSC converter. Thus, this section presents the coordinated control for multiple wind farms connection (this section details how the different modifications introduced into the power converters are going to be seen i.e. how the feed-forward signals are taken from the wind farm substations and then introduced into the voltage controller). In addition, in this section a mathematical analysis is also introduced for key parameters of the wind turbines and VSC converters.

5.1 Introduction

This chapter presents simulation studies of the control systems for DFIG/FRC wind turbines and principally on the VSC-HVDC control systems. Simulation results are expected to validate the VSC-HVDC power system, the VSC converter controllers and modifications discussed in Chapter 3 and Chapter 4. The results would also validate the proposed offshore scenarios "layouts" which are discussed in this chapter.

There has already been an increase in the number of offshore wind farms being placed in shallow waters. In recent years, offshore wind farms have also been planned and also installed in deep waters [135, 136]. This increase of the number of offshore wind farms installed in deep water will increase offshore power production and therefore will increase the necessity to adapt the existing electrical power systems. Furthermore, in order to determine the proper measures to be taken before this offshore power system is established, it has become necessary to carry out power system assessments for offshore wind power. Figure 5-1 shows a single point configuration of an offshore power system which has an offshore wind farm connected to an onshore single point connection. This figure represents the offshore connection similar to that installed in BorWin1 [135, 136].

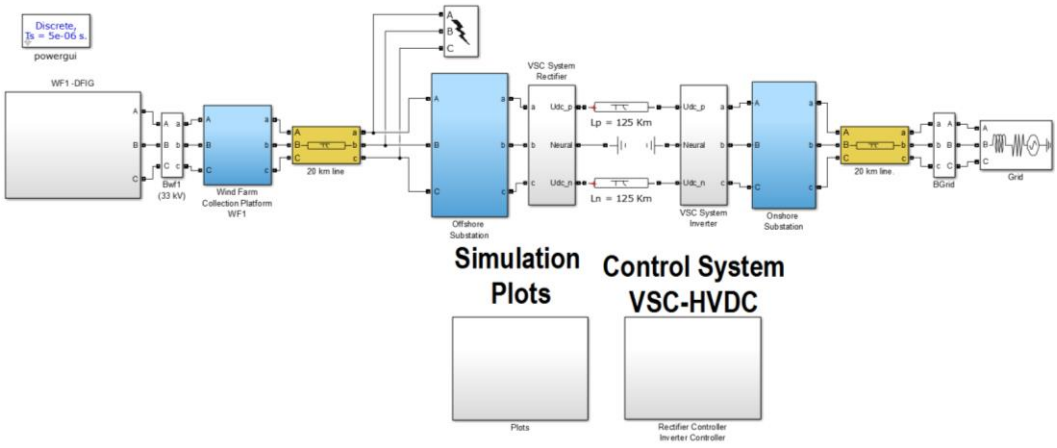

Figure 5-1: Large offshore wind farm in a single point connection

A definition of power system stability is the ability of an electrical network to keep the electrical power system stable after a disturbance. The proposed transient stability assessments for the examined VSC-HVDC power systems are set to determine the proper control action to restore the power system, reduce its fluctuations, and to adjust the power output in response to the power or frequency alterations. This thesis' stability assessment is set to ensure that the proposed power system could maintain stability during large transients. In order to understand the behaviour of the cluster substation and thus to fully examine the

functionality of the dynamic behaviour of the entire VSC-HVDC system - including wind turbines - a large transient has been incorporated into the offshore layout. The operability of the point to point converters during this transient is determined by the behaviour of the power system. Thus, power system stability studies must prove the ability of the control systems to restore the steady state, principally, of the offshore electrical power system and also the onshore. In addition, this thesis will also determine whether the proposed and presented offshore and onshore scenarios, the HVAC and HVDC transmission lines, are adequate for power transmission. The proposed scenarios have to validate the adequacy of the calculated values of the PI controllers [27, 116, 117, 137]. Therefore, to achieve the objectives of this thesis and to investigate and provide an explanation of the operational system of the DFIG/FRC wind turbines, their interconnection to the offshore cluster substation (VSC converter) and the HVDC connection; first of all, basic models of the wind turbines and also the VDC-HVDC system have been designed, analysed and tested. Then, a variety of modifications in the control system of the VSC converters have been applied. The results of these modifications in the power converters have been compared with the basic control models to facilitate the analysis of both different systems.

The thesis analyses the differences in the power flow variations, the power converter performances, and also DFIG and FRC wind farm performances. Therefore, this chapter is based on simulation studies of large offshore wind farms connected to an offshore cluster substation which has to control the stability of the offshore layout and at the same time to transfer the offshore power to onshore through a single point connection. Matlab/Simulink software has been used for modelling the offshore/onshore schemes.

5.2. Case Studies: Implementation Approach

To observe the difference in performance of each of the mentioned scenarios, and thus analyse the different behaviour of the power system after the modifications have been applied to the control system of the wind turbines and VSC converters, two different power system scenarios have been studied. These two scenarios have also been divided into different groups of simulations. Thus, the first group of simulations (5.3 Case Study 1: Basic Scheme Analysis) is divided into three case studies. The first and the second case studies (5.3.1, 5.3.2) investigate the performance of DFIG and FRC wind turbines when they are connected to an HVAC transmission system. The third case study (5.3.3) involves a VSC-HVDC scenario in which the modifications mentioned in Chapter 3 have been incorporated, one at a time. Moreover, this VSC-HVDC scenario has only one offshore wind farm which is connected

onshore by a single point connection. As mentioned, to analyse each modification applied to the control system of the wind turbines and the VSC-HVDC, and thus to analyse the performance of the power system, it was decided that the modifications would be applied to the wind turbine's control system one at a time. To differentiate the applied power control system modifications from the basic scheme they have been labelled as 'filter' scheme, 'frequency' scheme and 'third harmonic' or '3 Har' scheme. The filter scheme has first and second order filters applied to the control of the rotor and stator, voltage and current, the frequency scheme has the frequency controller, and the 3Har has the third harmonics technique installed in the power control system. The second case study group (5.4 Case Study 2: Coordinated Control for offshore Wind Farms: Single point Connection) evaluates a more complex offshore scenario which incorporates several offshore wind farms connected to one offshore cluster substation. This section is also divided into three case studies: DFIG (5.4.1), FRC (5.4.2), and a mixed scenario (5.4.3). The key point of this part of the chapter is to examine the coordinated power control of the offshore substation which can incorporate several wind farms into the offshore grid without significantly altering the power control system of the offshore substation. Thus, the modifications analysed in the previous chapter added to this coordinated power control. Furthermore, this scenario (coordinated power control scenario) is also compared with another scenario in which a feed-forward signal from each wind farm has been introduced - these feed-forward signals are taken from the wind farm substations and then are introduced into the voltage controller - to improve the dynamics of the offshore substation. Thus, the most advanced scenario contains a signal from each wind farm which is sent to the control system of the cluster substation which is then added to the coordinated power control of the VSC converter in the offshore substation system. The purpose of this modification is, principally, to analyse the behaviour of the entire offshore power system and in particular the offshore cluster substation.

5.3 Case Study 1: Basic Scheme Analysis

5.3.1 Case Study 1.1 DFIG Wind Farms

As discussed, in order to obtain an accurate overview of the control systems of both types of wind turbines, and thus to compare the performance of the different power systems separately; the explained modifications have been applied to the DFIG/FRC wind turbines at different times. The features of these hypothetical scenarios are based on an onshore wind farm which consists of five wind turbines which deliver a total of 7 MW and 10 MW (5X1.4

DFIG and 5X2 FRC respectively). In these scenarios, these wind turbines are connected to a wind farm substation and this substation is connected to the grid by an HVAC connection. In the wind farm substation, a large transient is trigger at 8s and has a duration of 130 ms. The transient produces higher fault currents, and thus the power system is lead to higher disturbances. Therefore, the control system of the wind turbines is also subjected to high disturbances. The control system of the wind turbines has to help to restore the steady state of the wind turbine and also to help to restore the steady state of the electrical power system. Furthermore, the DFIG grid side converter is set to control the DC power and the generator side converter is set to control active and reactive power output. The FRC case study has only one VSC converter which is controlled to comply with the grid requirements. The generator side has a diode bridge which rectifies the AC power into DC power. Table 5-1 shows this scenario's specifications.

Table 5-1: Specifications of parameters used in the wind turbine models

Power Flow Scenario		
Parameters	**DFIG Wind farm**	**FRC wind farm**
Rated WTs	1.4 MW	2.4 MW
Rated Power (Sn)	7 MW	12 MW
Reactive Power	0 MW	0 MW
WT Voltage	575V/33 kV	575V/33 kV
Transmission Voltage	33kV/132 kV	33kV/132 kV
DC Voltage	1100 V	1150 V
Base frequency, ω_b	50Hz	50 Hz
Choke impedance	(99.19 μΩ+ j26.31μH)	----------
Transmission Line	30 km	30 km

5.3.1.2 Mathematical Analysis

The values of C_{dc}, V_{dc} and the S_n are taken from Matlab/Simulink wind turbine demos.

$$\tau_{DFIG} = \frac{C_{dc} * V_{dc}^2}{2S_n} = \frac{0.05 * 1150^2}{2 * 7.5x10^6} = 0.00440s = 4.408ms \quad (5.1)$$

$$\tau_{FRC} = \frac{C_{dc} * V_{dc}^2}{2S_n} = \frac{0.45 * 1100^2}{2 * 10X10^6} = \frac{544500}{20X10^6} = 0.027225s = 27.225ms \quad (5.2)$$

The choke impedance of the DFIG wind turbine parameters are: r = 99.19 μΩ, L = 26.31μH and the base frequency, ω_b=50. The switching frequencies of the carrier signal in both converters are defined as f_{switch} and the average delay time of both converters are calculated as follows:

$$T_{DFIG}(rotor) = \frac{T_{r-switch}}{2} = \frac{1}{2f_{r-switch}} = \frac{1}{2*1629} = 0.031\text{ms} \quad (5.3)$$

$$T_{DFIG}(grid) = \frac{T_{g-switch}}{2} = \frac{1}{2f_{g-switch}} = \frac{1}{2*2700} = 0.0185ms \quad (5.4)$$

The $f_{r-switch}$ is the switching frequency of the rotor side converter of the DFIG wind turbine and the $f_{g-switch}$ is the switching frequency of the grid side converter of the DFIG wind turbine.

5.3.1.3 Grid Fault Analysis

As mentioned, the transient is triggered in the wind farm substation at 8s with a duration of 130ms. Under balanced conditions (three-phase fault) the large transient produces distortions in the currents and voltages. Thus, this transient produces unbalanced conditions in the wind turbine and in the electrical power system and therefore reactive power is suddenly increased from 0.0 pu (the reference reactive power) to much higher reactive power values. Furthermore, the transient also produces high fluctuations in the active power. At the beginning of the transient, the active power decreases from 1 pu to 0.0 pu and then the control system of the wind turbine recovers its output (after the transient is cleared). Figure 5-2 presents the DFIG analysed scenario and also presents a single onshore wind farm (7MW) which is connected to strong onshore grid thought a wind farm substation.

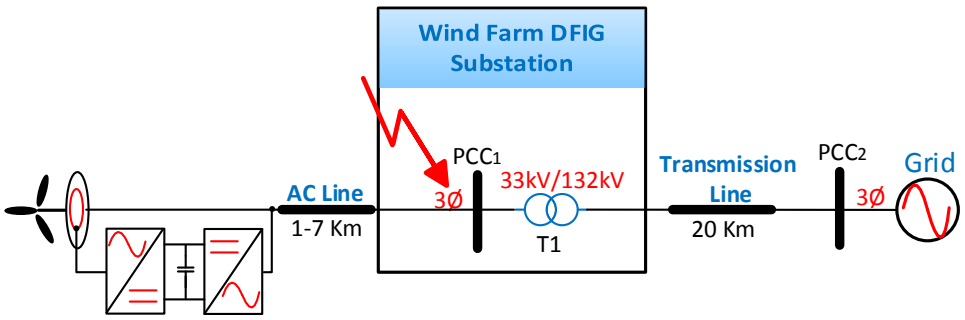

Figure 5-2: DFIG Scenario

5.3.1.3.1 Transient Analysis

The following section shows the performance plots of the active and the reactive power, DC voltage and index modulation of the DFIG wind turbine scenario. Figure 5-3 (a)1 shows the active power performance during the large transient applied in the substation. Figure 5-3 (a)2 shows the DC voltage in the four investigated schemes and Figure 5-3 (a)3 shows the index modulation.

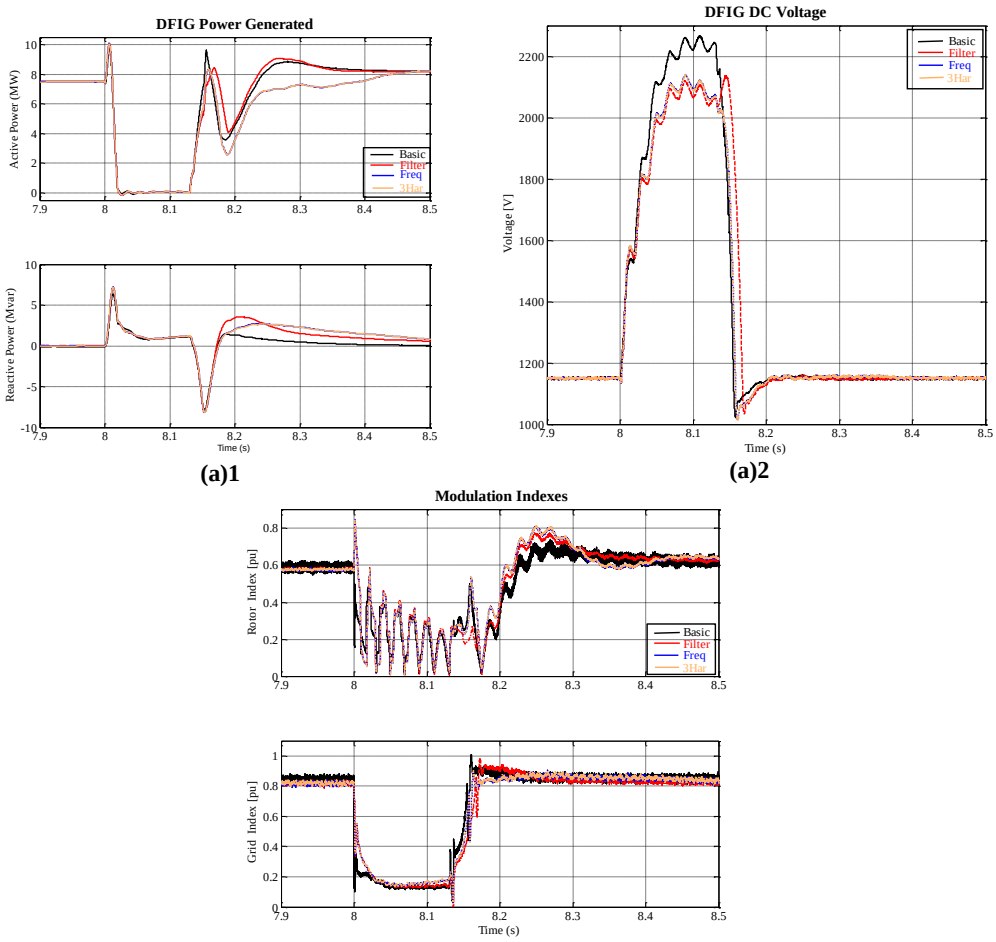

Figure 5-3: Transient responses for three-phase fault at the DFIG wind farm substation

The active and reactive power measurements are taken from the PCC at the wind farm side. This power system needs almost 8s to reach the steady state. At 8.5s, after the transient is cleared, the control system of the wind turbines partially recovers the power output and thus partially reaches the steady state. The DFIG wind turbines then need an additional 8s to fully reach the steady state (making a total of 16s), see Figure 5-3(a). At 8.5s, the reactive power production is also reduced to 0.0 pu. After the fault is cleared the control system of the wind farm begins to recover the steady state of the wind turbines. The circumstances are similar in the case of the active power. The active power peaks when the fault is triggered and then peaks again when the power system clears the fault. The DC voltage suffers a high increase during the fault and suddenly recovers the steady state after the fault is cleared (the control system of the wind turbines allows the overshoot DC voltage because a crowbar protection system has not been implemented). This sudden recovery of the DC voltage is preceded by the increase of the active power of the wind turbine which charges the DC capacitor. Therefore, the above results show large benefits from the application of each

modification; the adjustments applied to the control systems of both converters have enhanced the response of the active and reactive power, and DC voltage.

5.3.1.3.2 Transient Analysis

The following section shows the transient stability analysis of a basic scenario with respect to the most improved scenario. The first configuration shows a scenario in which no improvement has been implemented in the control system of the VSC power converters (Basic Configuration: Figure 5-3 (a)4 and Figure 5-3 (a)5). The second configuration shows a scenario which has implemented the improvements in the VSC power converters (Improved Configuration: Figure 5-3 (a)6 and Figure 5-3 (a)7.). Both scenarios show the performance of the AC voltage and the AC current on the wind farm substations at the PCC_1 point and also the AC voltage and the AC current on the grid side (PCC_2). Furthermore, Figure 5-3 (a)4 and Figure 5-3 (a)5 show the performance of the AC voltage and AC current of the basic scenario is shown in Figure 5-3 (a)6 and Figure 5-3 (a)7 respectively.

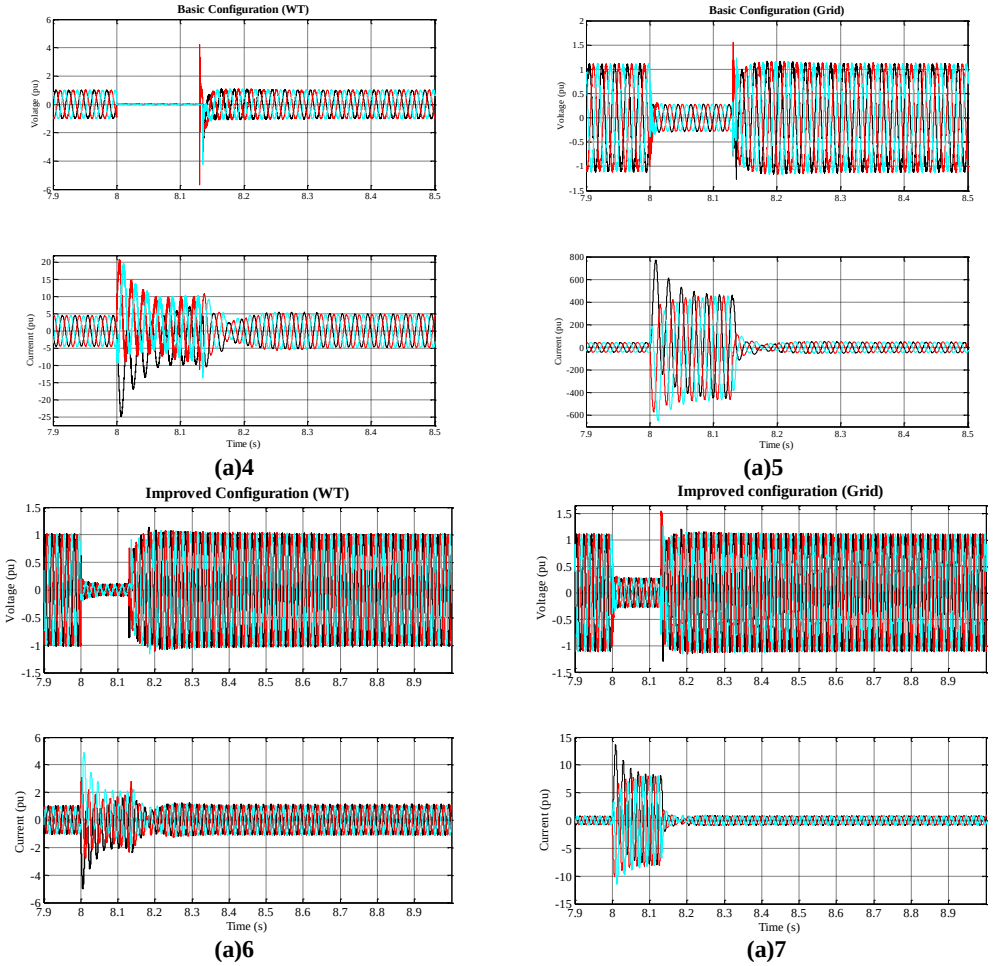

Figure 5-3: Transient responses for three-phase fault at the DFIG wind farm substation.

By examining the above plots, it can be seen that the performances of the AC voltage and the AC current have been improved. The installation of filters in the control of the VSC converter

plus the installation of V_{dqs}control system and the third harmonic injection technique has to improve the performance of the VSC converters and therefore improve the performance of the AC grid. Thus, the performance of the AC voltage and the AC current in the improved scenario, Figure 5-3: (a)6 and (a)7, show a clear decrease in the voltages and currents peaks and troughs an also a reduction in the recovery time of the scenario. Thus, the AC voltage maximum peak and trough have decreased by almost 14 per unit between the Basic Configuration (WF) and the Improved Configuration (WF). Similarly, the AC current maximum peak and trough is decreased around 1 per unit. Thus, the implementations introduced in the power control system of the VSC converters of the DFIG wind turbines have reduced the AC voltages and the AC currents peaks and also have reduced the drop of the AC voltage during the transient. Even during the transient, the drop of the AC voltages and the AC current is better controlled. The drop of the AC voltage, during the large transient is smaller comparing the Basic Configuration with the Improved Configuration. This allows a slightly longer time to recover the entire electrical power system before this is disconnected, [23, 138, 139]. Therefore, the incorporation of the improvements in the VSC converters have clearly improved the fault ride-through capability of the electrical power system.

5.3.2 Case Study 1.2 FRC Wind Farms: Stability Analysis

Figure 5-4 shows the analysed layout of the onshore FRC scheme. Thus, Figure 5-4 present the onshore layout and the internal structure of the FRC wind turbine, for more information see Table 5-1.

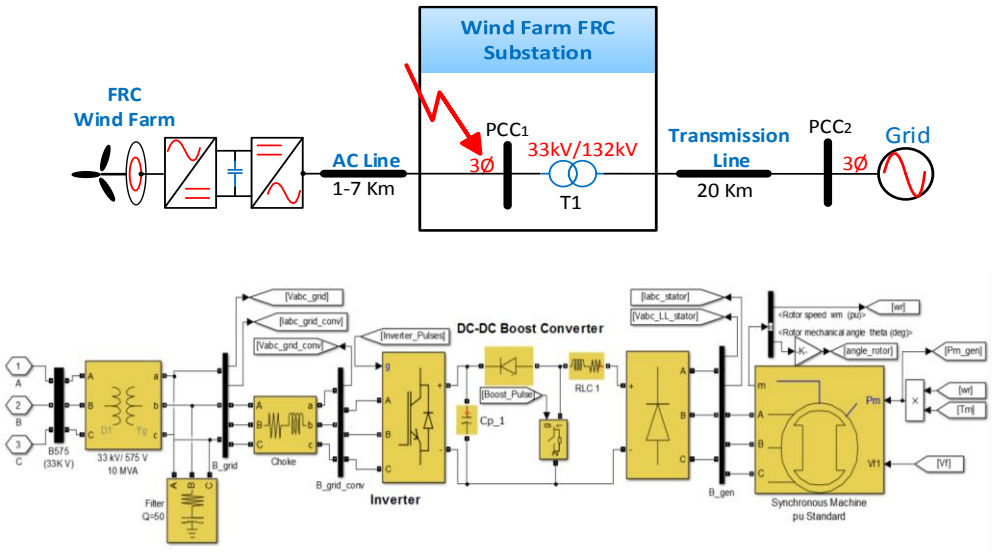

Figure 5-4: FRC Scheme and the converter Scheme inside of the wind turbine, [134]

The average delay time of FRC converter is then:

$$T_{FRC}(grid) = \frac{T_{switch}}{2} = \frac{1}{2f_{g-switch}} = \frac{1}{2*3000} = 0.01666ms \quad (5.5)$$

The $f_{g-switch}$ is the switching frequency of the grid side converter of the FRC wind turbine.

5.3.2.1.1 Transient Analysis

The following results show the performance of active and reactive powers, DC voltage and index modulation of the FRC wind turbines. The applied modification has improved the response of the wind turbines, decreasing the power peaks, troughs and the fluctuations of the power system. The improvements applied to the control system of the power converter have also improved the recovery time of the wind turbines. Figure 5-5 (b)1 shows the active and reactive power performance during the large transient applied in the substation. Figure 5-5 (b)2 shows the performances of the DC voltage, (b)3 the modulation index performances.

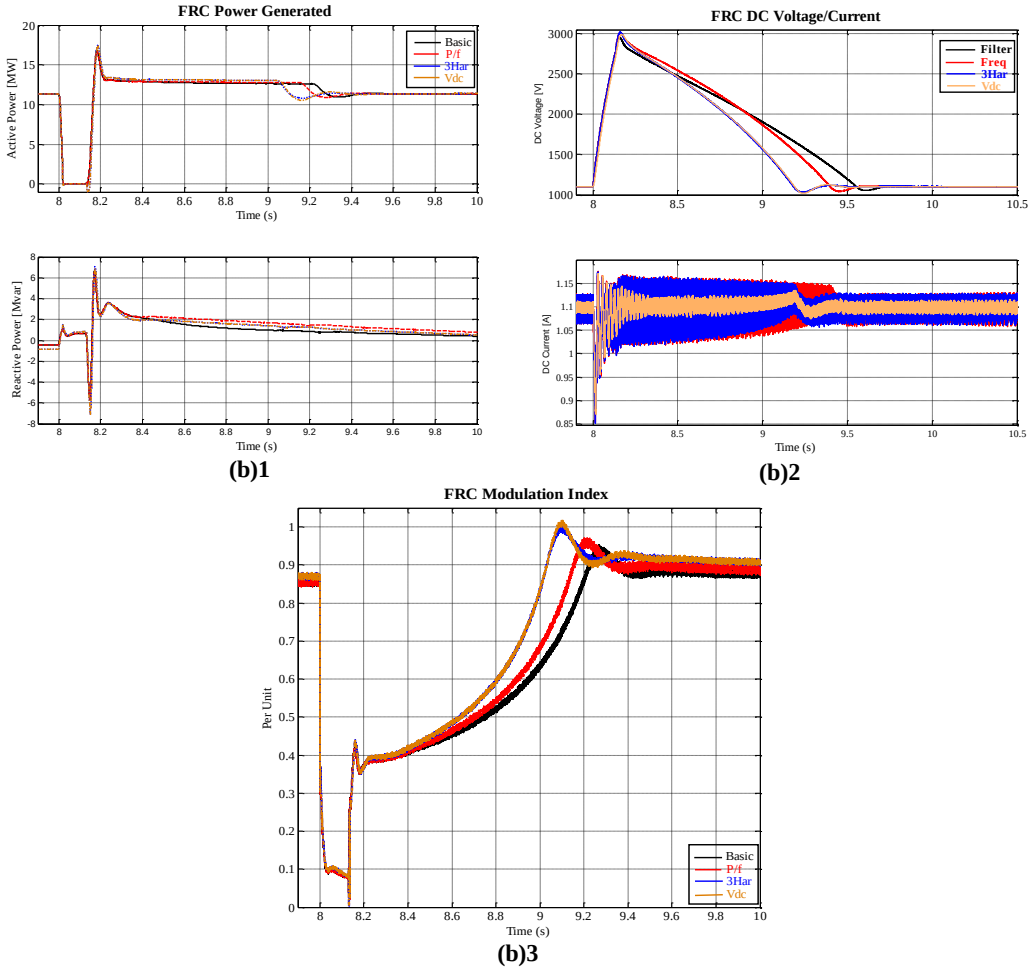

Figure 5-5: Transient responses for three-phase fault at the FRC wind farm substation

As shown in the previous configuration, DFIG scenario, the result of the installation of 1st and 2nd order filters and the frequency controller applied into the control system of the grid side converter, GSC, had displayed a significant improvement in the reduction of the recovery time of the power system. Principally, the filter modifications applied to the control

system of the stator and rotor parameters had significantly enhanced the control system of the power converter. Furthermore, the implementation of the third harmonic injection technique into the control system of the GSC had also shown a significant improvement of the reduction of the active power peaks and troughs and also had reduced the active power fluctuations. Finally, the modification applied in the control DC voltage slightly improves the performance of the wind turbine. However, the wind turbines performance does not change significantly, the DC voltage improvement still enhances the wind turbines performance during the large transient.

5.3.2.1.2 Transient Analysis

The following section shows the transient analysis of a basic scenario with respect to the most improved scenario. Both scenarios results show the performance of the AC voltage and the AC current on the wind farm substations at the PCC_1 point and also the AC voltage and the AC current on the grid side (PCC_2). The first configuration shows a scenario in which no improvement has been implemented in the control system of the VSC power converters (Basic Configuration: Figure 5-5 (b)4 and Figure 5-5 (b)5). The second configuration shows a scenario in which the improvements in the VSC power converters have been implemented (Improved Configuration: Figure 5-5 (b)6 and Figure 5-5 (b)7). Furthermore, Figure 5-5 (b)4 and Figure 5-5 (b)5 show the performance of the AC voltages and AC currents of the basic scenario and Figure 5-5 (b)6 and Figure 5-5 (b)7 shows the AC voltages and AC currents taken from the most improved scenario.

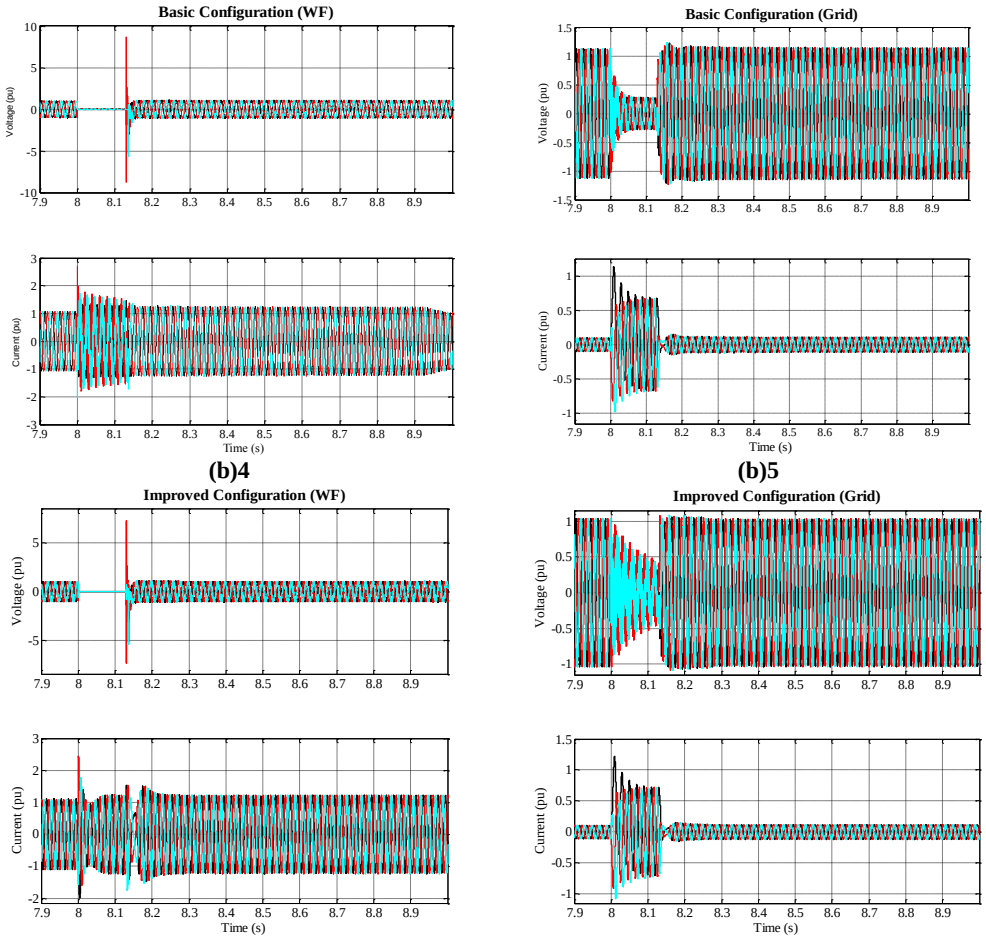

Figure 5-5: Transient responses for three-phase fault at the FRC wind farm substation

The installation of filters in the control of the VSC converter plus the installation of V_{dqs} control system and the third harmonic injection technique has to improve the performance of the VSC converters and therefore the network. Thus, the performance of the AC voltage and the AC current in the improved scenario Figure 5-5 (b)6 and (b)7, show a clear decrease in the voltages and currents peaks, troughs and in the recovery time of the most improved scenario. Thus, the AC voltage maximum peak has decreased by almost 1 per unit between the Basic Configuration (WF) and the Improved Configuration (WF). Similarly, the AC current maximum peak decreases around 1 per unit Figure 5-5 (b)4 and Figure 5-5 (b)6). Furthermore, the simulations Figure 5-5 (b)5 and Figure 5-5 (b)7) do not show significant improvement in the PCC_2. The implementations introduced in the power control system of the VSC converters of the DFIG wind turbines have reduced the AC voltages and the AC currents peaks and also have reduced the drop of the AC voltage during the transient. Even during the transient, the drop of the AC voltages and the AC currents are better controlled. The drop of the AC voltage, during the large transient, in the cluster substation is smaller comparing the Basic Configuration with the Improved Configuration; this allows a

slightly longer time to recover the entire electrical power system before this is disconnected [23, 138, 139]. Therefore, the incorporation of the improvements in the VSC converters have clearly improved the fault ride-through capability of the electrical power system.

5.3.3 Case Study 1.3 VSC-HVDC System

The objective of this case study is to monitor the operation of the control system modifications installed in both power converters of the VSC-HVDC system. Particularly, the interest of this case study is to monitor the performances produced by the modifications in the point to point control systems, explained in Chapter 3. To examine and determine the dynamic behaviours of the control and the transmission systems of the VSC-HVDC link. A large transient has been triggered in the offshore part of the power system under consideration. In this case study, the control system of the VSC-HVDC link is tested with an ideal block which provides the rated AC voltage and frequency for the offshore scheme. This decision simplifies the examined scenario and thus avoids the need to run the scheme until wind turbines reach the steady state. To analyse the mentioned control system modifications; the VSC-HVDC layout consists of two VSC converters linked by two DC cables with a length of 125 km. The power system in this scenario is rated at 300MW. Furthermore, the offshore/onshore grid voltage is rated at 132 kV, while the DC voltage is rated at ±150 kV, for more information see Table 5-2. Figure 5-6 shows a basic configuration of a VSC based HVDC transmission system.

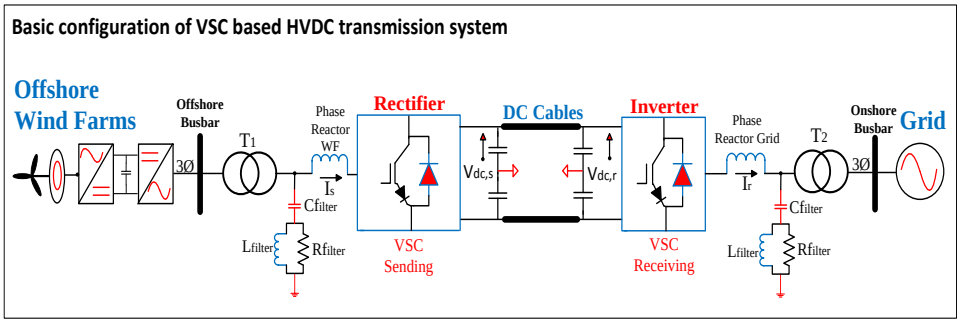

Figure 5-6: Basic VSC-HVDC power system

5.3.3.1 Mathematical Analysis: PI Controllers

To understand the performance of a VSC-HVDC power system, it is necessary to understand the behaviour of its control system. The VSC control system is based on the idea of fast tracking signals which can easily re-establish the network system after a large transient is applied. In order to re-establish the normal operation of the power system, the optimum values of each parameter of the PI controllers - k_p and k_i - have to be calculated in a steady

state. The performances of the PI controllers of the VSC converters are evaluated by applying the obtained mathematical results into the PI controllers of the VSC-HVDC power system. Then, after evaluating the obtained results; these parameters will be adapted to the necessity of the VSC-HVDC power system.

Table 5-2: Specification parameters use in the VSC-HVDC models

Parameters	Rating
Rated Power	300 MW
Rated AC Voltage	132 kV
Rated DC Voltage	300 kV
DC Current	1 kA
Base Frequency	50 Hz
ω_b	2Πf
AC Transmission Line	20 km
DC Transmission Line	125 km
Transformers Substation T_{loff}/T_{lon}	300 MVA – 33/132kV
DC Capacitors	2500μF
(r+jωL)	0.006+j0.092 (pu)

The control parameters - k_p and k_i - are calculated as follows [50, 52, 64, 106, 140]. First of all, the average time delay of the carrier signal used to modulate the VSC converter (the switching frequency, f_{switch}) is calculated. The imposed switching frequencies of the IGBT switches in both VSC converters, in this case study, are 2.25 kHz. Therefore, the time delay produced by the switching of the IGBT valves is calculated as follows:

$$T_a(offshore) = T_{a-off} = \frac{T_{switch}}{2} = \frac{1}{2f_{r-switch}} = \frac{1}{2*2250} = 222.22\mu s \quad (5.6)$$

$$T_a(onshore) = T_{a-on} = \frac{T_{switch}}{2} = \frac{1}{2f_{g-switch}} = \frac{1}{2*2250} = 222.22\mu s \quad (5.7)$$

To calculate the values of the parameters, k_p and k_i, the VSC-HVDC equipment (resistances, impedances and capacitances) must be converted into per-unit values. The phase reactor impedance is converted into pu values and the delay time is extracted as follows [140]:

$$L_{Phrec-pu} = \frac{LZ_{Base}}{\omega_b} = L * \frac{V_{dc}^2/S_n}{\omega_b} = \frac{0.5\left(132k^2/300e^6\right)}{2\pi 50} = \frac{17.124}{314.16} = 0.0924\ pu \quad (5.8)$$

The natural frequency is taken as ω_b =314.16 rad/s. The m_a is set to be at maximum value, thus the phase reactor integration time of the system is given by (3.2) [64, 68]:

$$V_{ac}max = \frac{\sqrt{3}*1*300e^6}{2\sqrt{2}} \approx 0.612V_{dc} \approx 183.712kV \quad (5.9)$$

$$\tau_{ph-rec} = \frac{0.9*0.0924}{314.16(183.712k-132k)}0.612V_{dc} \approx 939.87\mu s \quad (5.10)$$

The transformer delay time is given by:

$$\tau_{trafo-pu} = \frac{L_{pu}}{r_{pu}*\omega_b} = \frac{0.015}{6.0e^{-4}*314.16} = 0.0796s \quad (5.\ 11)$$

Thus, the k_p and k_i for the inner and outer current controller of the offshore cluster substation is given as follows [50, 70, 71, 76, 141]:

$$k_{p1} = \frac{T_{i-total}{}^{4} r_{pu}}{2T_a} = \frac{0.0805*6.0e^{-4}}{2*222.22\mu} = \frac{48.32\mu}{444.44\mu} = 0.1087 \quad (5.12)$$

$$k_{i1} = \frac{k_{p1}}{\tau_{ph-rec}} = \frac{0.1087}{939.87\mu s} = 115.654 \quad (5.13)$$

In this thesis, the reactive power of both networks are set to be similar, i.e. zero. Thus, the k_{p2} k_{i2}, and k_{p5} k_{i5}, values for the reactive power are 0.005 and 0.000175 respectively. The damping factor of the offshore power system is calculated by [76]:

$$\zeta = \frac{1}{2}\sqrt{\frac{T_{i-total}*r_{pu}}{k_{p1}*T_a}} = 0.5\sqrt{\frac{0.0805*6.0e^{-4}}{0.1087*222.22\mu}} = 0.5\sqrt{\frac{48.3\mu}{24.15\mu}} = 0.5 * 1.414 = 0.71 \quad (5.14)$$

The DC PI controller parameters, k_{p3} and k_{i3}, are calculated as follows [50, 115, 142, 143]:

$$a = \frac{1+\cos\varphi}{\sin\varphi} = \frac{1+\cos 45}{\sin 45} = 2.4142 \quad (5.\ 15)$$

$$T_i = a^2 * T_{eq} = a^2 * 4 * T_a = 2.4142^2 * 4 * 222.22\mu = 5.181e^{-3} \quad (5.16)$$

Thus, the control parameters for the DC controller are given as follows [50, 71, 141, 143]:

$$k_{p3} = \frac{4C_{dc}}{9*a*V_{d,dc}T_i} = \frac{4*2500e^{-6}}{9*2.4142*1*5.181e^{-3}} = 0.3 \quad (5.17)$$

$$k_{i3} = \frac{k_{p3}}{T_i} = \frac{0.3}{5.181e^{-3}} = 59.19 \quad (5.18)$$

In this simulation, the charging time of the DC capacitances (offshore and onshore) are set at 375ms. The value of the capacitor is calculated using the following equation:

$$C_{dc} = \frac{2S_n*\tau}{V_{dc}^2} = \frac{2*300e^6\ 375x10^{-3}}{(300x10^3)^2} = \frac{225x10^8}{9x10^{10}} = 0.0025F = 2500\mu F \quad (5.19)$$

Table 5-3 shows the calculated k_p and k_i parameters of the PI controllers in the VSC-HVDC power system. The table is divided in three sections.

Table 5-3: PI parameters of the inner and outer current controllers and dc controller

Calculated Scheme Offshore Control Loop				**Calculated Scheme Onshore Control Loop**					
Inner Controller		Outer Controller		DC Controller		Inner Controller		Outer Controller	
$\boldsymbol{k_{p1}}$	0.112	$\boldsymbol{k_{p2}}$	------	$\boldsymbol{k_{p3}}$	0.3	$\boldsymbol{k_{p4}}$	0.1087	$\boldsymbol{k_{p5}}$	------
$\boldsymbol{k_{i1}}$	115.64	$\boldsymbol{k_{i2}}$	------	$\boldsymbol{k_{i3}}$	59.19	$\boldsymbol{k_{i4}}$	115.65	$\boldsymbol{k_{i5}}$	------

[4] $T_{i-total} = \tau_{ph-rec} + \tau_{trafo-pu}$

Basic Scheme Offshore Control Loop				Basic Scheme Onshore Control Loop					
Inner Controller		Outer Controller		DC Controller		Inner Controller		Outer Controller	
k_{p1}	1	k_{p2}	0.005	k_{p3}	25	k_{p4}	1	k_{p5}	0.005
k_{i1}	500	k_{i2}	0.0017	k_{i3}	100	k_{i4}	600	k_{i5}	0.0017
Improved Scheme Offshore Control Loop				**Improved Scheme Offshore Control Loop**					
Inner Controller		Outer Controller		DC Controller		Inner Controller		Outer Controller	
k_{p1}	1.5	k_{p2}	0.005	k_{p3}	7.5	k_{p4}	1.5	k_{p5}	0.005
k_{i1}	500	k_{i2}	0.0017	k_{i3}	25	k_{i4}	600	k_{i5}	0.0017

The first section shows the calculated values; the second section shows the basic scenario values for the k_p and k_i; and the third section shows the parameters taken from the most improved VSC-HVDC scheme.

5.3.3.2 Power Losses Calculation

5.3.3.2.1 Theoretical Power Losses

In the ABB report "*HVDC Light®: It's time to connect*" it is possible to see the expected losses for different VSC-HVDC systems [144]. The power losses of the ABB power system are under 2%. These power losses are produced by the conversion of the power, AC/DC, and the transmission system. Therefore, the power losses occur in the switches, the $R_{snubber}$ resistance and the resistance of the DC cables [29, 101]. In, [29], the power losses of the M5 converter of the ABB system are calculated as follows [29, 101]:

$$P_{con-Losses} = \frac{P_{Sending} - P_{Reciving}}{2 * P_{Sending}} * 100 = \frac{373.4e^6 - 362e^6}{2 * 373.4e^6} * 100 = 0.0153 = 1.53\% \quad (5.20)$$

The cable rating is ±150 kV with a nominal current of 1.33 kA. This cable can transfer a nominal power of 400 MW. The cross-linked polyethylene, XLPE, and the cable cross-section has a conductor of 1200 mm^2 (copper) [29, 135]. Furthermore, it has been impossible to obtain the resistance value for the ABB cable and therefore it has been decided to calculate an ideal DC cable resistance with 1200 mm^2 at 60°, r_{dc} [5] [26, 145]. Therefore, the obtained power losses of the DC cable are not taken from ABB data. Thus, the following calculation cannot be considered as "correct" data analysis but this calculated DC cable data is still useful when it is compared with the expected power losses (power losses calculated with the applied data) and the obtained power losses (power losses obtained after the simulations).

[5] $r_{60} = r_{20}(1 + \alpha(T_{60} - T_{20}))$

$$r_{60} = 0.0151(1 + 0.00392(60 - 20)) = 0.0104\Omega/km \quad (5.\ 21)$$

The cable length is 125km and thus the DC cable power losses[6] are calculated as follows:

$$r_{dc-125} = 0.0104\Omega * 125 = 2.18346\Omega/km \quad (5.22)$$

$$P_{dc-cables-losses} = 2 * r_{dc} * I_{dc}^2 = 2 * 2.1835 * 1233^2 = 6.64\ \mathrm{M}W \quad (5.23)$$

5.3.3.2.2 Expected Converter Power Losses

The VSC converter losses have to be calculated when the power system is in steady state and also no conversion losses. The nominal losses estimated by ABB are 0.0165 pu of the S_{base}, the load losses are estimated to be 0.7pu of the S_{base} and the no-load losses are estimated to be 0.3pu of the S_{base}. The expected power losses of the VSC converter can be calculated as follows [106, 129, 144] [29, 101]:

$$P_{nom} = 0.0165 * \mathrm{S_{base}} = 0.0165 * 393e^6 = 6.5MW \quad (5.24)$$

$$P_{noload} = 0.3 * P_{nom} = 0.3 * 6.5e^6 = 1.95MW \quad (5.25)$$

$$P_{load} = 0.7P_{nom}\frac{\mathrm{P_{sent}}}{P_{sent-max}} = 0.7 * 6.5e^6\frac{300e^6}{373.4e^6} = 3.66MW \quad (5.26)$$

Total converter losses for one converter can be expressed as:

$$P_{conv,loss} = P_{noload} + P_{load} = 1.95MW + 3.66MW = 5.61MW \quad (5.27)$$

$$Total_{P_{conv,loss}} = 2 * P_{conv,loss} = 2 * 5.6MW = 11.211MW \quad (5.28)$$

The DC current and the $Z_{base\text{-}dc}$ are calculated as follows:

$$I_{dc} = \frac{P_{dc}}{V_{dc}} = \frac{300x10^6}{2*150x10^3} = 1kA \quad (5.29)$$

The DC cable length is 125km; the expected power losses produced in the DC cables are calculated as follows:

$$P_{cable-loss} = 2 * r_{dc} * I_{dc}^2 = 2 * 0.78155 * 1000^2 = 1.6\ \mathrm{M}W \quad (5.30)$$

The total power received in the onshore substation is calculated as follows:

[6] The DC cable losses have been calculated using an ideal DC cable resistance

$$P_{Reciving} = \mathrm{S_{base}} - 2P_{conv,losses} - P_{cable-los} = 300e^6 - 11.21e^6 - 1.6e^6 = 287.227 \text{ MW} \quad (5.31)$$

$$P_{con-Losses} = \frac{P_{Sending} - P_{Reciving}}{2 * P_{Sending}} * 100 = \frac{300e^6 - 287.272e^6}{2 * 300e^6} * 100 = \frac{12.8e^6}{2 * 300e^6} * 100 = 0.01864 * 100 = 2.13\% \quad (5.32)$$

5.3.3.2.3 Obtained Converter Power Losses: Onshore Grid

The VSC converter losses are calculated as follows [106, 129, 144] [29, 101]:

$$P_{con-Losses} = \frac{P_{Sending} - P_{Reciving}}{2 * P_{Sending}} * 100 = \frac{300 * 10^6 - 272 * 10^6}{2 * 300 * 10^6} * 100 = 0.0466 = 4.67\% \quad (5.33)$$

The power losses of the DC cables used in the scheme with actual DC current are:

$$P_{dc-cables-losses} = 2 * r_{dc} * I_{dc}^2 = 2 * 0.7815 * 933^2 = 1.4 \text{ M}W \quad (5.34)$$

Table 5-4: Power losses for a VSC-HVDC transfer capability of 600MW and DC cable lengths of 125 km

Parameters	ABB	Expected	Obtained
DC Cable Losses	6.64 MW	1.6 MW	1.4 MW
Converter Losses	11.4 MW	11.21 MW	26.6 MW
$\mathbf{P_{Losses}}$ %	1.53%	2.13%	4.67%

5.3.3.3 Grid Fault Analysis

5.3.3.3.1 Transient Analysis

The following section shows the power grid analysis of different VSC-HVDC power systems. Thus, the following plots show performance of four different scenarios. As mentioned in Section 5.2. Case Studies: Implementation Approach, each scenario has introduced one implementation into the control system of the power VSC converter at a time. Thus, it would be possible to differentiate the improvements produced by each modification in the control system of the VSC converter in the power system. The different scenarios are denominated as Basic scenario, Freq scenario, 3Har scenario, and V_{dc} scenario. Figure 5-7 shows the transient responses for three-phase fault at PCC of the offshore substation: (c)1 is the power transferred from the offshore substation, (c)2 is the power received in the onshore substation, (c)3 is the DC voltage in the link.

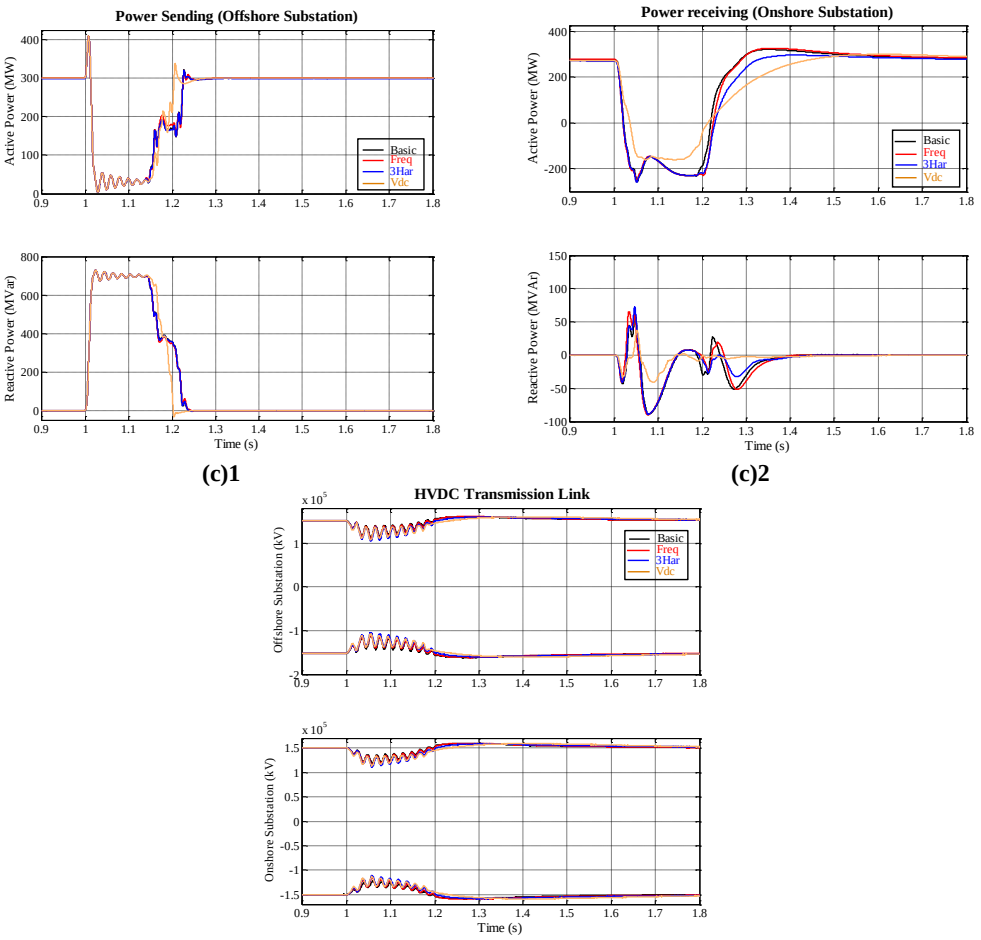

Figure 5-7: VSC-HVDC Power System

The comparing scenarios presented the performance of the four different control systems exposed in the previous paragraph. Thus, the scenario which has installed all the improvements in the control system behaves better than the other scenarios (V_{dc}scenario). Furthermore. In the top part, this figure shows the performance of the active power and the bottom part shows the performance of the reactive power during the transient (Figure 5-7 (c)1 and **(**c)2). The reduction of the active power fluctuation is significant and thus it starts to recover the steady state a few milliseconds before unlike the other three scenarios. Unfortunately, the results show that the steady state of the power system is fully recovered at the same time as the other scenarios. This control system slightly improves the power fluctuations after the transient is cleared. Furthermore, this scenario produces a slightly higher peak in the active power which reaches slightly over 400 MW. The reactive power behaviour is significantly improved, to recover the initial state of the reactive power, the control system of the VSC began slightly later than the other scenarios but it reaches 0 MVAr more quickly and also recovers the steady state a few milliseconds earlier, Figure 5-7 (c)1. Figure 5-6 (c)2 shows the performance of the active and reactive power performances on the

onshore substation Thus, the scenario which the transient produces less fluctuations is the V_{dc} scenario. The drop in the active power does not cross -200 MW and also starts to recover the steady state early. The reactive power is also improved and fluctuations produced by the transient are considerably reduced. Furthermore, the recovery of the steady state also begins early. Figure 5-7 (c)3 shows the HVDC performance during the large transient.

In all these simulations can be seen a significant improvement each time the control system of the VSC converter of the offshore and onshore substation had been modified. In addition, it is clear to see that the implementation of the third harmonic technique (3Har) and the V_{dc} technique produce the best improvement in the active and reactive power behaviour.

5.4 Case Study 2: Coordinated Control for Offshore Wind Farms

In this section, three different scenarios with a coordinated control system for two wind farms is evaluated. Thus, the composition of the offshore layout has three different types of wind farms: two DFIG wind farms, two FRC wind farms and a Mixed scenario which features one wind farm of each type. Furthermore, in these three examples, the connection points to onshore are single point connections. To study the performance of these three scenarios and their control systems, the modifications applied in the VSC-HVDC scenario, *5.5.3.VSC-HVDC System: Stability Analysis*, have been introduced in the control system of both power converters installed in the offshore and onshore substations. Then, these scenarios are compared with an extra control system modification system in which feed-forward signals have been introduced in the offshore cluster substation. These signals are obtained in the offshore wind farm substations and are fed into the power/voltage controller of the offshore cluster substation. The intention of comparing these two scenarios is to see if the control system of the offshore substation becomes more reliable with the introduction of feed-forward signals.

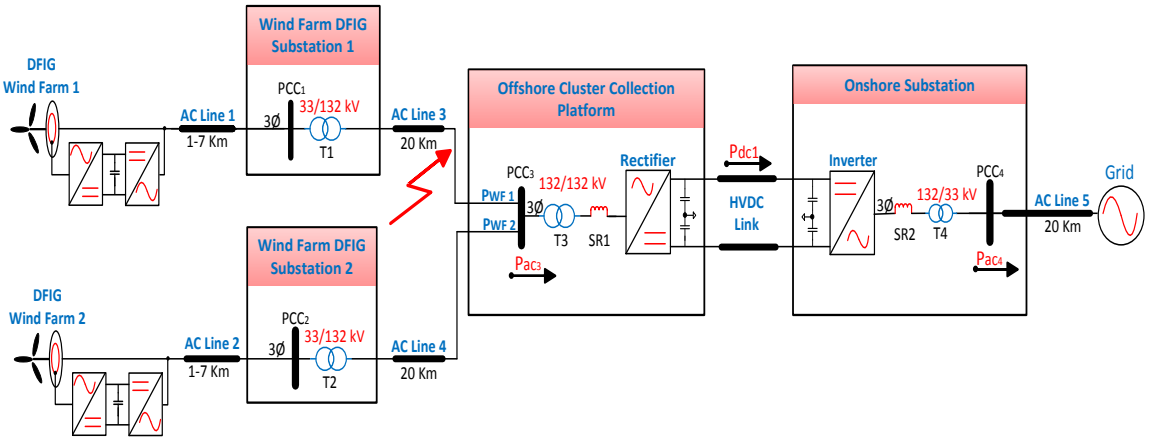

Figure 5-8: Block diagram of the DFIG scheme

Figure 5-8 represents a VSC-HVDC scenario which contains the two DFIG wind farms. The offshore layout is composed of two DFIG wind farms connected to a single cluster substation by HVAC cables rated at 132 kV. These AC cables have a length of 20 km respectively. Furthermore, each wind farm transfers 300 MW of power and thus the cluster substation controls and transfers 600 MW in total. The HVDC link is rated at ± 150 kV. In addition, in terms of improving the dynamic responses of the VSC-HVDC power system the high pass filter has been removed from the offshore layout. It has been replaced with a capacitor bank of 35 kVAr in the offshore cluster substation and 1st and 2nd order filters have been introduced inside the VSC converter (control system). As the active power control of the offshore substation has already been explained in Chapter 3, a short explanation of a feed-forward control technique is introduced in this section (this control technique is introduced in the VSC converter aiming to improve the dynamic performance of the offshore cluster substation).

The power produced by the wind turbines is collected in the wind farm substations and then sent to the offshore substation (cluster substation). The total power produced by the offshore wind farms is then collected in the PCC point at the offshore cluster substation. This total power is used to obtain the control signals for the inner and outer current controller. In terms of controlling the offshore substation, the AC voltage, at the PCC point, is used to obtain the reference signal. Figure 5-9 shows the approach of the control system applied in the offshore substation (VSC converter).

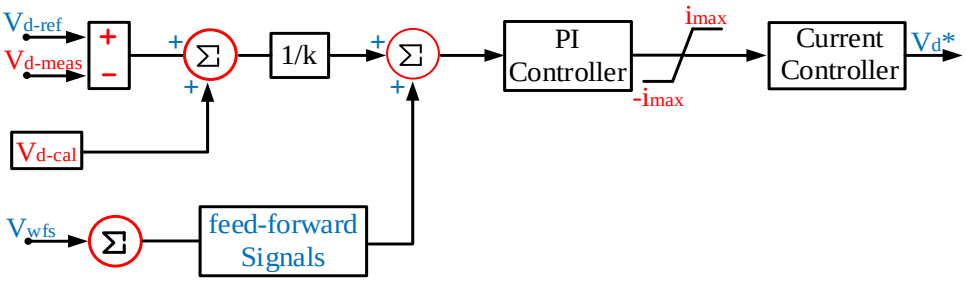

Figure 5-9: Control loop diagram of a voltage controller with a feed-forward control signals

The feed-forward signals obtained from the wind farm substations are then incorporated into the control system of the VSC converter (more information see Figure 3-10). In Figure 3-10, the P_{w1}/V_{s1} and the P_{w2}/V_{s2} are the power or voltage collected at the PCC point in the cluster substations. In this thesis, to obtain an accurate control of the power, the AC power sending is then compared with the DC power, $P_{ac} = \mathrm{P_{dc}}$. Considering no power losses in the power conversion, the power collected in the offshore substation should also be proportional to the P_{dc} and thus the reference signals can be calculated. The following equation is used to calculate the i_d^* control signal of the offshore substation (more information see equation (3.51-3.23).

5.4.1 Case Study 2.1 DFIG Scenario: Grid Fault Analysis

5.4.1.1 Scheme Analysis

As previously mentioned, to understand the performance of the VSC-HVDC system, the performance of the VSC control system and specifically their PI controllers have to be properly understood. In this scenario, the integration time of the offshore layout is influenced by the phase reactor and also by the AC transmission cables and power transformers. The mathematical approach used to calculate these parameters is similar to that used in the previous section. Although these parameters are calculated similarly, the time delay produced by all the components in the offshore layout will change the integration time and this will influence the final value of the k_p and k_i (offshore and onshore) [50, 52, 64, 65, 106, 140].

5.4.1.2 Mathematical Analysis: PI Controllers

To calculate the k_p and k_i values of the PI controllers, the magnitudes of each parameter of the power system (AC or DC cables, power transformers, etc…) have to be adapted in per-unit value. To simplify the calculation of the PI parameters and also to obtain the time delay between the wind farm and the offshore cluster substation (the time delay between the start-up of the power system and when the power system components reach the

steady state). The parameters introduced into the k_p and k_i equations are: the wind farm substation power transformer, the AC transmission lines, 132 kV and the offshore cluster substation equipment [146]. Figure 5-10 shows the scheme used to calculate the parameters of the offshore PI controllers.

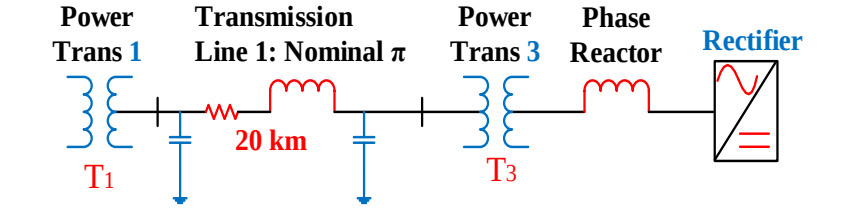

Data

Transmission Line 1	T1	T3	Sbase	Vbase
r_{l1} 0.0124Ω	300MVA	600MVA	600 MVA	132 kV
l_{l1} 1.05e-3H	33/132kV	132/132kV		
c_{l1} 1.33e-9F	R_{T1} 333.4μ pu	R_{T3} 0.0006 pu		
Ph_{rec} = 0.25H	L_{T1} 0.015 pu	L_{T3} 0.015 pu		

Figure 5-10: Basic diagram of the offshore power system

5.4.1.2.1 Offshore Analysis: Offshore PI Controllers

As mentioned, the total delay times of the offshore layout is the sum of the delay times of each component and thus the calculated delay time begins at the wind farm substation and ends at the cluster substation. To calculate the power system's delay all parameters have to be in per unit values, for more information see Appendix B. The integration time of the phase reactor system, τ_{ph-rec}, is calculated as follows [76, 140], [64, 68]:

$$L_{Phrec-pu} = \frac{LZ_{Base}}{\omega_b} = \frac{L\left(V_{ac}^2/S_n\right)}{\omega_b} = \frac{0.25\left(132k^2/600x10^6\right)}{2\pi 50} = \frac{7.26}{314.16} = 0.02311\ pu \quad (5.35)$$

$$\tau_{ph-rec} = \frac{0.9*0.02311}{314.16(183.712k-132k)}0.612V_{dc} \approx 2.351e^{-4}s \quad (5.36)$$

The total impedance and resistance of the power transformers (T1 and T3) and transmission cable (Line 1) are given by:

$$l_{pu} = Z_{l_{T1}-pu.new} + l_{l1-pu.new} + Z_{l_{T3}-pu.new} = 1.875e^{-3} + (7.77e^{-3} - 2.452e^{-6}) + 0.015 = 0.0172pu \quad (5.37)$$

$$L_{pu-tot} = L_{T1-pu} + L_{Phrec-pu} = 0.0172 + 2.351e^{-4} = 0.01743 \quad (5.38)$$

Thus, the total delay time of the offshore layout is calculated as follows [70, 71, 76]:

$$r_{pu-total} = 3.33e^{-4} + 0.092 + 0.0006 = 0.093pu \quad (5.39)$$

$$\tau_{pu} = \frac{l_{pu-total}}{r_{pu-total} * \omega_b} = \frac{0.01743}{0.093 * 314.16} = 5.961e^{-4} \quad (5.40)$$

$$T_{i-total} = \tau_{pu} + \tau_{ph-rec} = 5.961e^{-4} + 2.351e^{-4} = 8.312e^{-4}s \quad (5.41)$$

The k_{p1} and the k_{i1} are calculated as follows [50, 70, 71, 76, 141]:

$$k_{p1} = \frac{T_{i-total} * r_{pu-total}}{2T_a} = \frac{8.312e^{-4} * 0.093}{2 * 222.22\mu} = \frac{7.7301e^{-5}}{444.44e^{-6}} = 0.174 \quad (5.42)$$

$$k_{i1} = \frac{k_p}{T_i} = \frac{0.174}{8.312e^{-4}} = 209.25 \quad (5.43)$$

The damping factor of the calculated offshore scheme is given as follows [76]:

$$\zeta = \frac{1}{2}\sqrt{\frac{T_{i-total} * r_{pu-total}}{k_{p1} * T_a}} = 0.5\sqrt{\frac{8.312e^{-4} * 0.093}{0.174 * 222.22\mu}} = 0.5\sqrt{\frac{7.73e^{-5}}{3.87e^{-5}}} = 0.5 * 1.414 = 0.7074 \quad (5.44)$$

The calculated values of the ζ shows the adequacy of the $k_{p1}$and k_{i1} for the VSC-HVDC power system. Thus, the ζ value indicates a smooth transition of the power system until it reaches the steady state. A damping factor value higher than 1, $\zeta > 1$, indicates that the power system is over-damped and damping factor value lower than 0, $0 < \zeta$, indicates that the power system is under-damped. Both situations are not desirable for normal operations of the VSC-HVDC power system and thus with the calculated $k_{p1}$and k_{i1} have been avoided. In this simulation, the charging time of the DC capacitors "offshore and onshore" is computed at 375ms. The value of the capacitor is calculated using the following equation:

$$C_{dc} = \frac{2S_n * \tau}{V_{dc}^2} = \frac{2 * 600x10^6 * 375x10^{-3}}{(300x10^3)^2} = \frac{225x10^8}{9x10^{10}} = 0.0025F = 2500\mu F \quad (5.45)$$

5.4.1.2.2 Onshore Analysis: Onshore PI Controllers

The optimum symmetrical technique has again been used to calculate the parameters of the onshore PI controllers (the DC PI controller and the inner and outer current controllers). In order to obtain the parameters of the DC controller, the phase margin criterion "theta angle" is set at 45° and therefore the "a" parameter is set at 45°. Furthermore, the integration time is equal to $T_i = a^2 * T_{eq}$ and thus the transfer function is tuned as follows [50, 115, 142, 143]:

$$a = \frac{1+\cos 45}{\sin 45} = 2.4142 \quad (5.46)$$

$$T_i = a^2 * T_{eq} = a^2 * 4 * T_a = 2.4142^2 * 4 * 166.666\mu = 0.00392 \quad (5.47)$$

The control parameters for the DC controller are given as follows [50, 71, 141, 143]:

$$k_{p3} = \frac{4C_{dc}}{9*a*V_{d,dc}T_i} = \frac{4*2500e^{-6}}{9*2.4142*1*0.00392} = 0.11741 \quad (5.48)$$

$$k_{i3} = \frac{k_p}{T_i} = \frac{0.11741}{0.00392} = 29.952 \quad (5.49)$$

The parameters of the onshore scheme are calculated similarly to the offshore parameters and therefore the values for the inner and outer current controllers are calculated as follows:

$$L_{Phrec-pu} = \frac{LZ_{Base}}{\omega_b} = \frac{L\left(V_{dc}^2/S_n\right)}{\omega_b} = \frac{0.5\left(132k^2/600x10^6\right)}{2\pi 50} = \frac{14.52}{314.16} = 0.046\ pu \quad (5.50)$$

The m_a is set to be at maximum value, and thus the integration time of the system is given by (3.2) [64, 68]:

$$\tau_{ph-inv} = \frac{0.9*0.046}{314.16(183.712k-132k)} 0.612V_{dc} \approx 4.7e^{-4}s \quad (5.51)$$

The total impedance and resistance of the power transformers and transmission cables are given by:

$$l_{pu} = Z_{l_{T4}-pu.new} + l_{l2-pu.new} = (7.77e^{-3} - 2.452e^{-6}) + 0.015 = 0.0227pu \quad (5.52)$$

$$r_{pu-total} = r_{pu-T_4} + r_{pu-cable} = 0.092 + 0.0006 = 0.092pu \quad (5.53)$$

$$\tau_{pu} = \frac{l_{pu-total}}{r_{pu-total}*\omega_b} = \frac{0.0227}{0.093*314.16} = 7.854e^{-4} \quad (5.54)$$

The total delay time of the onshore layout is calculated as follows:

$$T_{i-total} = \tau_{pu} + \tau_{ph-rec} = 7.854e^{-4} + 4.7e^{-4} = 1.255e^{-3} \quad (5.55)$$

The k_{p4} and the k_{i4} are calculated as follows [70, 71, 76]:

$$k_{p4} = \frac{1.255e^{-3}*0.092}{2*222.22\mu} = \frac{1.2151e^{-4}}{444.44e^{-6}} = 0.262 \quad (5.56)$$

$$k_{i4} = \frac{k_p}{T_i} = \frac{0.262}{1.2151e^{-4}} = 213.92 \quad (5.57)$$

The damping factor of the calculated onshore scheme is given as follows [76]:

$$\zeta = 0.5\sqrt{\frac{1.255e^{-3}*0.092}{0.262*166.666\mu}} = 0.5\sqrt{\frac{1.127e^{-4}}{4.366e^{-5}}} = 0.5 * 1.6 = 0.803 \qquad (5.\ 58)$$

Table 5-5: PI parameters of the inner and outer current controllers and DC controller

Calculated Scheme Offshore Control Loop

Inner Controller		Outer Controller		DC Controller		Inner Controller		Outer Controller	
k_{p1}	0.12	k_{p2}	------	k_{p3}	0.12	k_{p4}	0.262	k_{p5}	------
k_{i1}	209.1	k_{i2}	------	k_{i3}	29.95	k_{i4}	213.92	k_{i5}	------

Calculated Scheme Onshore Control Loop

Basic Co-ordinate Control Scenario Offshore Control Loop

Inner Controller		Outer Controller		DC Controller		Inner Controller		Outer Controller	
k_{p1}	1	k_{p2}	0.005	k_{p3}	25	k_{p4}	1	k_{p5}	0.005
k_{i1}	500	k_{i2}	0.0017	k_{i3}	100	k_{i4}	600	k_{i5}	0.0017

Basic Co-ordinate Control Scenario Onshore Control Loop

Co-ordinate control Scenario with a Feed-Forward Scheme Offshore Control Loop

Inner Controller		Outer Controller		DC Controller		Inner Controller		Outer Controller	
k_{p1}	1.5	k_{p2}	0.005	k_{p3}	7.5	k_{p4}	1.5	k_{p5}	0.005
k_{i1}	500	k_{i2}	0.0017	k_{i3}	25	k_{i4}	600	k_{i5}	0.0017

Co-ordinate control Scenario with a Feed-Forward Scheme Onshore Control Loop

The most significant difference between the PI parameters shown in the above table is between the calculated scheme "k_{i1}" and the implemented k_{i1} values in the basic and the feed-forward scenarios). The calculated value is significantly higher and therefore, it is possible to assume that the integration time T_i needs to include other timing factors.

5.4.1.3 DFIG Scenario: Power Losses Calculations

5.4.1.3.1 Theoretical Power Losses

For more information, see section 5.3.3.2.1 Power Losses: ABB and the ABB report "*HVDC Light®: It's time to connect*"

$$P_{con-Losses} = \frac{P_{Sending} - P_{Reciving}}{2 * P_{Sending}} * 100 = \frac{569.7e^6 - 553.3e^6}{2 * 569.7e^6} * 100 = 1.44\% \qquad (5.\ 59)$$

5.4.1.3.2 Expected Converter Power Losses

As was calculated in Section 5.3.3.2.2; the expected power losses of the VSC converter can be calculated as follows [106, 129, 144]:

$$P_{nom} = 0.0165 * \mathrm{S_{base}} = 0.0165 * 667e^6 = 11MW \quad (5.60)$$

$$P_{noload} = 0.3 * P_{nom} = 0.3 * 6.5e^6 = 3.302MW \quad (5.61)$$

$$P_{load} = 0.7P_{nom}\frac{\mathrm{P_{sent}}}{P_{sent-max}} = 0.7 * 11e^6\frac{600e^6}{633e^6} = 7.32MW \quad (5.62)$$

Total converter losses for one converter can be expressed as:

$$P_{conv,loss} = P_{noload} + P_{load} = 3.302e^6 + 7.32e^6 = 10.6MW \quad (5.63)$$

$$Total_{P_{conv,loss}} = 2 * P_{conv,loss} = 2 * 10.6e^6 = 21.2MW \quad (5.64)$$

The DC current and the Z_{base} are calculated as follows:

$$I_{dc} = \frac{P_{dc}}{V_{dc}} = \frac{600x10^6}{2*150x10^3} = 2kA \quad (5.65)$$

The DC cable length is 125km and thus the expected power losses of the DC cable are calculated as follows:

$$r_{dc-125} = 0.0212568 * 125 = 2.66\Omega \quad (5.66)$$

$$P_{cable-loss} = 2 * r_{dc} * I_{dc}^2 = 2 * 2.66 * 2000^2 = 21.3\ \mathrm{MW} \quad (5.67)$$

The total power losses of the point to point converter are calculated as follows:

$$P_{Reciving} = \mathrm{S_{base}} - 2P_{conv,losses} - P_{cable-los} = 600e^6 - 21.2e^6 - 21.3e^6 = 557.5\ \mathrm{MW} \quad (5.68)$$

$$P_{con-Losses} = \frac{P_{Sending}-P_{Reciving}}{2*P_{Sending}} * 100 = \frac{600e^6-557.5e^6}{2*600e^6} * 100 = \frac{42.5e^6}{2*600e^6} * 100 = 3.541\% \quad (5.69)$$

5.3.3.2.3 Obtained Converter Power Losses

The power losses of the VSC-HVDC system are given by [106, 129, 144] [29, 101].

$$P_{con-Losses} = \frac{P_{Sending}-P_{Reciving}}{2*P_{Sending}} * 100 = \frac{600*10^6-560*10^6}{2*600*10^6} * 100 = \frac{40*10^6}{1200*10^6} * 100 = 3.33\% \quad (5.70)$$

The DC cable length is 125km; the obtained power losses produced in the DC cables are calculated as follows:

$$P_{dc-cables-losses} = 2 * r_{dc} * I_{dc}^2 = 2 * 2.66 * 1810^2 = 17.43\ \mathrm{MW} \quad (5.71)$$

Table 5-6: Power losses for a VSC-HVDC transfer capability of 600MW and a DC cable length of 125 km

Parameters	ABB	Expected	Obtained
DC Cable Losses	-------	21.3 MW	17.43 MW
Converter Losses	16.4 MW	21.2 MW	22.57 MW

P_{Losses} %	1.44 %	3.541%	3.33%

The P_{Losses} in the ABB section is calculated using the M6 converter data obtained from the [29] and with a total length of 100Km.

5.4.1.4 Grid Fault Analysis

The following section shows the simulation plots obtained from the DFIG scenario, in which the coordinated control for two offshore DFIG wind farms are implemented in the cluster substation. To investigate the ability of this coordinated control for the mentioned power system, a case study with two wind farms has been added to the offshore substation, in which a large transient has been triggered at 6s. To differentiate the control systems, in the following plots, the first control system is named "basic" (basic coordinated control). The basic scenario has the same modified scenario tested in the previous case studies. Thus, the basic scenario has all the modification applied in the wind turbines, 5.3.1 Case Study 1.1 and 5.3.2 Case Study 1.2, and the modifications implemented in the VSC-HVDC power system, 5.3.3 Case Study 1.3. The modified control system in which has been introduced the feed-forward signals from the wind farms is named (feed signal).

5.4.1.4.1 Transient Analysis: Power Analysis

The following plots show the performance of the two aforementioned VSC control systems. A basic coordinate control scenario "Basic Scenario" and the coordinate control system which has implemented the feed-forward idea.

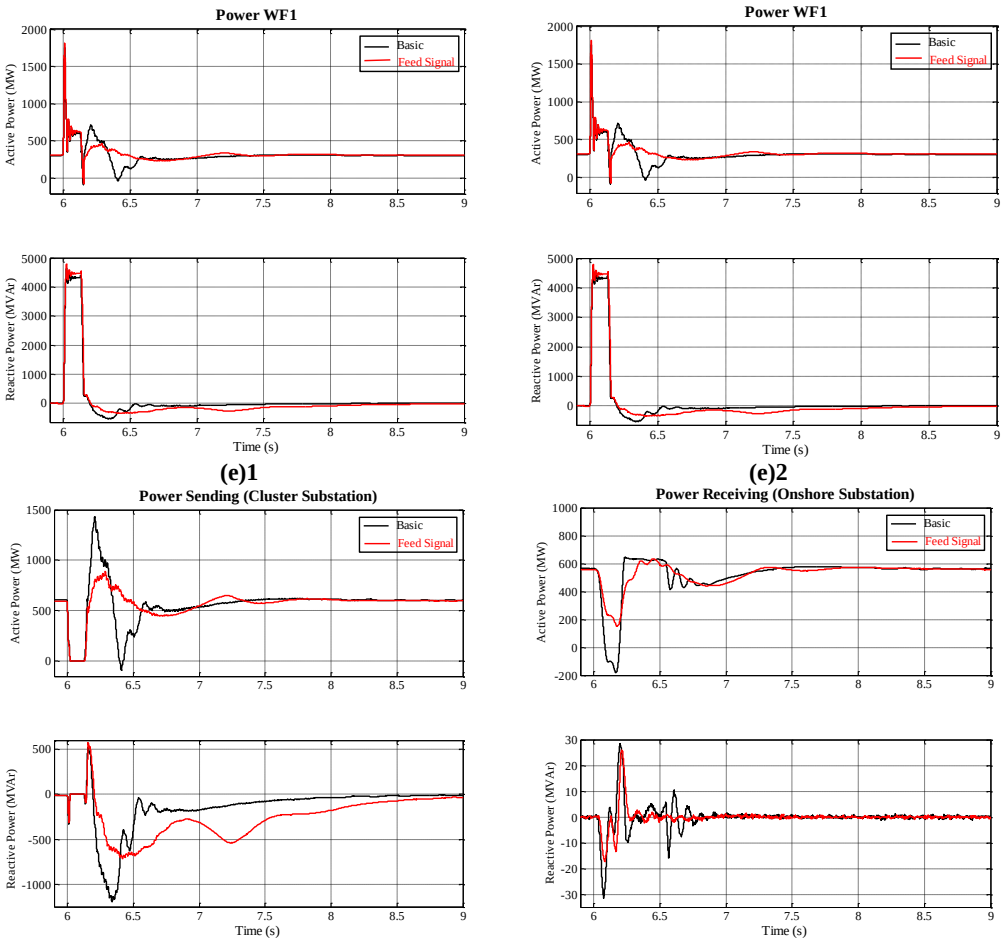

Figure 5-11: Transient responses for three-phase fault at the DFIG scenario

Figure 5-11 (e)1 to (e)4 show the performance of the active and reactive power performances on the wind farm substations and the offshore and onshore substations respectively. In the top part, these figures show the performance of the active power and in the bottom part show the performance of the reactive power during the transient. The introduction of the feed-forward technique does not change the reaction of the power system during the first 0.25ms. It is after the first 0.25ms that the behaviour of the power system changes (red line). Thus, the peaks and fluctuations have been significantly reduced. The performance of wind farm substations are also improved and thus they reach the steady state smoother; around 7.5sec. With the feed-forward technique the reactive power peaks are higher during the initial state. In contrast, the feed-forward technique reduces the power system fluctuations and enables the power system to reach the steady state without significant peaks and troughs. Figure 5-11 (e)3 shows the performance of the offshore cluster substation. The behaviour of the offshore cluster subtation is similar to the behaviour of both wind farm substations. Thus, with the basic coordinated control (black line) the maximum power peak reaches almost 1500 MWs and the lowest trough reaches 0 MW. In contrast, the maximum peak in the scenario which

has the feed-forward signals is significantly less, around 750 MW and the lowest trough is over 500 MW. In this scenario the fluctuations are also reduced and the power system reaches the steady state in a smoother transition. The onshore substation figure, Figure 5-11 (e)4, also shows the benefit that this implementation applied to the offshore substations produced in the VSC-HVDC power system. The reduction of the lowest trough is subtantial; from -200 MW with the basic configuration to 200MW with the feed-forward configuration. The feed-forward configuration also improves the active power performance and also its fluctuations. The feed-forward technique does not significantly improve the performance of the reactive power. Finally the peaks and troughs are reduced and thus the power system fluctuations.

5.4.1.3.2 Transient Analysis: Voltage and Current Analysis

The first results show the performance of the AC voltage and current offshore and onshore substation in per unit values, Figure 5-11 (e)5 and (e)6. The second plots show the same performance of the offshore and the onshore substations but in sinusoidal values, Figure 5-11(e)7 to Figure 5-11 (e)10. Thus, Figure 5-11 (e)7 and (e)8 show a scenario in which no improvement has been implemented in the control system of the VSC power converters (Basic Configuration) and Figure 5-11 (e)9 and (e)10 show a scenario in which the feed-forward technique has been implemented in the VSC power converter. These figures show the behaviour of the AC voltages and AC currents at the offshore/onshore substations at the PCC_3 and PCC_4, Figure 5-8.

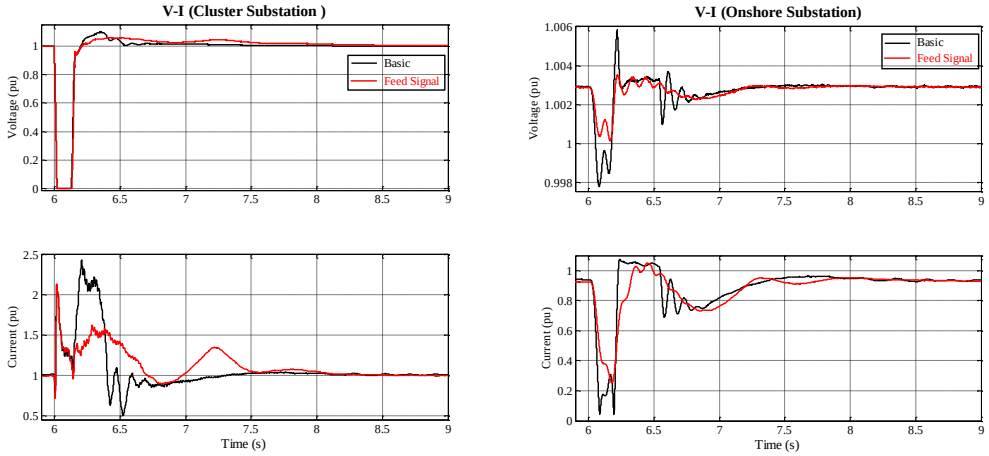

(e)5 **(e)6**

Figure 5-11: Transient responses for three-phase fault at the DFIG scenario

Figure 5-11 (e)5 shows the voltage and current in the offshore substation and Figure 5-11 (e)6 shows the voltage and current in the onshore substation. The feed-forward improvement implemented in the offshore cluster subsation clearly improves the current performances in both substations This implemetation has improved the behaviour of the AC voltage in both substations and significantly improved the behaviour of the AC curent in both substations.

The AC current peaks and troughs are reduced significantly by almost 0.5 pu in the offshore substation. The AC current behaviour, in the onshore substation, is slightly enhanced. Thus, the peak and trough are marginally improved but the AC current fluctuations are considerably decreased and thus the VSC-HVDC power system reaches the steady state in a smooth transition.

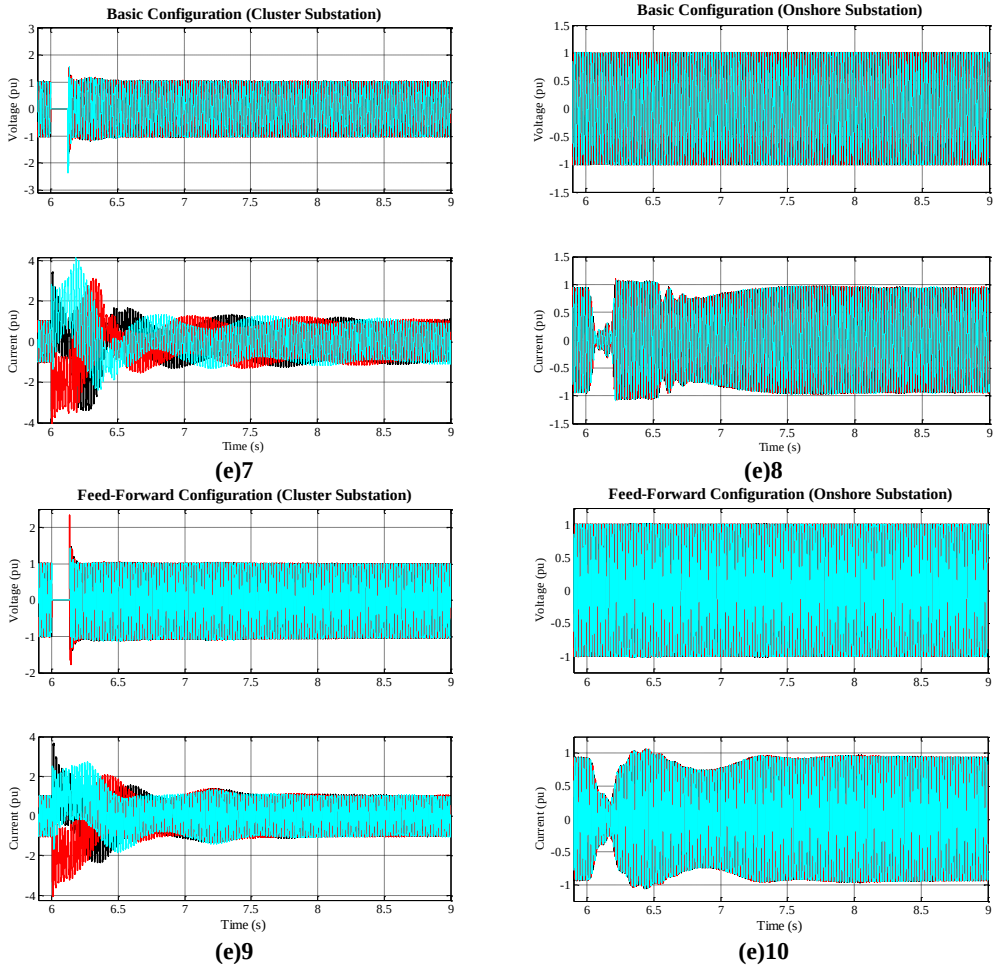

Figure 5-11: Transient responses for three-phase fault at the DFIG scenario

The performances of the AC voltages and the AC currents of the offshore and onshore substations are shown in Figure 5-11. The introduction of the feed-forward signals from the wind farms (WF1 and WF2) obtained in the wind farm substations have improved the behaviour of the AC voltages and AC currents. Clearly, the feed-forward signals produce an important impact in the behaviour of the AC currents which recovers the steady state more quickly (offshore substation) than the basic configuration, Figure 5-11 (e)7 to Figure 5-11 (e)9. Furthermore, the fluctuations produced by the large transient are also significantly reduced. In terms of the onshore substation, the AC voltage is not affected. However, the AC current is slightly affected by the large transient. In Figure 5-11 (e)8 can be appreciated that there is a current dip, followed by a sudden increase, finishing around 6.5s. Then, the AC

currents suffers a large but steady fluctuation until it recovers the steady state around 8 seconds. Furthermore, the currents maximum peaks produced during the recovery of the power system have also improved and thus they have reduced almost by 2 per unit (the initial current peak is still similar in both figures). In Figure 5-11 (e)10 can be clearly seen that the AC current dip is reduced and the large fluctuation is also reduced. Thus, the power system reaches almost the steady state around 7.4 sec. Therefore, it can be concluded that the behaviour of the electrical power systems - offshore/onshore grids - have been improved through the addition of these feed-forward signals from the wind farms (WF1 and WF2).

5.4.2 Case Study 2.2 FRC Scenario: Grid Fault Analysis

The FRC layout has the same power system characteristics as the DFIG layout (previous section) and thus the initial values of the PI parameters and the power losses are taken from the previous section. The Figure 5-12 shows the FRC scheme.

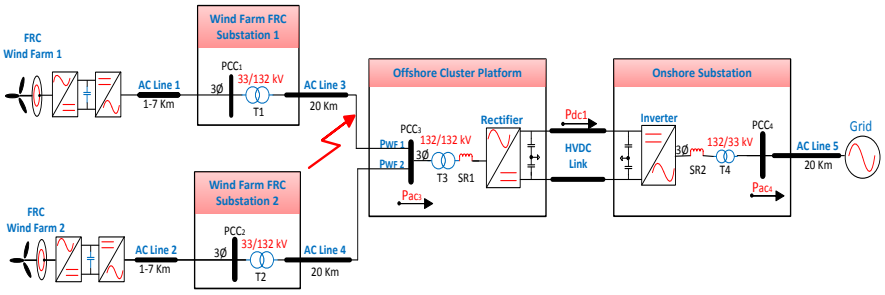

Figure 5-12: Block diagram of the FRC scheme

5.4.2.1 Scheme Analysis

The structure of the FRC layout is similar to the DFIG scenario. Thus, the calculated values of the PI controllers obtained in the previous Section, Section 5.4.1.2.2, have also used in this scenario. Therefore, the developed mathematical analysis has been shown above and thus the initial parameters have been taken from Table 5-5.

Table 5-7: PI parameters of the inner and outer current controllers and dc controller

Calculated Scheme Offshore Control Loop				**Calculated Scheme Onshore Control Loop**					
Inner Controller		Outer Controller		DC Controller		Inner Controller		Outer Controller	
k_{p1}	0.12	k_{p2}	------	k_{p3}	0.12	k_{p4}	0.262	k_{p5}	------
k_{i1}	209.1	k_{i2}	------	k_{i3}	29.95	k_{i4}	213.92	k_{i5}	------

Basic Co-ordinate Control Scenario Offshore Control Loop				Basic Co-ordinate Control Scenario Onshore Control Loop					
Inner Controller		Outer Controller		DC Controller		Inner Controller		Outer Controller	
k_{p1}	0.35	k_{p2}	7.5	k_{p3}	7.5	k_{p4}	1	k_{p5}	0.005
k_{i1}	2.05	k_{i2}	30	k_{i3}	50	k_{i4}	150	k_{i5}	0.0017
Co-ordinate control Scenario with a Feed-Forward Scheme Offshore Control Loop				**Co-ordinate control Scenario with a Feed-Forward Scheme Onshore Control Loop**					
Inner Controller		Outer Controller		DC Controller		Inner Controller		Outer Controller	
k_{p1}	0.35	k_{p2}	7.5	k_{p3}	2.0	k_{p4}	0.105	k_{p5}	0.005
k_{i1}	1.5	k_{i2}	30	k_{i3}	15	k_{i4}	150	k_{i5}	0.0017

The most significant difference between the PI parameters shown in the above table is between the calculated scheme "k_{i1}" and the implemented k_{i1} values in the basic and the feed-forward scenarios). The calculated value is significantly higher and therefore, it is possible to assume that the integration time T_i needs to include other timing factors.

5.4.2.2 FRC Scenario: Power Losses Calculations

The power system characteristics of the offshore layout offshore VSC-HVDC power system - when a DFIG and a FRC wind farms are added to the offshore layout - are equal to the DFIG power system. The theoretical power losses "Section 5.4.1.3.1", the expected power losses "Section 5.4.1.3.2", and the obtained power losses "Section 5.3.3.2.3" of the VSC-HVDC power system are expected to be equal. Thus, the values of the theoretical power losses, the expected power losses and the obtained power losses can be examined in the previous section. Therefore, as the power losses in this section should be equal to the power losses in the previous section, it has been decided to avoid further calculation of the VSC-HVDC power system and thus further information of the power losses system of the VSC-HVDC power system when the FRC wind turbines are added to the scenario can be checked in Section 5.4.1.3 Power Losses Calculations.

5.4.2.3 Grid Fault Analysis

The introduction of these wind farms has altered the performance of the VSC-HVDC power system (compared with the previous example). However, the behaviour of the power system is changed, the reaction of the control system of the cluster substation does not change significantly and thus achieves the voltage fault ride-through capability standards. Furthermore, the recovery of the FRC scenario is appropriately achieved to the recovery time seen in the DFIG scenario and thus achieve the steady state of the VSC-HVDC power system without major difficulties. Furthermore, the following section shows the power grid analysis

of the VSC-HVDC with the two mentioned scenarios in the previous section. The basic scenario has the same modified scenario tested in the previous case studies. Thus, the basic scenario has all the modification applied in the wind turbines, 5.3.1 Case Study 1.1 and 5.3.2 Case Study 1.2, and the modifications implemented in the VSC-HVDC power system, 5.3.3 Case Study 1.3. Then, two wind farms have been implemented into the offshore array (to simplify the simulations, both wind farms have the same characteristics). Finally, the coordinated power control has been added to the offshore cluster substation.

5.4.2.3.1 Transient Analysis: Power Analysis

Figure 5-13 shows the performance of: (f)1 P-Q at the WF1 substation, (f)2 P-Q at the WF2 substation, (f)3 P-Q at the offshore cluster substation, (f)4 P-Q at the onshore substation. Thus, Figure 5-13 shows the performance of the active and reactive power performances on the wind farms substations, the offshore and the onshore substations. The above plots show the performance of the basic scenario and the scenario in which the feed-forward signals have been added to the control system of the VSC converter. Furthermore, in the top part, these figures show the performance of the active power and the bottom parts show the performance of the reactive power during the transient.

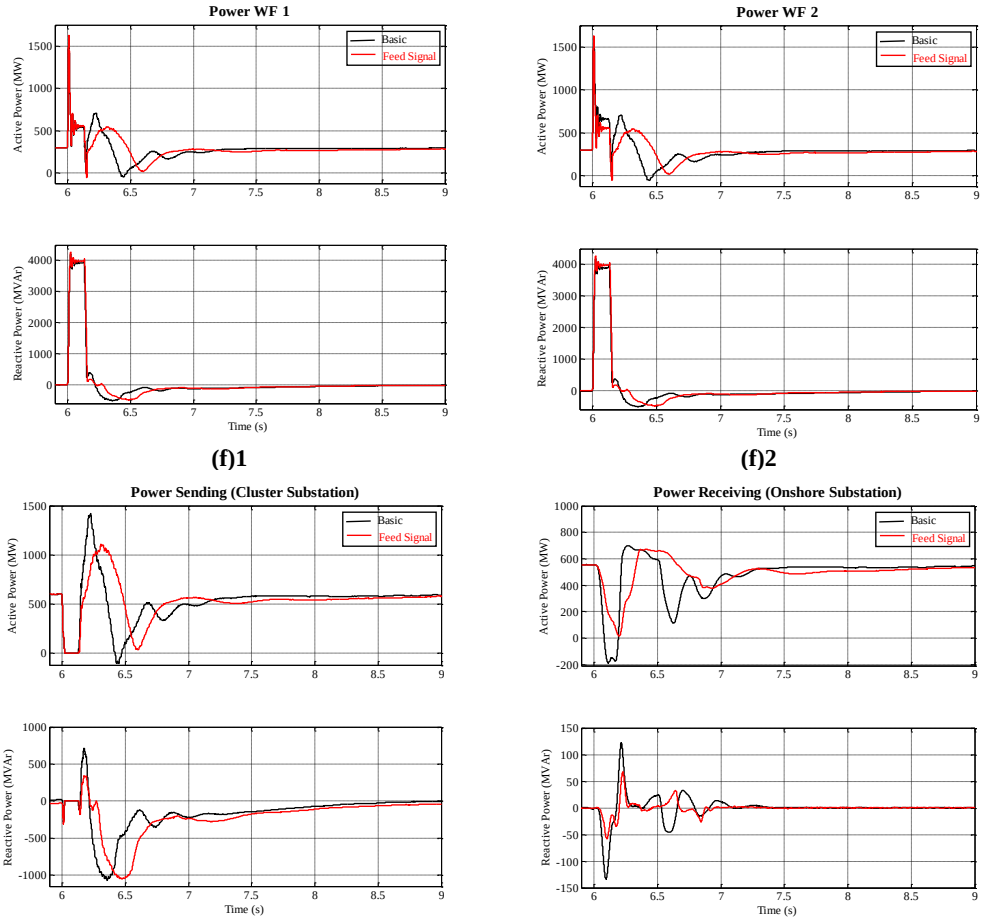

Figure 5-13: Transient responses for three-phase fault at the FRC scenario

Figure 5-13 (f)1 and (f)2 show the performance of the active and reactive power performances on the wind farm substations, WF1 and WF2. As mentioned, the above plots show the performance of the basic scenario and the scenario in which the feed-forward signals have been added to the control system of the VSC converter. In the top part, each figure shows the performance of the active power and the bottom part shows the performance of the reactive power. The introduction of the feed-forward technique has not changed the reaction of the power system during the first 0.25ms. It is after the first 0.25ms that the behaviour of the power system changes (red line). Thus, the maximum peak and also power system fluctuations have been reduced. In wind farm substations (WF1 and WF2) maximum power peak of the active power (red line) is around 500 MW while with the basic configuration is over 600 MW. In both scenarios the minimum of the active power is similar and thus is around 0MW. Furthermore, the reactive power performance is similar. However, the performance of the reactive power in both configurations are similar, the configuration within the feed-forward signals are installed the reactive power performance is slightly better. The performance of the active power in the offshore cluster substation is significantly

improved and thus in the feed-forward scenario, the peaks and troughs are significantly reduced by almost 400 MW (around 1500 MW to 1000 MW) and 100 MW (around -100 MW to just over 0 MW) respectively. The power fluctuation is also improved and the VSC-HVDC power system reach the steady state in a smoother transition, around 7.5sec. The reactive power performance is also improved and thus the maximum peaks is also reduced around 500 MVAr from a maximum peak around 1200 MVAr to 750 MVAr. Furthermore, the fluctuation of the reactive power is also significantly improved and thus the VSC-HVDC reaches the steady state smoother around 9s. In the onshore substation, Figure 5-13 (f)4, the minimum active power peak is significantly reduced and thus from a minimum of -200 MW (basic cinfiguration) to a minimum around 20MW. Thus, the active and reactive power behaviour in the onshore substation, Figure 5-13 (f)4, are also benefited by the implementation applied to the offshore substations.

In conclusion, even though the power behaviour has been changed, the control system in the offshore array ensure the complete recovery of the power system within the fault ride-through standards. Furthremore, the introduction of the feed-forward technique improves the behaviour of the power system and thus the small increment of the k_p and the k_i have significant benefit. In addition, the maximum and minimum peaks and thus the fluctuations of the power system have been improved.

5.4.2.3.2 Transient Analysis: Voltage and Current Analysis.

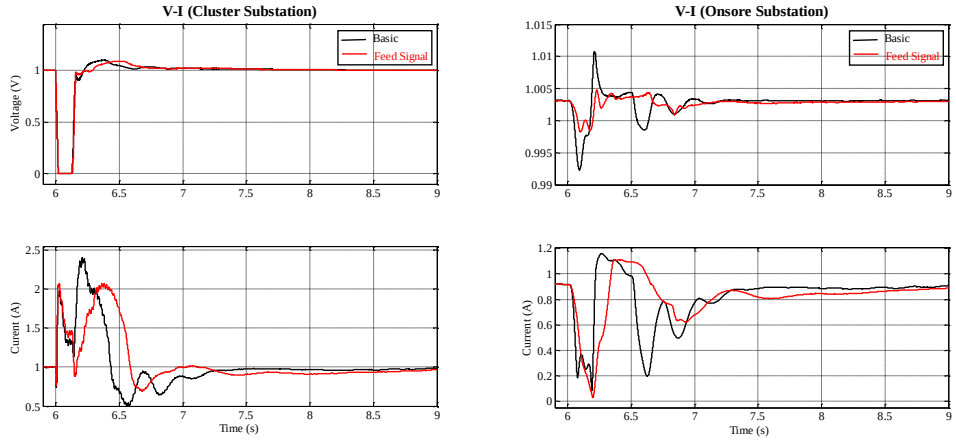

(f)5 **(f)6**

Figure 5-13: Transient responses for three-phase fault at the FRC scenario

As can be seen in both figures, the feed-forward technique implemented in the offshore cluster substation improves significantly the current performances in both substations (offshore and onshore). It also improves slightly the behaviour of the voltage but not as significantly as the current. The voltage transition, in the offshore substation, to the steady

state is slightly better achieved. In the onshore substation, the peak and troughs of the voltage are a bit reduced, from a maximum peak around 1.01 pu to a 1.005 pu and from a minimum around 0.99 pu to around 0.999 pu. The curent peak, in the offshore substation, is decreased around 0.5 pu and the trough around 0.25 pu. The implementation also reduces significantly the fluctuations of the current. In the onshore substation, the current peaks and troughs are slightly improved which makes the transition to the steady state smoother.

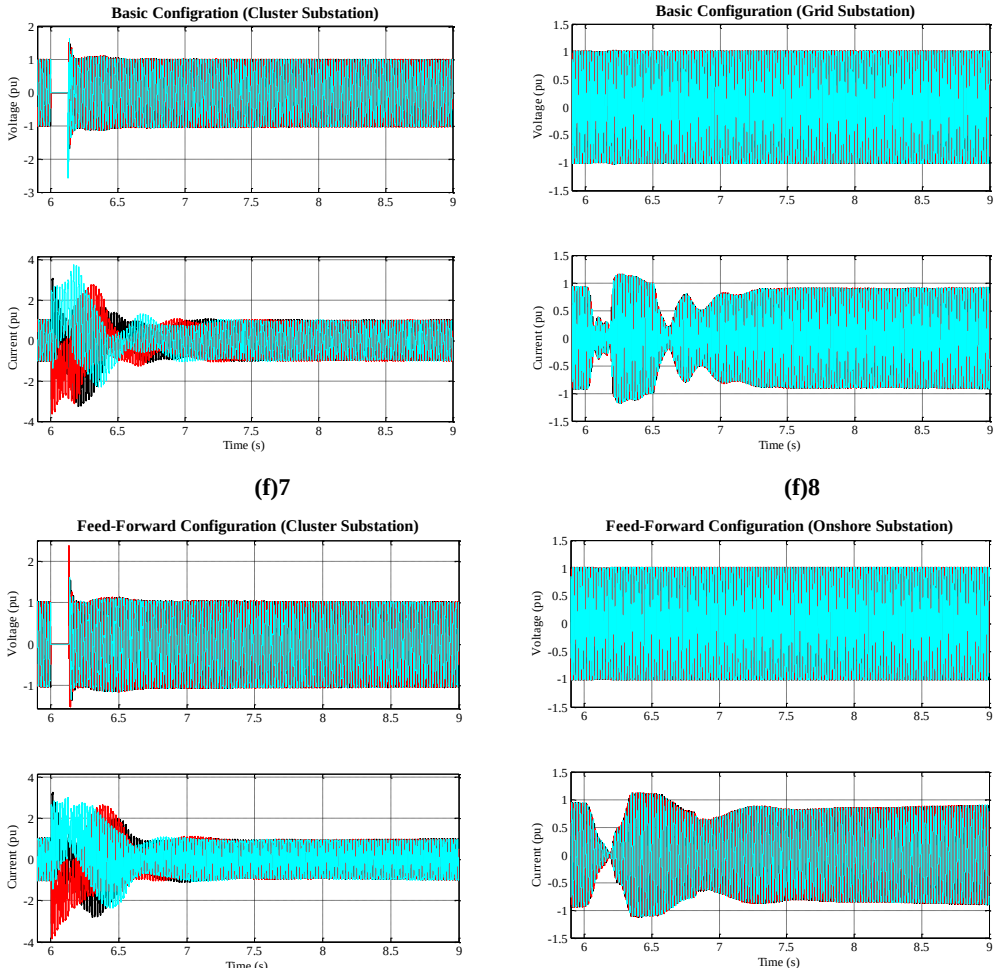

Figure 5-13: Transient responses for three-phase fault at FRC scenario

The introduction of the feed-forward signals has improved the overall behaviour of the AC voltages and AC currents. Clearly, the feed-forward signals produce an important impact in the behaviour of the AC currents which recover the steady state faster than the basic configuration, Figure 5-13 (f) 9 and Figure 5-13 (f) 9. The high current peaks produced by the large transient are significant mitigated and thus these peaks are reduced by almost 2 pu. Furthermore, the high fluctuations are also reduced and thus the offshore power system reach the steady state around 7 seconds while in Figure 5-13 (e) 9 reaches the steady state around 7.5 sec. In terms of the onshore substation, the AC voltage is not affected. In contrast, the AC

current in the onshore substation is slightly affected by the conversion of the transient. Thus, it produces fluctuations in the AC currents. The implementation of the feed-forward signals in the offshore substation has also improved the behaviour of the current and reducing peaks and troughs and the fluctuation of the power system.

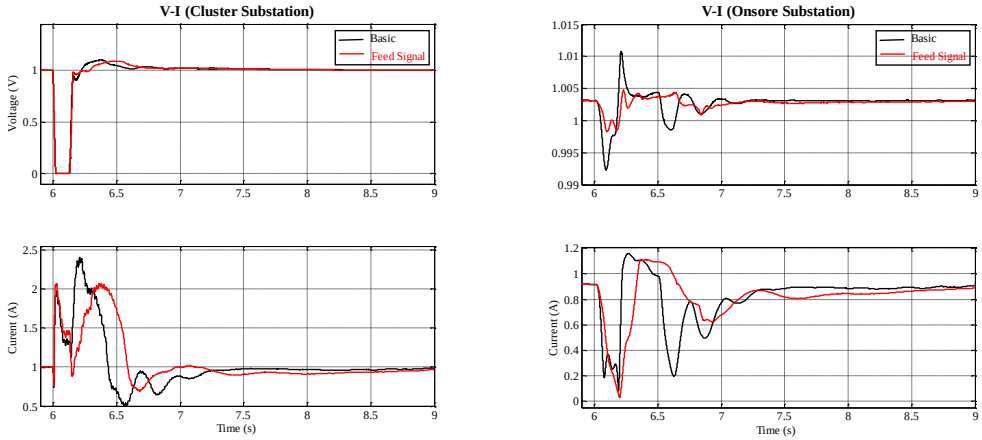

(f) 3 **(f) 4**

Figure 5-13: Transient responses for three-phase fault at the FRC scenario

As can be seen in Figure 5-13 (f)11 and (12), the feed-forward technique implemented in the offshore cluster substation improves significantly the current performances in both substations (offshore and onshore). It also improves slightly the behaviour of the voltage but not as significantly as the current. The voltage transition, in the offshore substation, to the steady state is slightly better achieved. In the onshore substation, the peak and troughs of the voltage are a bit reduced, from a maximum peak around 1.01 pu to a 1.005 pu and from a minimum around 0.99 pu to around 0.999 pu. The curent peak, in the offshore substation, is decreased around 0.5 pu and the trough around 0.25 pu. The implementation also reduces significantly the fluctuations of the current. In the onshore substation, the current peaks and troughs are slightly improved which makes the transition to the steady state smoother.

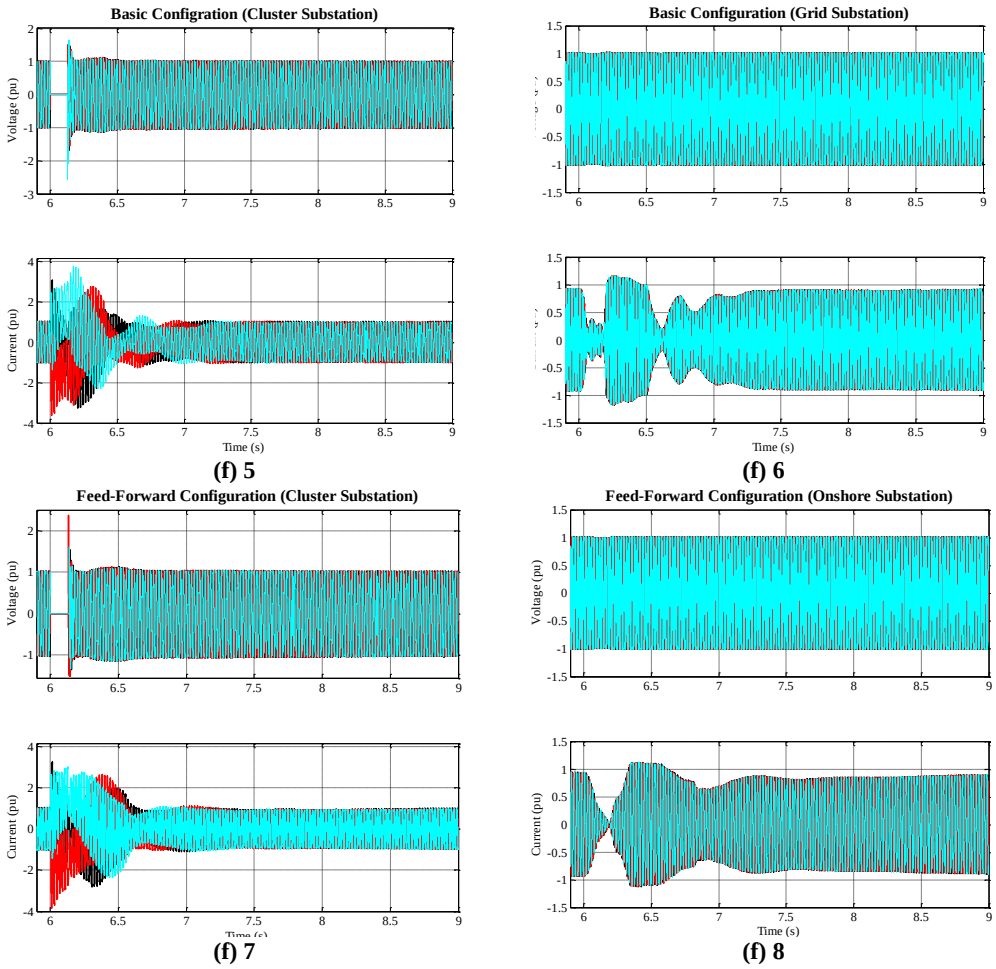

Figure 5-13: Transient responses for three-phase fault at FRC scenario

The introduction of the feed-forward signals into the basic configuration has improved the overall behaviour of the AC currents. These produce an impact in the behaviour of the AC currents which recover the steady state faster than the basic configuration (Figure 5-13 (f)13 and Figure 5-13 (f)14). Thus, the high current peaks produced by the large transient are significant mitigated. Furthermore, the current fluctuations are also reduced and thus the offshore power system reach the steady state around 7s while in the Figure 5-13 (e)13 reaches the steady state after 7s. In terms of the onshore configuration, the AC voltage is not significantly affected by the large transient. In contrast, the AC current in the onshore substation is slightly affected by transient. This produces fluctuations in the AC currents. The implementation of the feed-forward signals in the offshore substation has also improved the behaviour of the current in the onshore substation. These current peaks and troughs are reduced.

In conclusion, in this scenario the behaviour of the electrical power systems - offshore/onshore grids - have been improved through the implementation taken from the wind farms (WF1 and WF2). The implementation of feed-forward signals allows the

modification of the k_p and k_i parameters of the inner and outer current in both sides of the VSC-HVDC power system. Thus, the control system of the VSC converter can react faster to any disturbances.

5.4.3 Case Study 2.3 Mixed Scenario: Grid Fault Analysis

The structure of the Mixed scenario is composed of one DFIG and one FRC wind farms. Furthermore, the offshore layout has the same characteristics as the previous two layouts but the value of the phase reactance installed in the offshore cluster substation has been increased from 0.25 pu to 0.45 pu. This increment in the value of the phase reactor has been done because of stability problems.

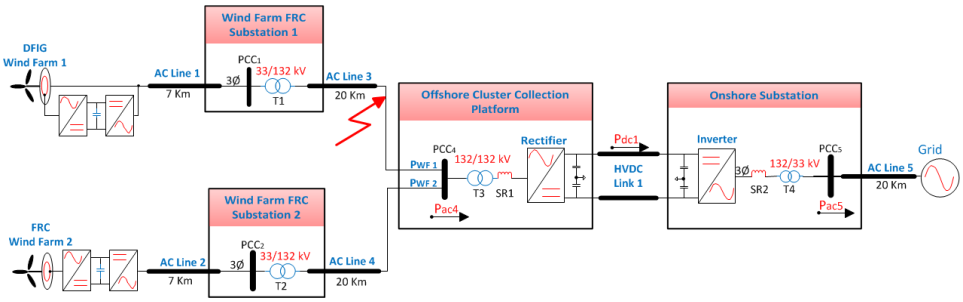

Figure 5-14: A block diagram of the DFIG scheme

Due to the change in the phase reactor of the offshore substation, higher reactive power peaks have been observed during the initialisation of the power system. The control system of the VSC-HVDC power system manages to control the entire system and reach the steady state after a few seconds. In contrast, the power flow fluctuations observed - in the initialization of the VSC-HVDC system - in previous scenarios have been avoided.

5.4.3.1 Mathematical Analysis: PI Controllers

The mathematical technique used to calculate the values of the PI controllers in the previous, DFIG scenario, has also been used to calculate the value of the PI parameters in this section. The imposed switching frequency of the IGBT switches in the offshore VSC converters is 2.25 kHz and the onshore is 3 kHz. The delay time produced by the switching of the IGBT valves is calculated as follows:

$$T_a(offshore) = \frac{T_{switch}}{2} = \frac{1}{2f_{switch}} = \frac{1}{2*2250} = 222\mu s \quad (5.72)$$

$$T_a(onshore) = \frac{T_{switch}}{2} = \frac{1}{2f_{switch}} = \frac{1}{2*3000} = 166.666\mu s \quad (5.73)$$

5.4.3.1 Offshore Analysis: Offshore PI Controllers

To simplify the calculation of the PI parameters and also to obtain the time delay between the wind farm and the offshore cluster substation, the delay time of each component is applied into only one transmission line [146]. Figure5-15 shows the scheme used to calculate the parameters of the offshore PI controllers.

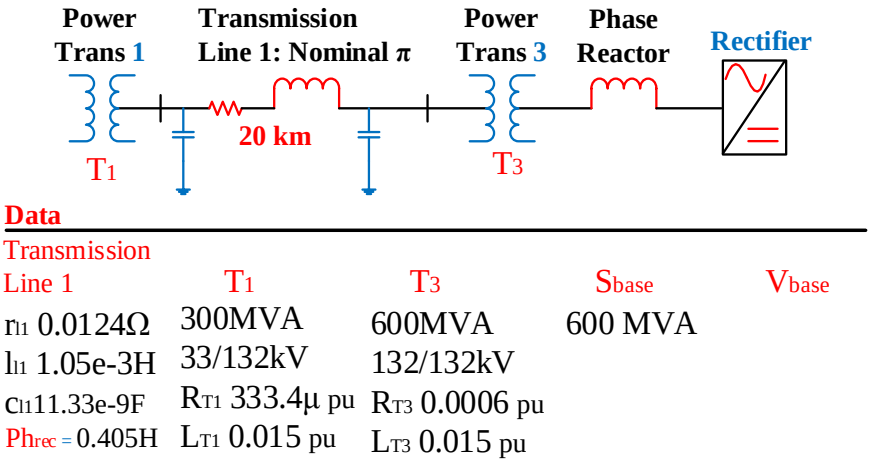

Figure 5-15: A basic diagram of the offshore power system

The delay time produced by each component of the examined layout is calculated as follows, for more information see 5.4.1.2 PI Controller: Mathematical Analysis. The integration time of the phase reactor system, τ_{ph-rec}, is calculated as follows [76, 140], [64, 68]:

$$L_{Phrec-pu} = \frac{LZ_{Base}}{\omega_b} = \frac{L\left(V_{ac}^2/S_n\right)}{\omega_b} = \frac{0.405\left(132k^2/600x10^6\right)}{2\pi 50} = \frac{11.7612}{314.16} = 0.03744\ pu \quad (5.74)$$

$$L_{Phrec-pu} = 0.03744\ pu$$

$$\tau_{ph-rec} = \frac{0.9*0.03744}{314.14(183.712k-132k)} 0.612V_{dc} \approx 0.000381s \quad (5.75)$$

The total impedance and resistance of the power transformers (T1 and T3) and transmission cable (Line 1) are given by (for more information see Appendix B).

$$l_{pu} = Z_{l_{T1}-pu.new} + l_{l1-pu.new} + Z_{l_{T3}-pu.new} = 1.875e^{-3} + (7.77e^{-3} - 2.452e^{-6}) + 0.015 = 0.0172pu \quad (5.76)$$

$$L_{pu-tot} = L_{T1-pu} + L_{Phrec-pu} = 0.0172 + 0.03744s = 0.05464 \quad (5.77)$$

The total delay time, $T_{i-total}$, of the offshore layout is calculated as follows:

$$r_{pu-total} = 3.33e^{-4} + 0.092 + 0.0006 = 0.093pu \quad (5.78)$$

$$\tau_{pu} = \frac{l_{pu-total}}{r_{pu-total} * \omega_b} = \frac{0.055}{0.093 * 314.16} = 1.883e^{-3}s \quad (5.79)$$

$$T_{i-total} = \tau_{pu} + \tau_{ph-rec} = 1.883e^{-3} + 0.000381 = 2.31e^{-3}s \quad (5.80)$$

The k_{p1} and the k_{i1} are calculated as follows [50, 70, 71, 76, 141]:

$$k_{p1} = \frac{T_{i-total} * r_{pu-total}}{2T_a} = \frac{2.31e^{-3} * 0.093}{2 * 222.22\mu} = \frac{2.11e^{-4}}{444.44e^{-6}} = 0.474 \quad (5.81)$$

$$k_{i1} = \frac{k_p}{T_i} = \frac{0.474}{2.31e^{-3}} = 205.04 \quad (5.82)$$ 83

The damping factor of the calculated offshore scheme is given as follows [76]:

$$\zeta = 0.5\sqrt{\frac{2.31e^{-3} * 0.093}{0.474 * 222.22\mu}} = 0.5\sqrt{\frac{2.15e^{-4}}{1.1e^{-4}}} = 0.5 * 1.398 = 0.699 \quad (5.84)$$

In this simulation, the charging time of the DC capacitors "offshore and onshore" is computed at 375ms and thus the value of the capacitor is calculated as follows (more information see equation 3.17):

$$C_{dc} = \frac{2S_n * \tau_{Vdc}}{V_{dc}^2} = \frac{2 * 600x10^6 * 375x10^{-3}}{(300x10^3)^2} = \frac{225x10^8}{9x10^{10}} = 0.0025F = 2500\mu F \quad (5.85)$$

5.4.3.2 Onshore Analysis: Onshore PI Controllers

The optimum symmetrical technique has again been used to calculate the parameters of the onshore PI controllers. In order to obtain the parameters of the DC controller, the phase margin criterion "theta angle" is set at 45° and therefore the "a" parameter is set at 45°. Furthermore, the integration time is equal to $T_i = a^2 * T_{eq}$and thus the transfer function is tuned as follows [50, 115, 142, 143]:

$$a = \frac{1+\cos 45}{\sin 45} = 2.4142 \quad (5.86)$$

$$T_i = a^2 * T_{eq} = a^2 * 4 * T_a = 2.4142^2 * 4 * 166.666\mu = 0.00392 \quad (5.87)$$

The control parameters for the DC controller are given as follows [50, 71, 141, 143]:

$$k_{p3} = \frac{4C_{dc}}{9*a*V_{d,dc}T_i} = \frac{4*2500e^{-6}}{9*2.4142*1*0.00392} = 0.11741 \quad (5.88)$$

$$k_{i3} = \frac{k_p}{T_i} = \frac{0.11741}{0.00392} = 29.952 \quad (5.89)$$

The parameters of the onshore scheme are calculated similarly to the offshore parameters and therefore for the values for the inner and outer current controllers are calculated as follows [76, 140], [64, 68]:

$$L_{phrec-pu} = \frac{LZ_{Base}}{\omega_b} = \frac{0.405\left(132k^2/_{600x10^6}\right)}{2\pi 50} = 0.0363pu \quad (5.90)$$

The m_a is set to be at maximum value and thus the delay time of the system is given:

$$\tau_{ph-inv} = \frac{0.9*o.0363}{314.16(183.712k-132k)}0.612V_{dc} \approx 3.6922ms \quad (5.91)$$

The total delay time, $T_{i-total}$, of the onshore layout is calculated as follows:

$$\tau_{trafo1} = \frac{L_{pu}}{r_{pu}*\omega_b} = \frac{0.015}{0.00266*314.16} = 0.018s \quad (5.92)$$

$$\tau_{i-cable} = \frac{7.76e^{-3}}{0.09176*314.16} = 269.2\mu s \quad (5.93)$$

$$T_{i-total} = \tau_{ph-rec} + \tau_{trafo1} + \tau_{i-cable} = 3.6922m + 0.018 + 269.2\mu += 0.02196$$

The k_{p4} and the k_{i4} are calculated as follows [70, 71, 76]:

$$k_{p4} = \frac{T_{i-total}*r_{pu-total}}{2T_a} = \frac{0.02196*0.09236}{2*166.66\mu} = \frac{2.028m}{333.32\mu} = 6.1 \quad (5.94)$$

Where $r_{pu\text{-}inv}$ is $r_{pu-inv} = r_{pu-T_4} + r_{pu-cable} = 0.0006 + 0.09176 = 0.09236$

$$k_{i4} = \frac{k_{p4}}{T_{i-total}} = \frac{6.1}{0.02196} = 277.77 \quad (5.95)$$

The damping factor of the onshore scheme can be calculated as follows [76]:

$$\zeta = \frac{1}{2}\sqrt{\frac{T_{i-total}*r_{pu-total}}{k_{p4}*T_a}} = 0.5\sqrt{\frac{0.02196*0.09236}{6.1*166.666\mu}} = 0.5\sqrt{\frac{0.00203}{0.001016}} = 0.5*1.413517 = 0.711 \quad (5.96)$$

Table 5-8: PI parameters of the inner and outer current controllers and DC controller.

Calculated Scheme Offshore Control Loop				**Calculated Scheme Onshore Control Loop**					
Inner Controller		Outer Controller		DC Controller		Inner Controller		Outer Controller	
k_{p1}	0.474	k_{p2}	------	k_{p3}	0.12	k_{p4}	6.1	k_{p5}	------
k_{i1}	205.04	k_{i2}	------	k_{i3}	29.95	k_{i4}	277.8	k_{i5}	------

Basic Co-ordinate Control Scenario Offshore Control Loop				Basic Co-ordinate Control Scenario Offshore Control Loop					
Inner Controller		Outer Controller		DC Controller		Inner Controller		Outer Controller	
k_{p1}	0.65	k_{p2}	7.5	k_{p3}	5.0	k_{p4}	1	k_{p5}	0.005
k_{i1}	4.0	k_{i2}	50	k_{i3}	15	k_{i4}	150	k_{i5}	0.0017
Co-ordinate control Scenario with a Feed-Forward Scheme Offshore Control Loop				**Co-ordinate control Scenario with a Feed-Forward Scheme Onshore Control Loop**					
Inner Controller		Outer Controller		DC Controller		Inner Controller		Outer Controller	
k_{p1}	0.65	k_{p2}	7.5	k_{p3}	4.0	k_{p4}	1.0	k_{p5}	0.005
k_{i1}	4.5	k_{i2}	50	k_{i3}	15	k_{i4}	259	k_{i5}	0.0017

The most significant difference between the PI parameters shown in the above table is between the calculated scheme "k_{i1}" and the implemented k_{i1} values in the basic and the feed-forward scenarios). The calculated value is significantly higher and therefore, it is possible to assume that the integration time T_i needs to include other timing factors.

5.4.3.2 Mixed Scenario: Power Losses Calculation

The AC offshore layout is basically equal to the two previous examples and therefore should produce similar power losses and also similar power flows (active and reactive power flows). Thus, the values of the theoretical power losses, the expected power losses should be similar to the previous calculation and thus it has been decided to avoid further calculation of the VSC-HVDC power system. For further information on the power losses of the VSC-HVDC power system see Section 5.4.1.3 Power Losses Calculations.

5.4.4.2 Grid Fault Analysis

5.4.4.2.1 Transient Analysis: Power Analysis

The following plots show the performance of two different control systems. A basic coordinate control scenario "Basic Scenario" with the coordinated power control and the control system which has implemented the feed-forward idea (this scenario also has the coordinated power control). Figure 5-16 shows the transient responses for three-phase fault at Mixed configuration: (g)1 shows the active and reactive power performances at wind farm substation WF1, (g)2 shows the active and reactive power performances at wind farm substation WF2, (g)3 shows the active and reactive power performances at offshore cluster substation, (g)4 shows the active and reactive power performances at onshore substation and (g)5 shows the DC voltage in HVDC link.

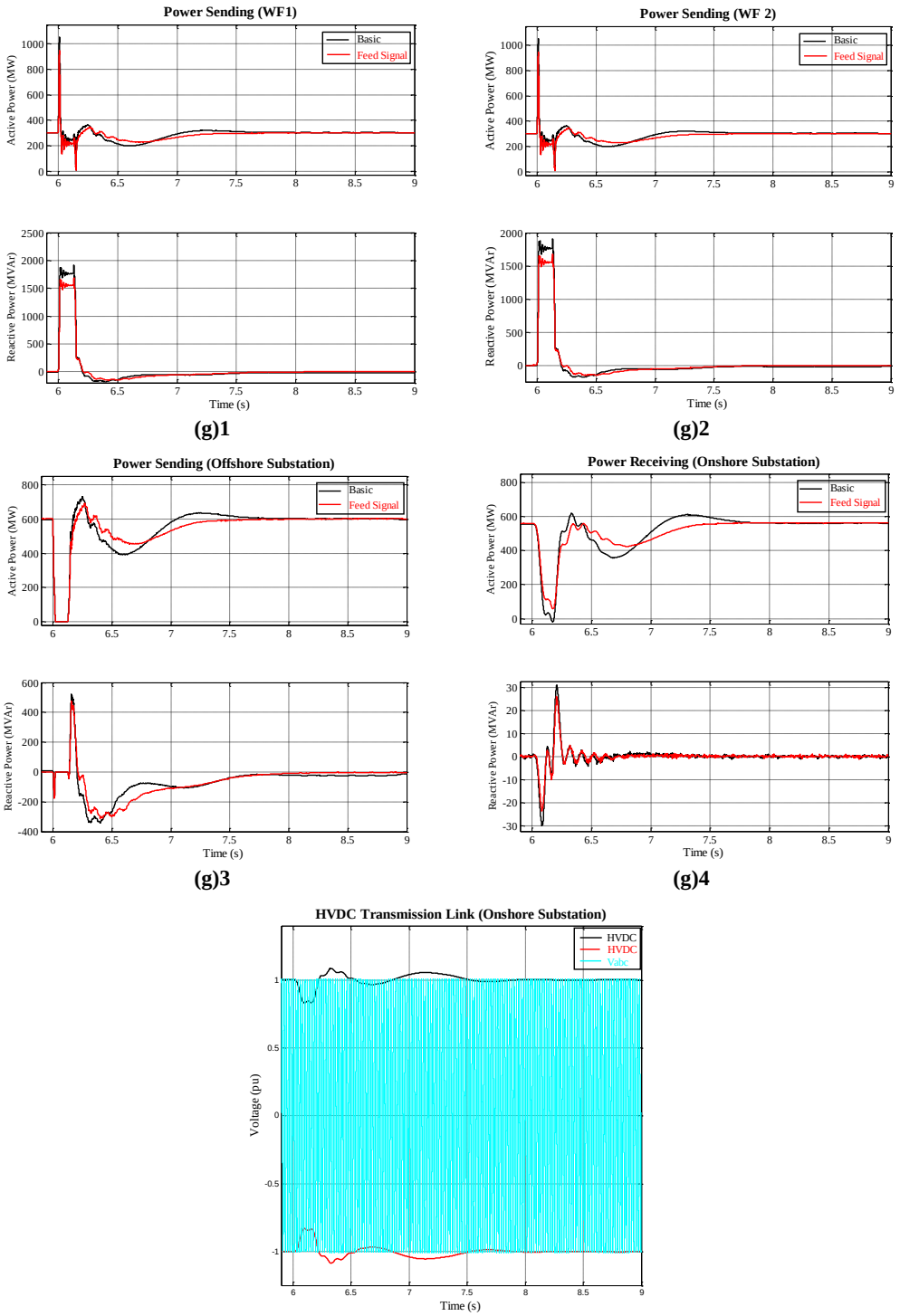

Figure 5-16: Transient responses for three-phase fault at the Mixed scenario

As mentioned, Figure 5-16 (g)1 and (g)2 show the performance of the active and reactive power performances on the wind farm substations. The WF1 is a DFIG wind farm and the WF2 is a FRC wind farm. However, the behaviour of the offshore power system has changed with the introduction of two different power sources; the reaction control system of the cluster substation after the transient is cleared is similar to the two previous sections and thus achieves the recovery of the entire VSC-HVDC power system appropriately and also

without major difficulties. Furthermore, in both scenarios the active power performances are similar and there are no major differences. Thus, the power peaks and the power system fluctuations produced by the transient are almost complementary. The reactive power performances are significantly different. The transient significantly affects the reaction of the reactive power and the peaks in the feed-forward scenarios are between 200 to 400 MVAr less high. The performance of the active power in the offshore cluster substation (in both simulations) are also similar. The Basic scenario and the Feed-Forward scenarios do not produce major changes in the peaks or trough of the active power or power system fluctuations. The major difference that can be observed is in the troughs which has been reduced by 100 MW, Figure 5-16 (g)3. The transition to the steady state is also smoother. In terms of reactive power, bottom part of Figure 5-16 (g)3, it can be observed that the trough has been slightly reduced and the fluctuations produced by the transient has been almost eliminated in the offshore power system. Furthermore, due to the most accurate control of the power system achieved in the feed-forward scenario; the active power performance in the onshore scenario is also improved and thus the maximum and minimum power peaks are slightly reduced Figure 5-16 (g)4. Moreover, the fluctuations are significantly improved and thus the VSC-HVDC power system reaches the steady state more smoothly around 8s. The reactive power performance is almost equal.

In conclusion, the combination of diferent generation elements do not alter significantly the control system of the offshore substation. However, the control system is not significantly altered, the phase reactor needed to be modifed. Thus, this could be the reason for which the active and reactive power performance is significantly different from the previous section. As it is possible to observe, the modification applied in the structure of the offshore array does not affect the control system of both offshore and onshore substations (VSC converters). Thus, the coordinated control restores the power transferred from the offshore substation without causing important alteration in the VSC-HVDC power system. In addition, the implementation of feed-forward signals allows the modification of the k_p and k_i parameters of the inner and outer current in both sides of the power system, thus improving the power system performance. Furthermore, the feed-forward modification also reduces the power system fluctuations.

5.4.3.3.2 Transient Analysis: Voltage and Current Analysis

This section shows the sinusoidal analysis of two mentioned scenarios: the basic and the feed-forward signal scenarios. Both figures show the behaviour of the AC voltages and

AC currents at the offshore/onshore substations at the PCC_4 and PCC_5 in Figure 5-14. Figure 5-16 (g)6 and (g)7 show voltages and currents at the offshore and onshore substations in per unit values.

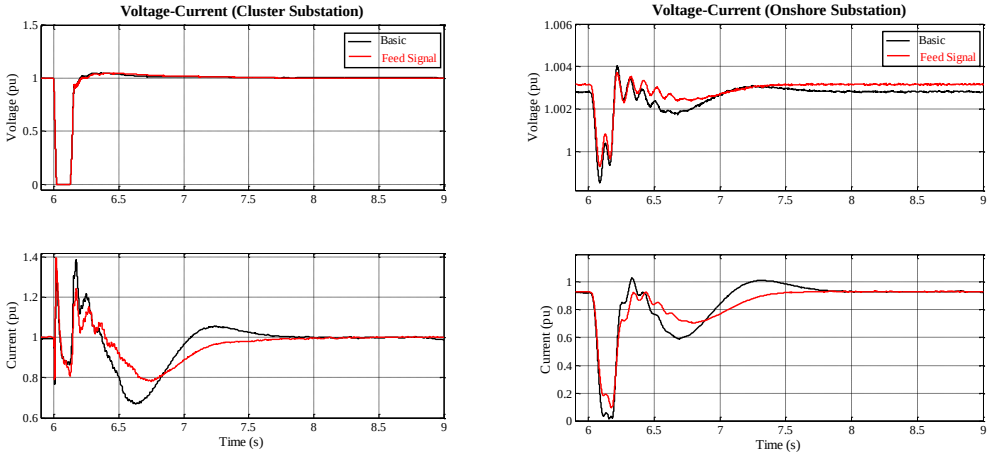

(g)6 **(g)7**

Figure 5-16: Transient responses for three-phase fault at the Mixed scenario

In Figure 5-16 (g)6, the voltage in the offshore cluster substation is not sigifiantly affected by the aforementioned implementation (in any of the two simulation cases). In contrast, In Figure 5-16 (g)7, the fluctuations on the voltage is slightly improved. The voltage drop is also slightly mitigated. In Figure 5-16 (g)6 and also in in Figure 5-16 (g)7, the current is significantly improved. Furthermroe, the current peaks and troughs are also reduced and thus the VSC-HVDC power system reaches smoothly to the steady state. In Figure 5-16 (g)8 and Figure 5-16 (g)10 show the sinusoidal AC voltage performance in the offshore cluster substations and Figure 5-16 (g)9 and Figure 5-16 (g)11 in the onshore substations.

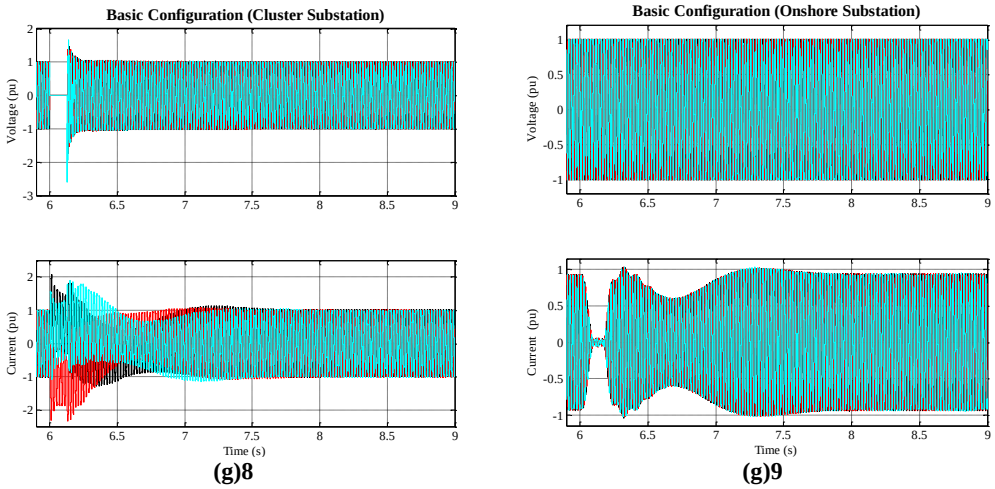

(g)8 **(g)9**

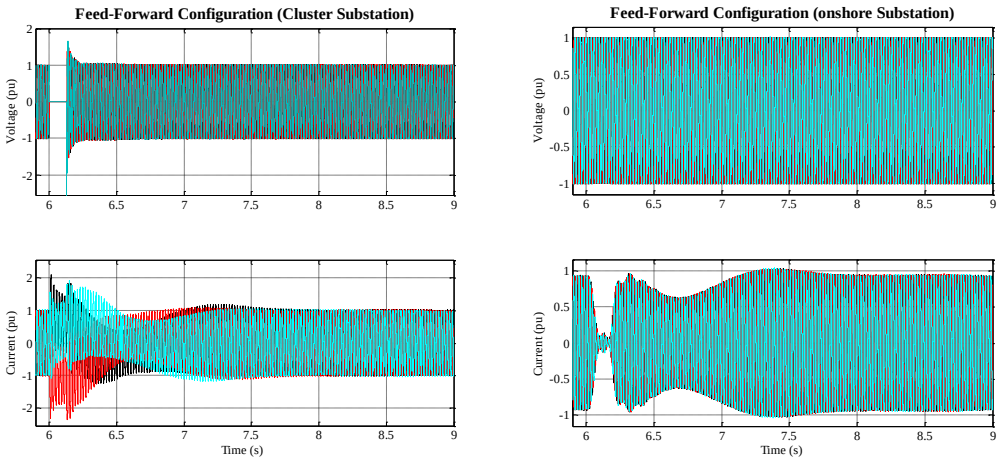

(g)10 **(g)11**

Figure 5-16: Transient responses for three-phase fault at the Mixed scenario

However, in this case study, the feed-forward implementation just produces a slight improvement on the performance of the AC voltage and current, it still improves the behaviour of the VSC-HVDC power system. The dynamic performance of the Mixed scenario is substantially different from previous scenarios. The combinations of the DFIG and FRC wind farms have significantly altered the power flow. Nevertheless, the alteration of the power flows in the offshore scenario does not significantly affect the VSC converter control and thus this recovers the steady state of the power system into grid standards without creating serious hazards.

5.5 Summary

To conclude, simulation results have validated the effectiveness of the applied modifications in the power control system of the VSC converter and thus in this chapter, it has validated the different control system modifications presented in Chapter 3, Chapter 4 and Chapter 5. Results have also validated specific modifications (feed-forward signals) applied in the control system offshore cluster substation which was shortly presented in this chapter.

Chapter 6: Coordinated Control for Meshed Multi-Terminal System

Chapter 6 presents a multi-terminal power system scenario with two onshore connection points. In this chapter, the coordinated control with the feed-forward signals introduced in the control system of the offshore cluster substation is analysed with a multi-terminal scenario. Furthermore, the purpose of this chapter is to verify that the controller system of the VSC-HVDC power system can still recover the power system after a large transient is triggered. Furthermore, the second intention of this simulation is to verify if the control system can re-direct the sending power from the offshore side to one connection point if one of the onshore connection points is disconnected.

6.1 Introduction

This VSC-HVDC power system example could be linked to one of the North Sea projects. The North Sea is one of the biggest potential areas for developing offshore wind energy resources in the European Union, [7], and thus help to create the Supergrid, (NSSG and NSCOGI) [7, 50, 147-150]. Therefore, the objective of this offshore infrastructure (MTDC grid) is to integrate large amounts of renewable power into onshore grids and also encourage power exchange between North Sea countries [149, 151]. The scenario in Figure 6-1 is proposed to fulfil one of the objectives of a multi-terminal offshore scenario (Offshore Grid and Statnett, [152, 153]).

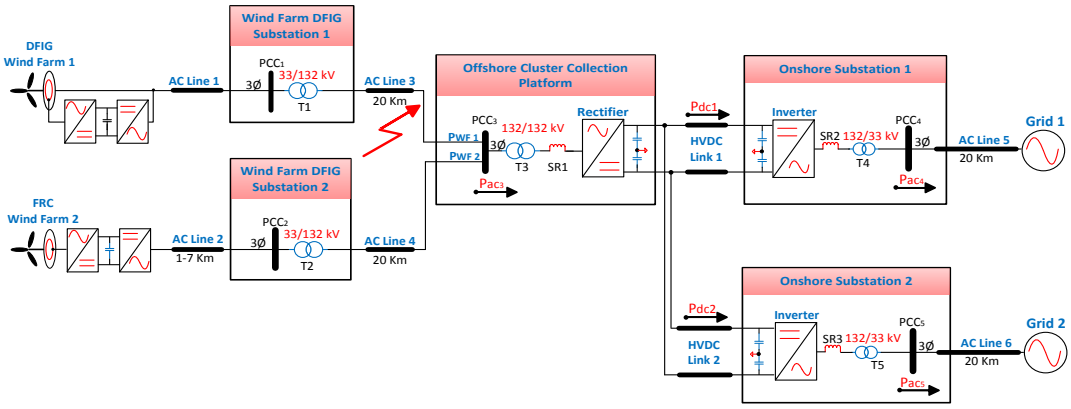

Figure 6-1: multi-terminal scenario

6.1.1 Challenges in Developing a Meshed Scenario

Furthermore, to understand the behaviour of the offshore system, it is necessary to understand the performance of its AC voltage and frequency. The normal operation of the

offshore layout should be similar to the onshore layout - the offshore power system should work within 1% of the frequency bandwidth around the normal frequency operation - 50Hz - and thus the frequency drop during normal operation should not be higher than ± 0.5 Hz, so 1%. During large transients, the offshore power system should operate in a range between 105% and 95% (if the frequency overstepped this range the power system operators must disconnect the entire power system) [12, 117]. Furthermore, in order to connect this power system and thus to stabilize a secure offshore power system; the offshore grid codes must be defined and establish periods where power plants must remain connected and help the power system by providing reactive power support [116, 117, 137].

The proposed control strategy is based on the control system analysed in Chapter 5. Thus, the control system in which the feed-forward signals are added to the control system of the offshore cluster substation is evaluating the multi-terminal power system. To simplify the analysis of the power MTDC, this thesis has evaluated the control system when the power flow is sent from offshore to onshore; so, only in one direction. It has not been attempted to change the power flow direction.

6.2 Modelling and Controlling a Multi-Terminal Power System

The control strategy of the MTDC is based on the idea of a master-slave control system (master-slave structure). This control method is used to integrate the MTDC power system into conventional AC power grids. The master substation (in this case study is the offshore substation) has entire control of the power system and therefore can decide which onshore substation is receiving the offshore power. Furthermore, the strategy for the control system of the MTDC is designed with the same idea applied in Chapter 5. Thus, the offshore cluster substation regulates the AC voltage by using a voltage controller. This voltage controller sets the AC voltage and also the frequency of the offshore system at the rated values. In the onshore substation, the DC controller controls the transferred DC power.

In this case study, the power transferred from the offshore cluster substation to the onshore substation is 900 MW, each wind farm produces 450 MW. The AC cables which link the wind farms with the cluster substation are rated at 132kV and the AC cables which link the wind farm substations with the wind turbines are rated at 33 kV. Furthermore, both DC transmission lines (HVDC links) are rated at ±150 kV. In this case study a large transient is also triggered in the offshore substation to test the overall performance of the offshore system. The first onshore connection, Grid 1has a length of 125 km and the second onshore connection, Grid 2, has a length of 165 km (HVDC link 2) respectively, see Figure 6-1.

Furthermore, this case study is set to share the offshore power equally in both substations. However, both onshore substations are rated equally, the transferring power could be influenced by the length of the DC transmission cable. Therefore, the power received in both substations could be different, $P_{dc1} \neq P_{dc2}$.

The equations equation for the control system of the offshore and onshore substation can be found in Section 3 from 3.5 until 3.3.1.

The total power transfer from the offshore substation to Grid 1 and Grid 2 is given as follow:

$$P_{dc-Grid1} = 300e^3 * 1.85e^3 = 555MW \quad (6.1)$$

$$P_{dc-Grid1} = 300e^3 * 85e^3 = 255MW \quad (6.2)$$

6.2.1 PI Controllers: Mathematical Analysis

The proposed multi-terminal scenario has the same characteristics as the Mixed scenario presented in the Chapter 5, section 5.4.3. Thus, the calculated values of the offshore and also onshore PI controllers are taken from this section. In the case of Grid 2, this thesis has assumed that the characteristic of these grids is similar to Grid 1 and therefore the calculated k_p and k_i values of the DC controller of Grid 1 can initially applied to the DC controller and the inner and outer current controller in the Grid 2. Figure 6-2 shows the analysed MTDC structure.

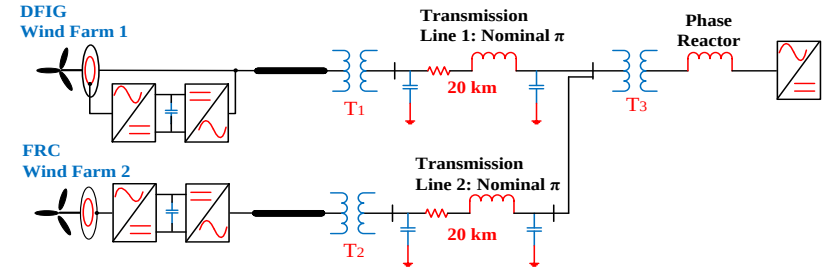

Data					
Transmission Line 1	Transmission Line 2	T1	T2	T3	VSC-HVDC
R_{l1} 0.0124Ω	R_{l2} 0.0124Ω	450MVA	450MVA	900MVA	900 MVA
L_{l1} 1.05e-3H	L_{l2} 1.05e-3H	33/132kV	33/132kV	132/132kV	± 150 kV
C_{l1}11.33e-9F	C_{l2}11.33e-9F	R_{T1} 0.08/30 pu	R_{T2} 0.08/30 pu	R_{T3} 0.0006 pu	
Ph_{rec} = 0.25mH		L_{T1} 0.015 pu	L_{T2} 0.015 pu	L_{T3} 0.015 pu	

Figure 6-2: Diagram of the offshore power system

However, both system have the same characteristics, there is one significant difference in this multi-terminal approach; the value of the phase reactor is reduced to 0.25mH.

6.2.1.1 Offshore Analysis: PI Controllers

The reaction of the converter depends on the delay time of the offshore layout which the sum of the delay time of each component. Thereby, this thesis has decided to calculate

delay time from the wind farm substation and to the cluster substation The integration time of the phase reactor system, τ_{ph-rec}, is calculated as follows [140], [64, 68]:

$$L_{Phrec-pu} = \frac{LZ_{Base}}{\omega_b} = \frac{L\left(V_{dc}^2/S_n\right)}{\omega_b} = \frac{0.25\left(132k^2/900x10^6\right)}{2\pi 50} = \frac{4.84}{314.16} = 0.0154\ pu \quad (6.3)$$

$$L_{Phrec-pu} = 0.0154\ pu$$

$$\tau_{ph-rec} = \frac{0.9*0.0154}{314.16(183.712k-132k)} 0.612V_{dc} \approx 1.572e^{-4}s \quad (6.4)$$

The total impedance and resistance of the power transformers (T1, T2 and T3) and transmission cables (Line 1 and Line 2) are given by:

$$L_{pu-tot} = Z_{l_{T1}-pu.new} + l_{l1-pu.new} + Z_{l_{T3}-pu.new} + L_{Phrec-pu} = 0.001875 + (5.24e^{-3} - 3.684e^{-6}) + 0.015 + 0.0154 = 0.0544 \quad (6.5)$$

The total delay time of the offshore is calculated as follow:

$$\tau_{pu} = \frac{l_{pu-tot}}{r_{pu-total}[7] *\omega_b} = \frac{0.0544}{0.08062 *314.16} = 2.15e^{-3}s \quad (6.6)$$

The total delay time, T_i, of the offshore layout is calculated as follows:

$$T_{i-total} = \tau_{pu} + \tau_{ph-rec} = 2.15e^{-3} + 1.572e^{-4} = 2.31e^{-3}s \quad (6.7)$$

The k_{p1} and the k_{i1} of the offshore substation are calculated as follow [50, 70, 71, 76, 141].

$$k_{p1} = \frac{T_{i-total} * r_{pu-total}}{2T_a} = \frac{2.31e^{-3}*0.07915}{2*222.22\mu} = \frac{1.842e^{-4}}{444.44e^{-6}} = 0.411 \quad (6.8)$$

$$k_{i1} = \frac{K_{p1}}{T_i} = \frac{0.411}{2.31e^{-3}} = 177.71 \quad (6.9)$$

The damping factor of the calculated offshore scheme is given as follows:

$$\zeta = \frac{1}{2}\sqrt{\frac{T_{i-total}*r_{pu-total}}{k_{p1}*T_a}} = 0.5\sqrt{\frac{2.31e^{-3}*0.07915}{0.411 *222.22\mu}} = 0.5\sqrt{\frac{1.83e^{-4}}{9.133e^{-5}}} = 0.5 * 1.4155 = 0.7077 \quad (6.10)$$

In this simulation, the charging time for the offshore and onshore DC capacitors are computed at 375ms and thus the value of the capacitors are calculated using the following equation (3.17):

[7] $r_{pu-total} = 0.01655 + 0.062 + 2.0666e^{-3} = 0.08062pu$

$$C_{dc} = \frac{2S_n * \tau}{V_{dc}^2} = \frac{2*600x10^6*375x10^{-3}}{(300x10^3)^2} = \frac{225x10^8}{9x10^{10}} = 0.0025F = 2500\mu F \quad (6.11)$$

6.2.1.2 Onshore Analysis: Onshore PI Controllers

The optimum symmetrical technique has again been used to calculate the parameters of the onshore PI controllers (the DC PI controller and the inner and outer current controllers). In order to obtain the parameters of the DC controller, the phase margin criterion "theta angle" is set at 45° and therefore the "a" parameter is set at 45°. Furthermore, the integration time is equal to $T_i = a^2 * T_{eq}$ and thus the transfer function is tuned as follow [50, 115, 142, 143]:

$$a = \frac{1+\cos 45}{\sin 45} = 2.4142 \quad (6.12)$$

$$T_i = a^2 * T_{eq} = a^2 * 4 * T_a = 2.4142^2 * 4 * 166.666\mu = 0.00392 \quad (6.13)$$

The control parameters for the DC controller are given as follows [50, 71, 141, 143]:

$$k_{p3} = \frac{4C_{dc}}{9*a*V_{d,dc}T_i} = \frac{4*2500e^{-6}}{9*2.4142*1*0.00392} = 0.11741 \quad (6.14)$$

$$k_{i3} = \frac{k_{p3}}{T_i} = 29.952 \quad (6.15)$$

Figure 6-3 shows the onshore power system scenario.

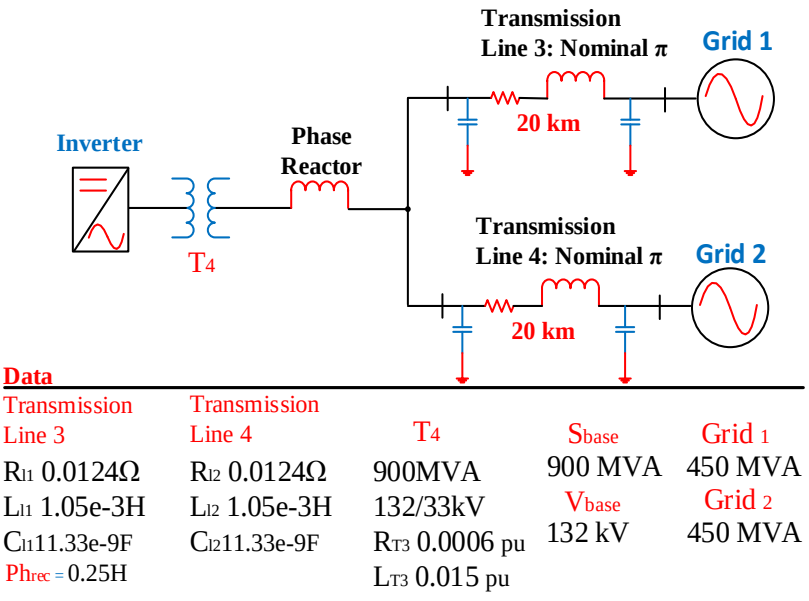

Figure 6-3: Diagram of the onshore power system

The parameters of the onshore scheme are calculated similarly to the offshore parameters and therefore for the values for the inner and outer current controllers are calculated as follows [140], [64, 68]:

$$L_{Phrec-pu} = \frac{LZ_{Base}}{\omega_b} = \frac{L\left(V_{dc}^2/S_n\right)}{\omega_b} = \frac{0.405\left(132k^2/900x10^6\right)}{2\pi 50} = \frac{7.8412}{314.16} = 0.025\ pu \quad (6.16)$$

The m_a is set to be at maximum value, and thus the integration time of the system is given by:

$$\tau_{ph-inv} = \frac{0.9*0.025}{314.16(183.712k-132k)} 0.612V_{dc} \approx 2.543e^{-4}s \quad (6.17)$$

The total impedance and resistance of the power transformers (T1, T2 and T3) and transmission cables (Line 1and Line 2) are given by:

$$L_{pu-tot} = l_{l1-pu.new} + Z_{l_{T3}-pu.new} + L_{Phrec-pu} = (5.24e^{-3} - 3.684e^{-6}) + 0.015 + 0.025 = 0.0452\ pu \quad (6.18)$$

$$r_{pu-total} = r_{pu-T_4} + r_{pu-cable} = 2.666e^{-3} + 0.062 = 0.0651\ pu \quad (6.19)$$

$$\tau_{pu} = \frac{l_{pu-total}}{r_{pu-total}*\omega_b} = \frac{0.0452}{0.0651*314.16} = 2.21e^{-3}s \quad (6.\ 20)$$

The total delay time of the onshore layout is calculated as follows

$$T_{i-total} = \tau_{pu} + \tau_{ph-rec} = 2.21e^{-3} + 2.543e^{-4} = 2.41e^{-3}s \quad (6.\ 21)$$

The k_{p4} and the k_{i4} are calculated as follows [70, 71, 76]:

$$k_{p4} = \frac{T_{i-total}* r_{pu-total}}{2T_a} = \frac{2.41e^{-3}*0.0651}{2*222.22\mu} = \frac{1.6043e^{-4}}{444.44e^{-6}} = 0.361 \quad (6.22)$$

$$k_{i4} = \frac{k_{p4}}{T_{i-total}} = \frac{0.361}{2.41e^{-3}} = 149.78 \quad (6.23)$$

The damping factor of the calculated onshore scheme is given as follows [76]:

$$\zeta = \frac{1}{2}\sqrt{\frac{T_{i-total}*r_{pu-total}}{k_{p4}*T_a}} = 0.5\sqrt{\frac{2.41e^{-3}*0.0651}{0.361*166.666\mu}} = 0.5\sqrt{\frac{1.57e^{-4}}{6.02e^{-5}}} = 0.5*1.615 = 0.812 \quad (6.24)$$

Table 6- 1: PI parameters of the inner and outer current controllers and DC controller

Calculated Scheme				**Calculated Scheme**					
Inner		Outer Controller		DC		Inner		Outer	
k_{p1}	0.411	k_{p2}	------	k_{p3}	0.12	k_{p4}	0.361	k_{p5}	------
k_{i1}	177.71	k_{i2}	------	k_{i3}	29.95	k_{i4}	149.78	k_{i5}	------

Calculated Scheme

Applied Offshore Control Loop				**Applied Onshore Grid 1 Control Loop**					
Inner		Outer Controller		DC		Inner		Outer	
k_{p1}	0.35	k_{p2}	7.5	k_{p3}	2	k_{p4}	1	k_{p5}	0.005

k_{i1}	2.05	k_{i2}	30	k_{i3}	15	k_{i4}	359	k_{i5}	0.0017

Applied Onshore Grid 1-2 Control Loop

6.2.3 Case Study 2.4 Multi-terminal

Even though the complexity of calculating a multi-terminal VSC-HVDC, the ABB report "*HVDC Light®: It's time to connect*" has been used as a reference to calculate the overall power losses of the VSC-HVDC system [144] [29].

6. 2.3.1 MTDC: Power Losses Calculations

The converter used to calculate the power losses of the ABB VSC-HVDC is the M9 [29]. Furthermore, result shown below is taken from a power system with DC cable's length of 100 Km. The DC voltage is also ±320 kV symmetric base modules.

$$\boldsymbol{P_{con-Losses} = \frac{P_{Sending}-P_{Reciving}}{2*P_{Sending}} * 100 = \frac{1215.3e^6-1186.7e^6}{2*1215.3e^6} * 100 = \frac{28.6e^6}{2430.6e^6} * 100 = 1.178\%} \quad (6.25)$$

The calculation power losses showed in (6.32) are similar to the calculated in previous sections.

6. 2.3.2 Obtained Power Losses: VSC-HVDC

The total power losses of the VSC-HVDC system which include Grid 1 and Grid 2 power losses are given by [29, 101].

$$P_{Con-Total\_Losses} = \frac{P_{Sending}-P_{Reciving}}{2*P_{Sending}} * 100 = \frac{900*10^6-780*10^6}{2*900*10^6} * 100 = \frac{120*10^6}{1800*10^6} * 100 = 6.66\% \quad (6.26)$$

The calculation power losses showed in (6.33) is higher to previous sections. The increase in the power transferred through the VSC-HVDC system and the fact that the DC voltage is maintain at ±150 kV has made that the power losses has increased significantly with respect to previous sections.

Table 6-2 shows the power losses for a VSC-HVDC transfer capability of 900MW and a DC cable length of 125 km and 165 km.

Table 6-2: Power losses for a VSC-HVDC transfer capability of 900MW

Parameters	Obtained
Converter Losses	120 MW
P_{Losses} %	6.66%

In the ABB proposal, [29, 101], VSC-HVDC power system which is capable of transferring similar power to the scenario currently under discussion (almost 1GW) has a voltage level higher than ±150kV.

6. 2.3.3 Grid Fault Analysis

To demonstrate the capacity of the multi-terminal VSC-HVDC control system to restore the power after a large transient is triggered, the following simulations have been subjected to fault ride-thought capability analysis. During the transient period, the offshore wind farms are delivering constant power to the offshore cluster substation which after the transient is cleared, this is then sending the wind power to the onshore grids.

6. 2.3.3.1 Transient Analysis: Power Analysis

The below simulations show results of the multi-terminal VSC-HVDC power system with the coordinated control system installed in the cluster offshore substation is not affected by the change in the onshore layout. Thus, it can be observed that the voltage dip and the large fault currents created by the transient have similar impact than in the point-to-point layout. Furthermore, the control can also restore consequently the entire power system. Figure 6-4 (h)1 and Figure 6-4 (h)2 show the active and reactive power transferred at the wind farms substations. Figure 6-4 (h)3 shows the active and reactive power transferred at the offshore cluster substation. Figure 6-4 (h)4 shows the active and reactive power deliver at the onshore substation (Grid 1 and Grid 2). Figure 6-4 (h)5 shows the DC voltage link and Figure 6-4 (h)6 shows the modulation indexes in the offshore and onshore substations. In addition, these figures show the behaviour of the AC voltages and AC currents at the offshore/onshore substations at the PCC_3, PCC_4, and PPC_5, Figure 6-1.

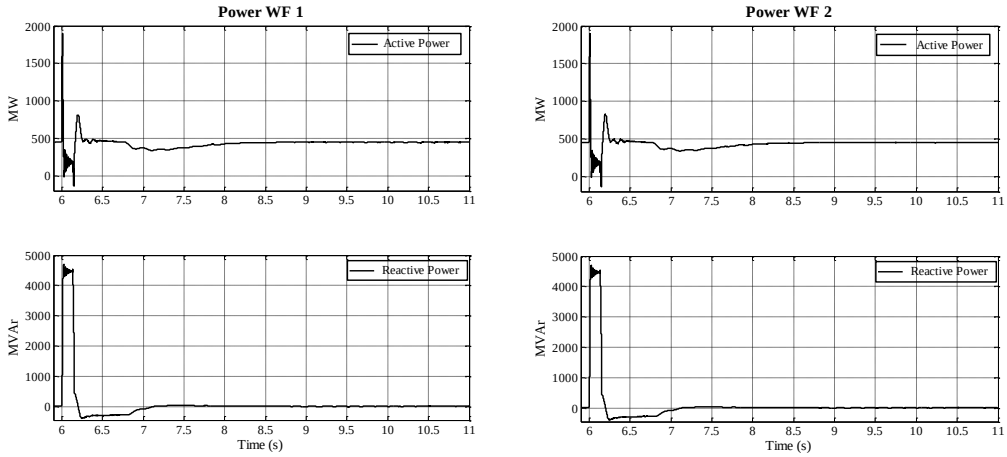

(h)1

(h)2

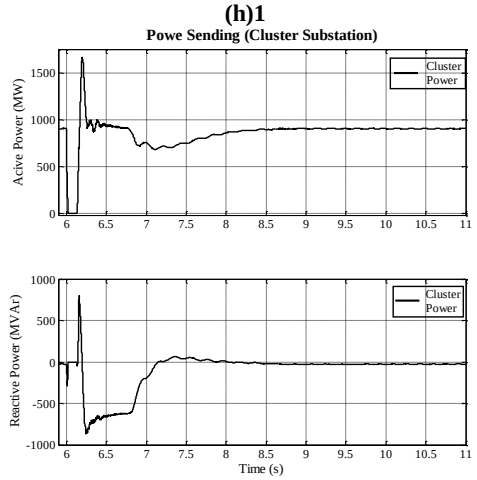

(h)3

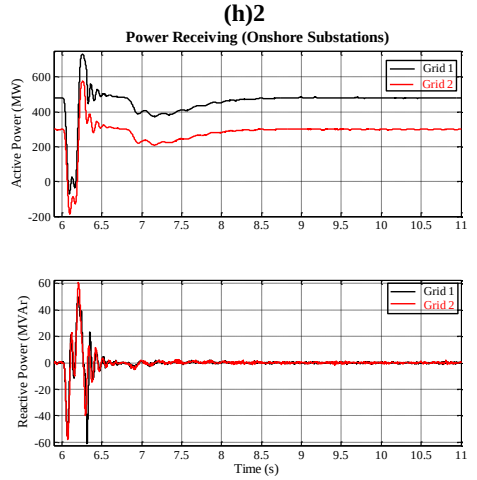

(h)4

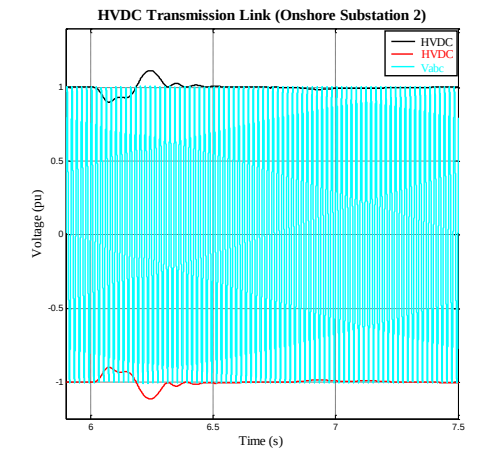

(h)5

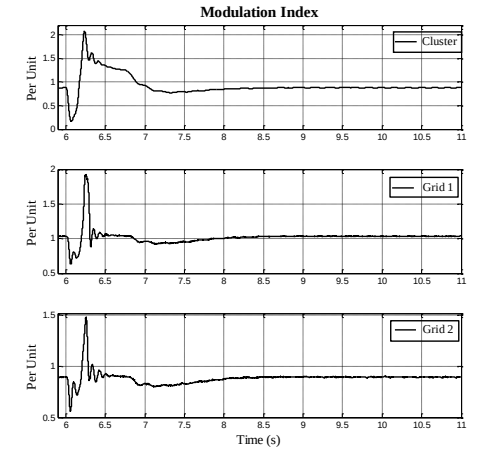

(h)6

Figure 6-4: Transient responses for three-phase fault in the multi-terminal scenario

Figure 6-4 (h)1 and (h)2 show the performance of the active and reactive power at the wind farms substations, WF 1 and WF2. Due to that the characteristics of both wind farm substations are similar, the behaviour of these substations, during entire simulation, are similar. The peaks and troughs of the active and reactive power and behaviour during the recovery are similar in both substations. Thus, the maximum active power peak reaches almost 2000 MW and the reactive power reaches almost 5000 MVAr. After the transient is cleared, the maximum active power peak reaches almost 750 MW and the reactive power

reaches almost 450 MVAr. Then, it cannot be appreciated, in the figures, another significant active or reactive power peak. Furthermore, the control system of the offshore substation recovers the steady state in both substations around 8.5s. Figure 6-4 (h)3 and (h)4 show the performance of the active and reactive power performances in the offshore and onshore substations. During the transient, the active power in the offshore cluster substation is clearly 0 MW. After the transient is removed from the system, the maximum active power peak is over 1500 MW and the trough is around 750 MW. The offshore power system suffers a slightly fluctuation until the control system recovers the steady state around 9s. After the first peak and the first trough, there are no significant peaks and troughs in the offshore power system. The maximum and minimum power peaks of the reactive power are around ± 900 MVAr. In case of both onshore substations, the active and reactive power perform similarly (the Grid 1 is connected to onshore by an underwater dc cable with a length of 125 km and the Grid 2 by dc cable with a length of 165 km). Thus, the power received at the onshore substation 1, Grid 1, is around 450 MW and in the onshore substation 2, Grid 2, is around 350 MW. The reactive power behaviour is very similar and the maximum and minimum peaks are ± 60 MVAr. Figure 6-4 (h)5 shows the performance of the HVDC transmission. This link connected the offshore substation and the Grid 2. As can be seen, the DC voltage still affected by the transient. The DC link transfers the transient to the onshore substation and therefore, as can be seen in Figure 6-4 (h)4, the active and reactive power in Grid 2 is affected by this transient. The control system of the VSC-HVDC link recover the steady state around 7.5s.

6. 2.3.3.2 Transient Analysis: Voltage and Current Analysis

Figure 6-4 (h)7 and (h)8 show the voltages and currents at the offshore cluster substation at the both onshore substations in per unit values. These voltages and currents values are taken at the offshore substation, PCC_3, and the onshore substations at the PCC_4 and PCC_5, Figure 6-1. Furthermore, Figure 6-4 (h)7 and (h)8 show the voltage and current performances of the offshore cluster substation and both onshore substations in per unit values. Figures (h)9, (h)10 and (h)11 show the voltage and current of the offshore cluster substation and both onshore substations in their sinusoidal values.

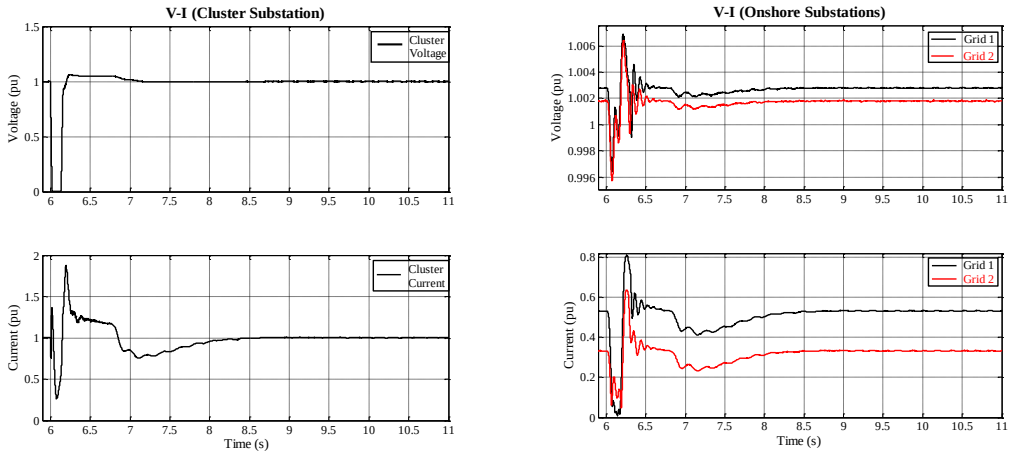

(h)7

(h)8

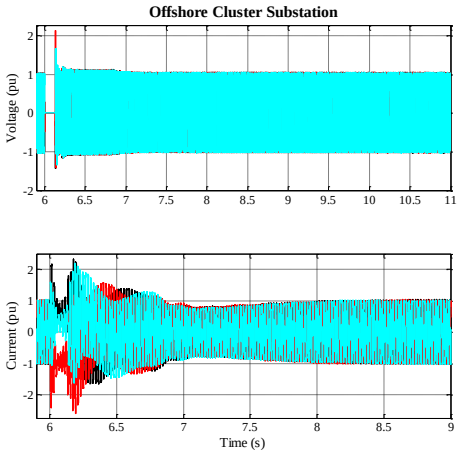

(h)9

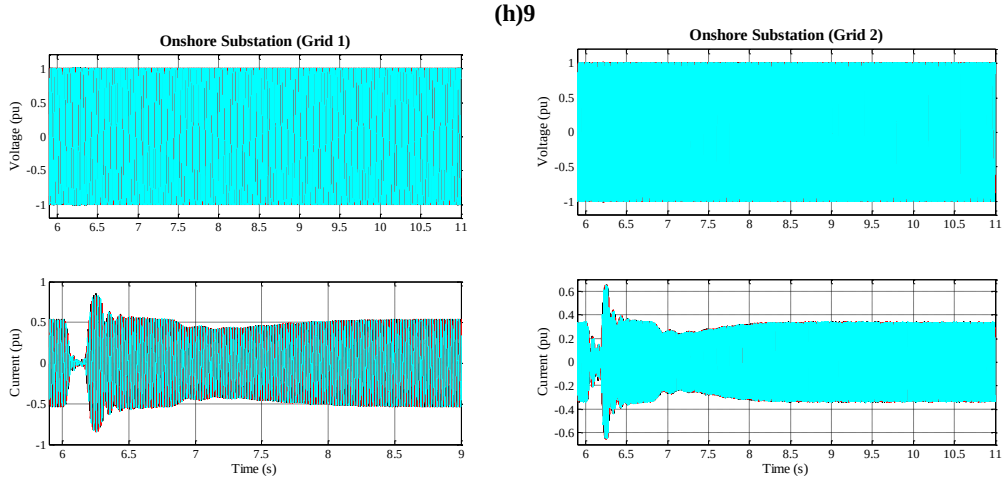

(h)10 (h)11

Figure 6-4: Transient responses for a three-phase fault at the multi-terminal scenario

As can be seen in these figures, the transient affects significantly the AC current in the offshore and onshore substation. The AC voltage in both sides of the VSC-HVDC is not significantly affected. Therefore, the large transient affect significantly the AC current of the offshore cluster substation and this reaches a maximum and a minimum peak over 2 pu at the beginning of the transient. Then, the control system of the offshore cluster substation recovers the steady state of the AC current around 8.5s, Figure 6-4 (h)9. In addition, the control system of the offshore substation smooths the behaviour of the AC current and

thereby not significant fluctuations can be seen between the maximum peak, 6.26s, and when the power system reaches the steady state, 8.5s. The AC current peaks, in both substations, reach a maximum and minimum of ±0.8 pu and ±0.6 pu, respectively. After the first AC currents peak, the offshore substation controls the behaviour of the AC current and thus it cannot be appreciated significant fluctuations, around 6.35s, in both onshore substation Grid 1 and Grid 2. Furthermore, the VSC-HVDC links reaches the steady state around 9s.

As mentioned before, the AC voltage in the offshore and onshore substation are not significantly affected. However, the AC voltage, in the offshore substation, is 0 pu during the duration of the transient. When the transient is cleared the control system of the offshore substation begins to recover steady state of the AC voltage. It is also clear to see that the control system smooths the voltage transition and thus no significant fluctuations can be appreciated in Figure 6-4 (h)9. Thus, the AC voltage goes over 2 pu just after the transient is cleared (from 6.25s to 7s). In contrast, in both onshore substations, the AC voltage is not affected and no fluctuations can be appreciated.

6.3 Summary

A model of a MTDC power system is presented in this chapter. It has also been mathematically analysed the offshore scheme and thus the values of the PI controllers have been calculated. The simulations results have shown the efficient performance of this MTDC power system and the consistency of the power control system of the offshore cluster substation.

Chapter 7: Discussion

7.1 Introduction

This thesis has studied and analysed the performance of the VSC-HVDC power system and also the two most common types of wind turbines (DFIG and FRC) for offshore applications. The main objective of this thesis was to study, analyse and improve the power converter installed in the offshore and onshore section of the VSC-HVDC power system. The second objective was also to study and analyse the power converters of the DFIG and FRC wind turbines. The intention of this was to improve the conventional control system of these converters and thus to improve performance of the entire VSC-HVDC power system. Therefore, the improvement in the dynamic performance of these wind turbines will also improve the dynamic performance of the offshore cluster substation and thus to the entire VSC-HVDC power system.

To improve the behaviour of these power converters (the VSC-HVDC system and wind turbines) this thesis has decided to study, firstly, the conventional control system of the VSC converter. Then, each studied modification was introduced into the dynamic behaviour of the VSC converters separately. Thus, to study the behaviour of these modifications and thus the reaction of the VSC-HVDC power system and the WTs this thesis has divided the simulations into three main case studies. These case studies have also been divided into different scenarios. The first studied case included the study of VSC converter in the two types of wind turbines (DFIG FRC). The second case studied was a basic VSC-HVDC power system. The third case studied contained a more complex offshore scenario - two offshore wind farms connected to the offshore cluster substation - in which the coordinated power control was introduced in the offshore layout. Furthermore, this case study was also divided into three scenarios. These case studies, 2.1 to 2.3, contain three different offshore wind farms, DFIG OWF, FRC OWF and MIXED OWF. Finally, the Chapter 6 analysed a MTDC power system. This power system had the MIXED scenario in the offshore layout and two similar links to onshore. To understand the importance of the control and the transmission system of the VSC-HVDC, this research has studied the difference between the existing LCC-HVDC and the VSC-HVDC. Thus, to understand the purposes of installing a VSC-HVDC power system for offshore applications; this thesis has explained the difference over the LCC-HVDC system. This comparison highlighted the benefits of the VSC control system opposite to the LCC control system. In addition, the HVDC transmission system had been

compared with HVAC transmission system. To understand the ability and benefits of the HVDC for power transmission over long distances both transmission systems had been compared and thus the pros and cons had been highlighted.

The control system and transmission systems of the VSC-HVDC had been detailed explained and also had mathematically analysed in Chapters 2. Chapter 2 ends with a mathematical explanation of the VSC control system, the vector control technique. This technique has been used to decoupled powers, voltage and current and thus obtains more accurate control of the VSC converters (offshore and onshore). This analysis benefited for further control system modifications. In Chapter 3, the overall functionality of each substation has been explained and analysed. Furthermore, the composition of the offshore and onshore substations has been introduced and extensively described. Thus, the function of each component inside of the VSC-HVDC system (the VSC converters - which are the key of this power system - power transformers, the phase reactors and DC capacitors) have been discussed, have been analysed and have also been mathematically analysed. In Chapter 4, a mathematical explanation of the control system of the most common wind turbines has been given. Thus, the discussion of how the control system of the generator converter adapts the torque to the power generator and the rotor and stator voltages and currents to the grid requirements through the grid side converter had been explained and had been mathematically analysed. In chapters 5 and 6 the plot simulations of the different case studies have been shown. Thus, these two chapter show the results of the creation of a unified offshore power network for several large OWFs and also their integration into the onshore network. Furthermore, this research has decided to develop AC star offshore power network which has two offshore wind farms connected to one offshore cluster substation. This offshore connection could simulate future displays of the unified offshore network. The key factor of these simulations was to demonstrate the reliability of the modifications applied in the control system of the VSC power converter. Thus, Chapter 5 showed and also highlighted the enhancements modifications applied to the VSC power/voltage controller applied in the offshore cluster substation. Chapter 6 showed the reliability of the coordinated control system.

7.1.1 Discussion of the Case Studies

As mentioned, to achieve enhancements in the power control system of the VSC converters - DFIG/FRC wind turbines and principally VSC-HVDC power system - this research has analysed three main case studies. The first case study analysed the reliability of the wind

turbines power converters. This case study was structured as AC wind turbine scenarios in which the group of simulations had investigated the performance of DFIG and FRC wind turbines when they worked in an HVAC transmission system. The second case study analyses a basic VSC-HVDC power system, in which several control system modifications have been applied in the VSC converter in an offshore cluster substation. Thus, this VSC-HVDC scenario had only one offshore wind farm. This was connected to onshore by a single point connection. In this scenario the different modifications, mentioned in Chapter 3, were applied in the VSC converter, one at a time. To differentiate the applied modifications of the control system of the power converter from a basic scheme to the most improved scheme; simulations had been labelled as 'filter' scheme, 'frequency' scheme and 'third harmonic' or '3 Har' scheme. The third case study analysed the coordinated power controller for a VSC-HVDC power system when different offshore wind farm layouts were added to the offshore cluster substation. As mentioned previously, this case study was also divided into three scenarios which DFIG and FRC and a mixed of both wind farms are connected to the offshore cluster substation. The third case study group had evaluated the coordinated power controller also proposed in Chapter 3. This scenario had incorporated several offshore wind farms connected to one offshore cluster substation. To examine the performance of the proposed control system and also to improve its performance; this researched has also developed an improved power control system. Thus, in the power control system of the VSC converter, a feed-forward signal taken from each offshore wind farm was implemented into the control technique of the inner and outer current controller. This control technique was compared opposite to the basic coordinated control.

Case Study 1

Case Studies: 1.1, 1.2 and 1.3: Basic Scheme Analysis

To identify the benefits of each implemented modification in the control system of the VSC converters; these were tested separately, one at the time. In the final scheme each modified model was compared to the other modifications. Thus, this way of comparing the different schemes has shown the significant differences in each simulation performances. For example, the modifications incorporated into the control of the reactive power applied to the RSC and the GRC grid converters had mainly improved the active and reactive power performances and the DC power "DC voltage" transmission. As a result of the installation of 1^{st} and 2^{nd} order filters applied to the rotor and stator voltages and currents (RSC), the

performance VSC converters had displayed a significant improvement in the reduction of the recovery time of the power system. The filter modifications applied to the control system of the stator and rotor parameters had significantly enhanced the control system of the power converter in Case Study 1.1 DFIG Wind Turbine: Stability Analysis and Case Study 1.2 FRC Wind Turbine: Stability Analysis. Furthermore, the combination of the active power, the DC voltage and the frequency controllers had displayed a high benefit on the performance of the active power and reactive power performances of the DFIG and FRC wind turbines. Furthermore, the implementation of the third harmonic injection technique into the control system of both VSC converter (RSC and GSC) has also shown a significant improvement in the reduction of the active power peaks and had also reduced the active power fluctuations. Therefore, this control technique has helped to reduce the recovery time of the offshore power system. In conclusion, the modifications applied into the wind turbines control systems has shown a significant reduction of the power peaks (sending power).

In the Case Study 1.3 VSC-HVDC System: Stability Analysis, the research has shown the performance of the VSC-HVDC power system in which an offshore substation had been connected to an onshore substation by an HVDC link. This research also implemented the aforementioned control techniques, power controller, frequency controller and the third harmonics technique, and has also implemented a specific numerical controller for the control of the DC voltage in each substation (offshore/onshore). The display of these simulation results have principally shown the powers, the AC voltage, the AC current and the DC voltage in both substations. In this particular case study, the fault ride-through capability of the power system was obtained in each modification applied in the control of the VSC converter. Especially in the last modification, V_{dc}, the numeric control of the DC voltage significantly reduced the power flow fluctuation. The power system also achieved the steady state of the power system smoother than previous simulations. Furthermore, the third harmonic technique also significantly improved the performance of the active and reactive powers. Consequently, the AC voltage and the AC current have been improved too. In conclusion, the combination of the active power, the DC voltage and the frequency controllers have shown the highest benefits on the performance of the active and reactive power. Furthermore, the recovery of the power system significantly improved after each modification had been applied into the control system of the VSC converters.

To summarise this section, the modifications made in the power control system of the DFIG and FRC wind turbines (converters) improved the overall power system and also displayed an efficient power system recovery. The modifications applied in the power

converters of the VSC-HVDC have also shown benefits in the recovery of the power system. Thus, the simulations results had validated the modifications applied in the control system of the VSC converters.

Case Study 2

Case Studies: 2.1, 2.2 and 2.3: Coordinated Control for Offshore Wind Farms: Single Point Connection

These case studies showed the impact of the multiple offshore wind farms installed in the offshore layout. Furthermore, these case studies also analysed the impact of the coordinate power controller installed on this substation cluster substation. In addition, in these case studies have also evaluated the control implementations analysed in the case study 1.3 VSC-HVDC System: Stability Analysis. Thus, the dynamic simulations of the three scenarios, the coordinated power control system have also shown a correct achievement of the recovery of the VSC-HVDC power system. The robustness coordinate control installed in the offshore substation of the VSC-HVDC power system showed the accuracy of the independent of the active and reactive power control. In addition, the fast response of the core of the VSC control system along with the correct operation of the coordinate power controller helped to achieve a successful and realistic power transferring. Furthermore, the coordinate power controller was analysed opposite to the similar control system in which a modification had been introduced. This modification consisted in a feed-forward signal sent from each offshore wind farm substation. This modification of the control system called feed-forward signal and in the plots results was named feed-forward. This implementation allowed the control system of the VSC converters to reorganize the k_p and k_i parameter values and thus add a slightly higher flexibility of the VSC-HVDC power system. Furthermore, this modification of the control system in the offshore substation has also reduced the high peaks of the AC voltage and AC current. In addition, the introduction of the feed-forward signal into the control system of the offshore cluster converter also reduced the power flow fluctuation produced by the large transient.

In terms of the necessity of removing the high pass filter of the offshore substation; this high pass filter has been substituted by the incorporation of 1^{st} and 2^{nd} order filters for the control system of the VSC converter in the offshore cluster substation. After the disconnection of the high pass filter, problems related to the voltage level in the offshore substation had increased and therefore, a shunt capacitance had been incorporated into the structure of the offshore cluster substation. The reactive power compensation produced by the

shunt capacitance had been varied depending of the scenario but this has been applied in order to achieve a minimum power factor of cos (δ) = 0,95. Thus, the value of the shunt impedance varied in each scenario, from almost 30 MVAr in the 2.1 DFIG scenarios to almost 50 MVAr to the 2.3 Mixed scenario. Furthermore, assuming that the shunt capacitance had been adapted to each scenario, if in the future new offshore wind farms or existing oil & gas power station will be added to any offshore VSC-HVDC power systems, the value of this shunt capacitance will need to be re-addressed.

The mathematical analyses of the PI controllers had shown a significant difference between the calculated and the applied PI controllers (in each analysed scenario). The obtained values of the PI controllers "$k_{p,}$ and k_i values" had led the offshore power system to have high fluctuations and the control system could not let the VSC-HVDC power system get into a steady state. Therefore, the tuning values of the PI controller of the offshore substation has been re-examined. Thus, by trial and error, the applied values of the $k_{p,}$ and k_i were re-addressed and the most suitable values for these parameters were introduced. Furthermore, all parameters of the five PI controllers, k_{i1} to k_{i5}, have been adapted to the grid requirements. Therefore, the method of modulus optimum criteria had given an introductory approach of the values of the k_p and k_i parameters. In addition, due to the results further investigation for the calculation of these parameters needs to be introduced into this mathematical technique. Thus, more accurate $k_{i1}$to k_{i5} values could be obtained. The mathematical analyses of the power losses in the VSC-HVDC power system, in the different case studies, had shown great similitudes between the ABB power losses report, [29], the expected power losses and the power losses obtained during the simulations. The power losses showed in ABB report, [29], are not higher than 2% [29, 101], depending on the case study, the obtained results showed a power losses variation between 3.33% and 7%. Nevertheless, further investigation on DC submarine cables had to be carried out.

In conclusion, the simulation results had validated the displayed coordinate power controller installed in the offshore cluster substation which had been described and had also mathematically analysed in Chapter 3 and Chapter 5. In addition, the research had helped to clarify concepts of the control system of the VSC converters and had also helped to clarify concepts of the sending power though the HVDC links. Furthermore, the simulation plots had shown the achievement of the fault ride-thought capability of the VSC-HVDC power system. Thus, each analysed scenario had validated the control ideas applied to the VSC converters. Furthermore, the tuning approach of the PI controllers explained in the Chapter 3 had shown

significant difference in the k_p to k_i parameters between the calculated values, using the modulus optimum criteria, and the applied k_p to k_i values. This criterion was widely used to calculate the initial state of the mentioned controllers. Hence, it had to be considered that the complexity of the offshore scenario affected significantly to the calculations of the k_p to k_i parameters and thus further investigation of the proposed scenario had to be carrying out.

Case Study 3

Case Study 3.1: Modelling and Implementing a Multi-Terminal Power System

According to the literature, [29, 50, 154, 155], the MTDC gird has several advantages with respect to the single point connection. Principally, the wind power integration or offshore interconnection. The MTDC gird has the principal disadvantage of a high value of power losses and the cost of the offshore infrastructure. However, this power losses, the capacity of transferring power to a different onshore grids have bigger strength than the power losses produced in the VSC converter. The MTDC power system is the key for the future wind energy sector. The multi-terminal power system has the same technical characteristics those described in Chapter 3 and operates similarly to the control system described in Chapter 3 and in Chapter 5. The simulations plots have shown a correct performance of the MTDC power system. Therefore, the simulation results had also validated the reliability of the coordinated power control system of the offshore cluster substation. The simulation results showed the concordance of the control of the offshore power system exposed in the previous section.

Due to the problems with the stability of the HVDC link, the impedance of the DC cables had been increased and therefore the overall power losses of the MTDC scenario have also increased. Furthermore, the tuning of the DC controller did not affect the increase of the parameters of the DC cable.

Chapter 8: Conclusion and Future Work

8.1 Conclusion

The necessity of achievement of the European targets of CO_2 emissions have proportionated the opportunity of increasing the energy production from offshore wind farm grids. The flexibility of the VCS-HVDC allows converting the AC power into DC with higher quality and then allows transferring this power with a high control over it. Thus, the first achieved objective of this thesis was to study and then to analyse the VSC power converters which its mean function was to control the HVDC link. The second achieved objective was to improve the dynamic response of the power converters installed in the both substations. In the process of developing a more suitable scenario for the large offshore wind farms this research thesis also studied and improved the dynamic behaviour of the two existing wind turbines. Thus, this third objective was to incorporate and then to improve of the dynamic behaviour of the power converters of the DFIG and FRC wind turbines. Finally, these wind turbines were then introduced in the offshore layout of the VSC-HVDC power system. The intention of this was changing the dynamic of the VSC-HVDC. This allowed analysing the reaction of the control system of the VSC converters, principally, in the offshore substation and secondary in the onshore substation. This lead to the fourth achieved objective of the thesis, the creation of an adequate coordinated power control for the offshore cluster substation. This coordinated power control of the VSC converter controls the entire behaviour of the offshore layout and with the introduction of the feed-forward control signal. The behaviour of the offshore layout had significantly improved and thus the peaks and through the active and reactive power had significantly reduced. Furthermore, the recovery time had also improved.

The importance of improving the wind turbine behaviour had become essential. In this research, the behaviour of the VSC-HVDC power system depends also on the behaviour of the wind turbines installed offshore layout. In terms of improving the performance of the existing wind turbines, DFIG and FRC wind turbines, this thesis first targeted to improve the voltages and currents of the stator and rotor and also to improve the control techniques of the VSC power converters. Thus, the implementation of the 1^{st} and 2^{nd} order filters in the control system of the wind turbines had produced direct impact on the control system. Furthermore, the impact of this filter in the wind turbine had also influenced in the recovery time of these which had significantly reduced. In addition, the reactive power peaks and troughs were

significantly reduced. The frequency controller, third harmonics technique had also improved the dynamic behaviour of the wind turbines and thus had also reduced the recovery time and has also reduced the active and reactive power peaks and troughs.

The implementations applied into the control system of the basic VSC-HVDC scenario, the frequency controller, third harmonics technique and also the implementation of the DC voltage controller in both substations (offshore and onshore), had shown significant benefit for the power transferred. They had dramatically enhanced the control of the power system of the power converters and thus the behaviour of the VSC-HVDC power system and particularly offshore layout. The optimum tuning criteria technique - the mathematical method used to calculate the PI controllers - had given to this research an approach for obtaining the k_p and k_i initial values. This technique thereby allowed understanding the importance of the layout and thus the importance of the appropriate calculation of these parameters for the control of the VSC-HVDC power system. Furthermore, the complexity of the offshore power system had created mismatch between the calculated k_p and k_i values and the applied k_p and k_i parameters into the inner and outer current controller. Thus, further investigation need to be done to obtain more accurate parameters for the control system of the VSC converter.

The introduction of multiple offshore wind farms in the offshore layout had created the necessity of developing a basic coordinated power control for the offshore cluster substation. Thus, this coordinated power had shown relevant control of the active power transfer through the HVDC link. The introduction of the feed-forward signals - these signals were taken from the wind farm substations - had shown relevant reduction of the peaks and troughs of the active and reactive power system in the offshore and onshore substations. The introduction of these signals allowed a slight modification on k_p and k_i parameters which produces an important reduction in the recovery of the power system and thus the active and the reactive behaviours.

This research had also worked with the length of the submarine AC cables and with the parameter values of the DC cables. These significantly influenced the quantity, quality of the power transfer and also in the controllability of the entire VSC-HVDC power system. The value of shunt capacitance installed in the offshore substation needed to be adapted as the length of the AC submarine cable was modified. The values of the parameter of the DC cable influenced the controllability of the offshore and onshore substation. With low values of the parameter DC cables and even though the k_p and k_i values of the inner and outer controller were adapted, the recovery of the VSC-HVDC system was impossible to achieve. With low values of the parameter DC cables the power transferred was reduced significantly.

8.2 Future Work

The offshore technology and thus offshore wind farms scenarios have to be analysed and tested before they will be installed into the sea. Different large wind farm topologies for offshore wind scenarios have been analysed in this thesis and suggestions of further scenarios are as follows:

- In order to reduce power losses in the VSC-HVDC schemes and thus to increase the energy transferred, sending power to onshore; it would be interesting to study and also to analyse the multi-level voltage converters in the analysed offshore schemes.
- However, the VSC converter can stop partially the fault current produced by the large transient, the fault current is still influence the performance of the VSC-HVDC scenario. Therefore, further protection has to be installed in the VSC-HVDC scenarios. Thus, the DC fault current can be removed from the HVDC system. Therefore, if a DC chopper is introduced in the VSC-HVDC system as a protection. This protection system can prevent the rise of the DC current and the DC voltage. To prevent the increment of the V_{dc} in the capacitor and also again I_{dc} in the DC cable. This DC chopper has to be connected in parallel to the system capacitors [24, 129, 155, 156].
- In the coming years, the energy produced by a singular wind turbine will rise; this power increase will happen because the size of the wind turbines will also increase to Ø150m and probably Ø250m and thus producing 10MW or 12MW. Thus, the power penetration into the conventional grids will be significantly increased and therefore, the conventional grids will need to be adapted to this high increment coming from offshore wind farms. Furthermore, considering that the ABB report, [29], shows

different symmetric VSC-HVDC models which each have different transmission capacities ±320 kV or ±500kV, future simulation work should be kept in the direction of creating an UHVDC.

- The MTDC power system has been developed which the idea of creating a future offshore meshed grid and thus introducing another offshore cluster substation. Therefore, considering the connection possibility of re-organizing the control system of the MTDC-HVDC power system. Offshore substation should have a DC controller while the onshore substation should control the sending power

References:

[1] P. Skarby, "Special Report: 60 Years of HVDC," July 2014.

[2] A. Papadopoulos, *et al.*, "Collection and transmission losses of offshore wind farms for optimization purposes," *2015 IEEE Energy Conversion Congress and Exposition (ECCE)*, pp. 6724-6732, 20-24 Sept. 2015 2015.

[3] M. Barnes and A. Beddard, "Voltage Source Converter HVDC Links–The State of the Art and Issues Going Forward," *Energy Procedia*, vol. 24, pp. 108-122, 2012.

[4] J. Arrillaga, *et al.*, *Flexible power transmission: the HVDC options*: John Wiley & Sons, 2007.

[5] S. Sawyer and K. Rave. (2012) Annual market update 2011. [magazine]. 1- 65.

[6] E. T. E. W. E. Association, *Pure Power: Wind Energy Targets for 2020 and 2030; a Report by the European Wind Energy Association-2011*: EWEA, 2011.

[7] Dr. Nicolas Fichaux and J. Wilkes. (2009) Oceans of opportunity: Harnessing Europe's largest domestic energy resource.

[8] P. HALLBERG and M. PAUN, "Smart grids and networks of the future: EURELECTRIC views," *Union of the Electricity Industry – EURELECTRIC*, 2009.

[9] P. Schavemaker and L. Van der Sluis, *Electrical power system essentials*: Wiley, 2008.

[10] J. Wilkes, *et al.*, "Wind in power: 2011 European statistics," *EWEA, Brussels (BE)*, 2012.

[11] D. Energi. *Energinet. dk (2010)*.

[12] p. National Grid Electricity Transmission. (2010, 27/11). *Value breakdown for the offshore wind sector* Available: https://www.gov.uk/government/uploads/system/uploads/attachment_data/file/48171/2806-value-breakdown-offshore-wind-sector.pdf

[13] C. Ogilvie. (2013, 26/11). *Offshore Wind: Decision Time*. Available: http://www.renewableuk.com/en/publications/reports.cfm/offshore-wind-report

[14] BWEA. (2010, 27/11). *What does the Round 3 announcement mean?* Available: http://csmres.co.uk/cs.public.upd/article-downloads/Round%203%20Briefing%20from%20BWEA_a6293.pdf

[15] T. C. State. (2015). *Leasing rounds*. Available: https://www.thecrownestate.co.uk/energy-minerals-and-infrastructure/offshore-wind-energy/working-with-us/leasing-rounds/

[16] p. National Grid Electricity Transmission and T. C. ESTATE. (2010). *Round 3 Offshore Wind Farm Connection Study* Available: http://www.thecrownestate.co.uk/media/214799/round3_connection_study.pdf

[17] W. E. Technology. (11 Mar 2010). *Supergen Wind Energy Technologies Consortium*. Available: http://www.supergen-wind.org.uk/

[18] Iván Pineda and Paul Wilczek. (2012) Creating the Internal Energy Market. *EWEA*.

[19] Airtricity and C. Vea, "European Offshore Supergrid® Proposal
Vision and Executive Summary," www.Airtricity.com2010.

[20] T. T. GmbH, "Requirements for Offshore Grid Connections in the Grid of TenneT TSO GmbH," ed, 2012.

[21] J. De Decker and P. Kreutzkamp. (2011) Offshore Electricity Grid Infrastructure in Europe. *A Techno-Economic Assessment, Final Report*.

[22] J. Svensson, "Active Distributed Power Systems," *Lund University*, 2006.

[23] S. N. Sea, "Roadmap to the deployment of offshore wind energy."

[24] T. Ackermann, "Wind power in power systems," *Wind Engineering*, vol. 30, pp. 447-449, 2006.

[25] N. B. Negra, *et al.*, "Loss evaluation of HVAC and HVDC transmission solutions for large offshore wind farms," *Electric Power Systems Research*, vol. 76, pp. 916-927, 2006.

[26] T. Worzyk, *Submarine power cables: design, installation, repair, environmental aspects*: Springer, 2009.

[27] J. Machowski, *et al.*, *Power system dynamics: stability and control*: Wiley, 2011.

[28] A. Von Meier, *Electric power systems: a conceptual introduction*: John Wiley & Sons, 2006.

[29] P. Haugland, "It's time to connect: Technical description of HVDC Light® technology," 2008.
[30] B. Jacobson, *et al.*, "VSC-HVDC transmission with cascaded two-level converters," in *Cigré session*, 2010, pp. B4-B110.
[31] B. W. Williams, *Principles and elements of power electronics* vol. 377, 2006.
[32] S. Teeuwsen, *et al.*, "Modulation controller design for the 1400 MW New Zealand inter island HVDC link," *IFAC Proceedings Volumes*, vol. 45, pp. 337-342, 2012.
[33] J. Rodhe, "The large- scale circulation in the Skagerrak; interpretation of some observations," *Tellus A*, vol. 39, pp. 245-253, 1987.
[34] J. Arrillaga, *et al.*, *Flexible Power Transmission: The HVDC Options*: Wiley Online Library, 2007.
[35] ABB. (2010). *Economic and environmental advantages*. Available: http://new.abb.com/systems/hvdc/why-hvdc/economic-and-environmental-advantages
[36] A. Siemens. (2011) High voltage direct current transmission-proven technology for power exchange. *Energy Sector, Germany. Accessed at* http://www. *siemens. com/sustainability/pool/en/environmental-portfolio/products-solutions/power-transmission-distribution/hvdc_proven_technology. pdf*.
[37] T. H. Hansen, "Offshore Wind Farm Layouts," PhD, Department of Electrical Power Engineering, Norwegian University of Science and Technology, NTNU, ELKRAFT, 2009 July.
[38] M. P. Bahrman, "HVDC transmission overview," in *Transmission and Distribution Conference and Exposition, 2008. T&D. IEEE/PES*, 2008, pp. 1-7.
[39] V. K. Sood, *HVDC and FACTS controllers: applications of static converters in power systems*: Springer, 2004.
[40] P. F. de Toledo, "Modeling and control of a line-commutated HVDC transmission system interacting with a VSC STATCOM," 68, 2007.
[41] J. Arrillaga, *et al.*, *Flexible power transmission: The HVDC Options*: John Wiley & Sons, Inc., 2007.
[42] K. Giddani, "Control Design and Stability Assessment of VSC-HVDC networks for Large-Scale Offshore Wind Integration," Electronic and Electrical Engineering Doctor of Philosophy, Department of Electronic and Electrical Engineering, University Of Strathclyde, Glasgow, 2012.
[43] P. Kundur, *Power system stability and control* vol. 12: McGraw-Hill, Inc., 2001.
[44] A. Tadese, "Performance of a combined LCC and VSC Bipole HVDC link," Aalborg University, 2010.
[45] P. Kundur, *et al.*, *Power system stability and control* vol. 4: McGraw-hill New York, 1994.
[46] B. W. Williams, Ed., *Power electronics: Devices, drivers, and applications*. 1987, p.^pp. Pages.
[47] L. Chetty, "Design Synthesis of LCC HVDC Control Systems," University of KwaZulu-Natal, Durban, 2011.
[48] Jiuping Pan, *et al.*, "AC Grid with Embedded VSC-HVDC for Secure and Efficient Power Delivery.pdf," *IEEE Energy2030*, 2008.
[49] S. Chaudhary, "Control and Protection of Wind Power Plants with VSC-HVDC Connection," Aalborg UniversitetAalborg University, 2011.
[50] T. M. Haileselassie, "Control, Dynamics and Operation of Multi-terminal VSC-HVDC Transmission Systems," 2012.
[51] E. Koldby and M. Hyttinen, "Challenges on the Road to an Offshore HVDC Grid," 2009.
[52] A. Yazdani and R. Iravani, *Voltage-Sourced Converters in Power Systems* Yazdani, A. and Iravani, R, 2010.
[53] O. Anaya-Lara, *et al.*, *Offshore Wind Energy Generation: Control, Protection, and Integration to Electrical Systems*: John Wiley & Sons, 2014.
[54] O. Anaya-Lara, *et al.*, *Wind energy generation: modelling and control*: John Wiley & Sons, 2011.
[55] L. Zhang, "Modeling and control of VSC-HVDC links connected to weak AC systems," 2010.

[56] S. G. Johansson, *et al.*, "Power system stability benefits with VSC DC-transmission systems," in *CIGRE Conference, Paris, France*, 2004.
[57] M. Kirik, "VSC-HVDC for long term voltage stability improvement," Master's thesis, Royal Institute of Technology, School of Electrical Engineering, Departament of Electric power Systems, Stockholm, 2009.
[58] E. H. Watanabe, *et al.*, "Instantaneous p–q power theory for control of compensators in micro-grids," in *Nonsinusoidal Currents and Compensation (ISNCC), 2010 International School on*, 2010, pp. 17-26.
[59] D. J. Cooper. (2008). *Practical process control, proven methods and best practices for automatic pid control*.
[60] A. Yazdani and R. Iravani, *Voltage-Sourced converters in power systems: Modeling, Control, and Applications* Wiley Online Library, 2010.
[61] F. Renaudin, "Integration and Stability of a Large Offshore Wind Farm with HVDC Transmission in the Norwegian Power System," 2009.
[62] W. Xiaoguang and T. Guangfu, "Research of AC/DC Parallel Wind Farm Integration Based On VSC-HVDC," in *Power System Technology, 2006. PowerCon 2006. International Conference on*, 2006, pp. 1-5.
[63] B. Fox, *Wind power integration: connection and system operational aspects* vol. 50: Iet, 2007.
[64] C. Du, "The control of VSC-HVDC and its use for large industrial power systems," 2003.
[65] K. M. Høvik, "Control of Offshore Passive Platform System Voltage and Frequency through Control of Onshore Back-to-Back Voltage Source Converters," 2011.
[66] CUIQING DU, "VSC-HVDC for Industrial Power Systems," Goteborg, Sweden, CHALMERS UNIVERSITY OF TECHNOLOGY, 2007.
[67] CUIQING DU, "VSC-HVDC for Industrial Power Systems," *Goteborg, Sweden, CHALMERS UNIVERSITY OF TECHNOLOGY*, 2007.
[68] T. W. Shire, "VSC-HVDC Based Network Reinforcement," M. Sc. thesis Electrical power Engineering department, Delft University of Technology, 2009.
[69] H. Patel and V. K. Sood, "Modeling of Voltage Source Converter based HVDC system in EMTP-RV," in *Electric Power and Energy Conference (EPEC), 2010 IEEE*, 2010, pp. 1-6.
[70] A. Yazdani and R. Iravani, *Voltage-sourced converters in power systems: modeling, control, and applications*: John Wiley & Sons, 2010.
[71] S. Chaudhary, *Control and Protection of Wind Power Plants with VSC-HVDC Connection*: Aalborg UniversitetAalborg University, Faculty of Engineering and Science, Power Electronic Systems, 2011.
[72] T. Kalitjuka, "Control of Voltage Source Converters for Power System Applications," 2011.
[73] O. A. Giddani, *et al.*, "Control Strategies of VSC-HVDC Transmission system for wind power integration to meet GB grid code requirements," *International Symposium on Power Electronics, SPEEDAM 2010*, 2010.
[74] O. Giddani, *et al.*, "Grid integration of a large offshore wind farm using VSC-HVDC in parallel with an AC submarine cable," in *Universities Power Engineering Conference (UPEC), 2009 Proceedings of the 44th International*, 2009, pp. 1-5.
[75] C. Bajracharya, *et al.*, "Understanding of tuning techniques of converter controllers for VSC-HVDC," in *Nordic Workshop on Power and Industrial Electronics (NORPIE/2008), June 9-11, 2008, Espoo, Finland*, 2008.
[76] C. Bajracharya, "Control of VSC-HVDC for wind power," 2008.
[77] Q.-C. Zhong and T. Hornik, *Control of power inverters in renewable energy and smart grid integration*: John Wiley & Sons, 2012.
[78] O. LENNERHAG and V. TRAFF, "Modelling of VSC-HVDC for Slow Dynamic Studies."
[79] C. Du, "VSC-HVDC for industrial power systems," Chalmers University of Technology, 2007.
[80] E. Fuchs and M. A. S. Masoum, *Power quality in power systems and electrical machines*: Academic Press, 2008.
[81] S. Halpin, "Comparison of IEEE and IEC Harmonic standards," in *Power Engineering Society General Meeting, 2005. IEEE*, 2005, pp. 2214-2216.

[82] S. Kawasaki, *et al.*, "Restraint method of voltage total harmonic distortion in distribution system by power conditioner systems using measured data from IT switches," in *IPEC, 2010 Conference Proceedings*, 2010, pp. 636-641.
[83] J. Arrillaga and N. R. Watson, *Power system harmonics*: John Wiley & Sons, 2004.
[84] E. Krige, "Harmonic interaction between weak AC systems and VSC-based HVDC schemes," Stellenbosch: Stellenbosch University, 2012.
[85] G. Kalcon, "Control Design and Stability Assessment of VSC-HVDC networks for Large-Scale Offshore Wind Integration," 2011.
[86] R. Da Silva, *et al.*, "Optimization of Multilink DC Transmission for Supergrid Future Concepts," Renewable Power Generation (RPG 2011), IET, 2012.
[87] T. M. Haileselassie, "Control of multi-terminal VSC-HVDC systems," Norwegian University of Science and Technology, 2008.
[88] ENTSO-E, "EUROPEAN GRID TOWARDS 2020 CHALLENGES AND BEYOND," ed, 2010.
[89] M. Parker, "Electrical arrays for offshore wind farms " in *Offshore control schemes*, S. W. E. T. Consortium, Ed., ed, 2012, pp. 1-56.
[90] ENTSO-E and T. NSCOGI, "Offshore Transmission Technology," ed, 2011.
[91] A. Yazdani and R. Iravani, *Voltage-Sourced converters in power systems*: Wiley Online Library, 2010.
[92] T. M. Iversen, *et al.*, "Multilevel Converters for a 10 MW, 100 kV Transformer-less Offshore Wind Generator System," Department of Electric Power Engineering, Norwegian University of Science and Technology (NTNU), 2013.
[93] M. Davies, *et al.*, "HVDC plus–Basics and Principle of Operation," in *Special Edition for Cigré Exposition*, 2008.
[94] J. Rodriguez, *et al.*, "Multilevel inverters: a survey of topologies, controls, and applications," *Industrial Electronics, IEEE Transactions on*, vol. 49, pp. 724-738, 2002.
[95] S. Khomfoi and L. M. Tolbert, *Multilevel power converters*, 2007.
[96] M. Rashid and C. Press, *Power Electronics Handbook*, 2010.
[97] A. Antonopoulos, *et al.*, "On dynamics and voltage control of the Modular Multilevel Converter," in *Power Electronics and Applications, 2009. EPE '09. 13th European Conference on*, 2009, pp. 1-10.
[98] E. N. Abildgaard, "Exploring the Properties of a Modular Multilevel Converter Based HVDC Link: With Focus on Voltage Capability, Power System Relations, and Control System," 2012.
[99] J. Peralta Rodriguez, "Dynamic Averaged Models of VSC-Based HVDC Systems for Electromagnetic Transient Programs," École Polytechnique de Montréal, 2013.
[100] J. Glasdam, *et al.*, "Review on multi-level voltage source converter based HVDC technologies for grid connection of large offshore wind farms," in *Power System Technology (POWERCON), 2012 IEEE International Conference on*, 2012, pp. 1-6.
[101] P. K. M. Vormedal, "Voltage Source Converter Technology for Offshore Grids," ed: Norwegian University of Science and Technology, 2010.
[102] T. Haugsten Hansen, "Offshore Wind Farm Layouts: Performance Comparison for a 540 MW Offshore Wind Farm," 2009.
[103] W.-K. Chen, *Passive, active, and digital filters*: CRC Press, 2005.
[104] J. Dannehl, *et al.*, "Filter-based active damping of voltage source converters with filter," *Industrial Electronics, IEEE Transactions on*, vol. 58, pp. 3623-3633, 2011.
[105] A. Yazdani and R. Iravani, *Voltage-Sourced Converters in Power Systems*: Wiley, 2010.
[106] P. K. M. Vormedal, "Voltage Source Converter Technology for Offshore Grids: Interconnection of Offshore Installations in a Multiterminal HVDC Grid using VSC," 2010.
[107] A. Cetin, "Design and Implementation of a voltage source converter based STATCOM for reactive power compensation and harmonic filtering," MIDDLE EAST TECHNICAL UNIVERSITY, 2007.
[108] C. Stijn, "Steady-state and dynamic modelling of VSC HVDC systems for power system Simulation," PhD dissertation, Katholieke University Leuven, Belgium, 2010.

[109] D. G. Holmes and T. A. Lipo, "Pulse Width Modulation for Power Converters: Principles and Practice, 2003," ed: IEEE Press, 2003.
[110] B. Wu, *High-power converters and AC drives*: Wiley-IEEE Press, 2006.
[111] M. Knapczyk and K. PIEŃKOWSKI, "Analysis of Pulse Width Modulation Techniques for AC/DC Line-Side Converters," *Prace Naukowe Instytutu Maszyn, Napędów i Pomiarów Elektrycznych Politechniki Wrocławskiej. Studia i Materiały,* vol. 59, pp. 194-209, 2006.
[112] O. Gomis-Bellmunt, *et al.*, "Control of a wind farm based on synchronous generators with a central HVDC-VSC converter," *Power Systems, IEEE Transactions on,* vol. 26, pp. 1632-1640, 2011.
[113] J. Ögren, "PLL design for inverter grid connection: Simulations for ideal and non-ideal grid conditions," 2010.
[114] A. Timbus, *et al.*, "Synchronization methods for three phase distributed power generation systems - An overview and evaluation," in *Power Electronics Specialists Conference, 2005. PESC '05. IEEE 36th*, 2005, pp. 2474-2481.
[115] K. M. Høvik, "Control of Offshore Passive Platform System Voltage and Frequency through Control of Onshore Back-to-Back Voltage Source Converters," 2011.
[116] C. Sankaran, *Power quality*: CRC press, 2001.
[117] B. Fox, *et al.*, *Wind power integration: connection and system operational aspects*: Institution of Engineering and Technology, 2007.
[118] T. Ackermann, *Wind power in power systems* vol. 140: Wiley Online Library, 2005.
[119] L. Freris and D. Infield, *Renewable energy in power systems*: Wiley, 2008.
[120] O. Anaya-Lara, *et al.*, *Wind energy generation: modelling and control*: Wiley, 2011.
[121] J. Ekanayake, *et al.*, "Control of DFIG wind turbines," *Power Engineer,* vol. 17, p. 28, 2003.
[122] K. Lima, *et al.*, "Doubly-fed induction generator control under voltage sags," in *Energy 2030 Conference, 2008. ENERGY 2008. IEEE*, 2008, pp. 1-6.
[123] A. Perdana, "Wind turbine models for power system stability studies," 2006.
[124] B. Wu, *et al.*, *Power conversion and control of wind energy systems* vol. 77: John Wiley & Sons, 2011.
[125] O. Anaya- Lara, *et al.*, "Rotor flux magnitude and angle control strategy for doubly fed induction generators," *Wind energy,* vol. 9, pp. 479-495, 2006.
[126] J. I. Jang, *et al.*, "Active and reactive power control of DFIG for wind energy conversion under unbalanced grid voltage," in *Power Electronics and Motion Control Conference, 2006. IPEMC 2006. CES/IEEE 5th International*, 2006, pp. 1-5.
[127] J. A. Baroudi, *et al.*, "A review of power converter topologies for wind generators," *Renewable Energy,* vol. 32, pp. 2369-2385, 2007.
[128] T. Einervoll, "Impact on Wind Turbine Systems from Transient Fluctuations in Offshore Utility Grids," 2009.
[129] T. H. Hansen, "Offshore Wind Farm Layouts: Performance Comparison for a 540 MW Offshore Wind Farm," NTNU: Department of Electric Power Engineering 2009.
[130] A. Ashraf, "On reactive power compensation of wind farms-impact of wind farm controller delays," 2011.
[131] Z. Wu, *et al.*, "Operation and Control of a Direct-Driven PMSG-Based Wind Turbine System with an Auxiliary Parallel Grid-Side Converter," *Energies,* vol. 6, pp. 3405-3421, 2013.
[132] P. M. Pardalos, *et al.*, *Handbook of wind power systems*: Springer, 2014.
[133] P. Kundur, *et al.*, "Definition and classification of power system stability IEEE/CIGRE joint task force on stability terms and definitions," *Power Systems, IEEE Transactions on,* vol. 19, pp. 1387-1401, 2004.
[134] W. W. P. Nicholas W. Miller, Juan J. Sanchez-Gasca;, "Dynamic Modeling of GE 1.5 and 3.6 Wind Turbine-Generators," 2003.
[135] K. Johannesson, *et al.*, "HVDC Light Cables for long distance grid connection," in *European Offshore Wind Conference*, 2009, pp. 14-16.
[136] A. Bodin, "HVDC Light®-a preferable power transmission system for renewable energies," in *Energetics (IYCE), Proceedings of the 2011 3rd International Youth Conference on*, 2011, pp. 1-4.

[137] N. R. Ullah, "Wind Power-Added Value for Network Operation," Chalmers University of Technology, 2008.
[138] R. Grünbaum and N. Willemsen. FACTS to facilitate AC grid integration of large scale wind integration [Online]. Available: https://www.google.co.uk/search?q=Integration+of+large+scale+wind+farm+into+electrical+grids&oq=Integration+of+large+scale+wind+farm+into+electrical+grids&aqs=chrome..69i57j0.771j0j7&sourceid=chrome&espv=210&es_sm=93&ie=UTF-8
[139] T. T. B.V., "Market Integration Coupling of the European electricity markets ", ed, 2010.
[140] J. D. Glover, *et al.*, *Power System Analysis & Design*: Cengage Learning, 2011.
[141] T. Kalitjuka, "Control of Voltage Source Converters for Power System Applications," 2011.
[142] E. Prieto-Araujo, *et al.*, "Methodology for Droop Control Dynamic Analysis of Multiterminal VSC-HVDC Grids for Offshore Wind Farms," *IEEE Transactions on Power Delivery*, vol. 26, pp. 2476-2485, 2011.
[143] G. A. Raducu, "Control of grid side inverter in a b2b configuration for wt applications," *PED10-1015b, Aalborg University*, 2008.
[144] A. AB and G. S.-. HVDC, "HVDC Light® It's time to connect," 2012.
[145] J. Bird, *Electrical and electronic principles and technology* vol. Third edition: Elsevier Ltd., 2013.
[146] M. Wang, *Understandable electric circuits*: The Institution of Engineering and Technology, 2010.
[147] C. MaCilwain, "Supergrid," *Nature*, vol. 468, pp. 624-625, 2010.
[148] E.-E. AISL. (2013, 21/11). *Implementation Guideline for Network Code "Requirements for Grid Connection Applicable to all Generators"*. Available: https://www.entsoe.eu/major-projects/network-code-development/requirements-for-generators/
[149] M. H. R.Veguillas, *et al.*, "Project Objectives & KPI Deliverable nº 2.1," www. twenties-project. eu2010.
[150] B. M. A. Silva, "Multi-terminal HVDC Grids: Control Strategies for Ancillary Services Provision in Interconnected Transmission Systems with Onshore Wind Farms," Sustainable Energy Systems - MIT/Portugal, Faculty of Engineering of University of Porto, Porto, 2013.
[151] T. K. Vrana and O. B. Fosso, "Technical aspects of the North Sea super grid," *CIGRE Electra, November*, 2011.
[152] L. Meeus, *et al.*, "Offshore Grids: Towards a Least Regret EU Policy," 1977-3900, 2012.
[153] E. W. E. Association, *Wind Energy-the Facts: An Analysis of Wind Energy in the EU-25*: Corin Millais, 2004.
[154] Lie Xu, *et al.*, "Multi-Terminal DC Transmission Systems for Connecting Large Offshore Wind Farms," 2008.
[155] C. Ismunandar, "Control of Multi-Terminal VSC-HVDC for Offshore Wind Power Integration," TUDeft, Master's thesis, 2010.
[156] J. Yang, "Fault analysis and protection for wind power generation systems," University of Glasgow, 2011.
[157] p. National Grid Electricity Transmission. (2011). *Transmission Networks: offshore Development Information Statement*. Available: http://www.nationalgrid.com/NR/rdonlyres/B46EC9EF-2DD1-41DD-A650-93CAD1F246DA/43231/Future_Scenario_Consultation.pdf
[158] E. Plc, "Offshore Grid Study: Executive Report," 2010.
[159] O. Holmstrøm and N. B. Negra, "Survey of reliability of large offshore wind farms," in *European Wind Energy Conference, Milan, Italy*, 2007.
[160] L. Haarla, *Transmission Grid Security: A PSA Approach*: Springer, 2011.
[161] F. Van Hulle, *et al.*, "Integrating wind: Developing Europe's power market for the large-scale integration of wind power," European Wind Energy Association2009.
[162] N. S. C. O. G. Initiative, "Final Report-Grid Configuration," NSCOGl, intlNSCOGI2012.
[163] J. De Decker and A. Woyte, "D4. 2–Four Offshore Grid Scenarios for the North and Baltic Sea," 2010.
[164] L. Bergfjord, "Wind in the North Sea: Effects of offshore grid design on power system operation," Norwegian University of Science and Technology, 2011.

[165] S. SF. (2010) Annual Report 2010: The Norwegian Energy Regulator. Available: www.nve.no

Appendix A: Offshore Interconnection for North Sea Projects

A.1 Introduction

The European Union has started the expansion of the wind energy sector by supporting the economic development of the renewable energy industry and thus providing economic support to universities which can develop renewable projects. The EU has also proposed to develop a common offshore grid, which will allow transferring renewable energy through the North Sea when there is a lack of renewable energy or there is an energy surplus [19]. Given the high level of uncertainty over the achievement of CO_2 targets and also uncertainties regarding the development and installation of the future offshore network; the wind energy industry and government authorities are working with a degree of uncertainty regarding the potential power that this offshore infrastructure should deliver by 2020 or 2030. This necessary assumption of the offshore power delivery has to match with the assumption of the increment of the power demand in the upcoming years and should consider how this infrastructure will be accommodated by NETS or how it would be adapted to future power modifications. Therefore, these assumed scenarios should cover the energy progression of next to two decades from 2010 to 2030 from over 25 GW, a sustainable growth scenario, or over 67 GW, Sustainable Growth (SG) [157]. This exponential power increase is based on the proposal of four scenarios: Slow Progression (SP), Gone Green (GG), Accelerated Growth (AG) and Sustainable Growth (SG). These power production scenarios have also been compared with other technical studies such as: DECC's Pathway Analysis: Alpha Scenario, the ENA Report: "*Electrical Revolution Future Scenario, and also the TEC Register*" [157].

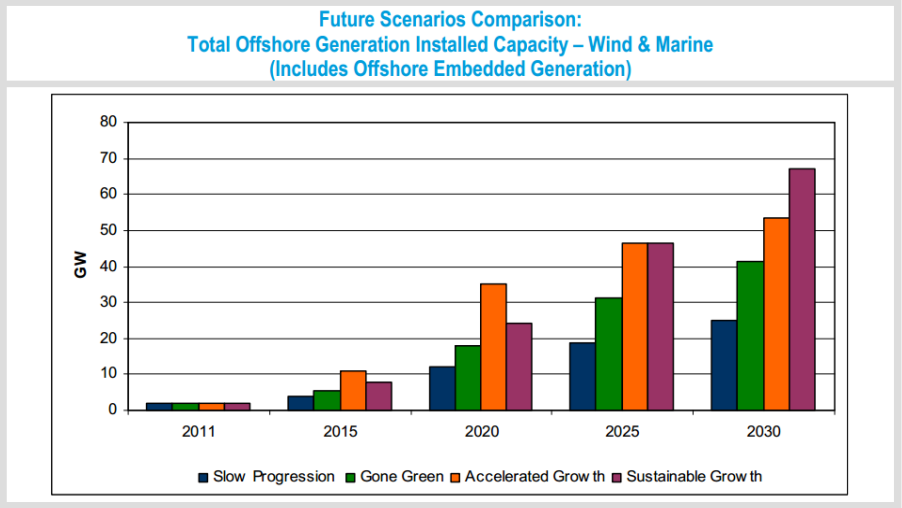

A-1: Total offshore generation expected capacity, this figure is taken from [157]

- Slow Progression (SP): Range (Installed Offshore Generation Capacity): 2 GW (2011) to 25 GW (2030).
- Gone Green (GG): Range (Installed Offshore Generation Capacity): 2 GW (2011) to 41.5 GW (2030).
- Accelerated Growth (AG): Range (Installed Offshore Generation Capacity): 2 GW (2011) to 53.5 GW (2030).
- Sustainable Growth (SG): Range (Installed Offshore Generation Capacity): 2 GW (2011) to 67.2 GW (2030).

The purpose of this offshore infrastructure is to supply the power demand to customers, it also need to be kept safety and also to keep the system working during disturbances. The correct design of the offshore infrastructure should avoid failures in energy supply and/or decrease the number of incidents in which the power supply is lost or the security power system is activated. Therefore, this large expansion of the renewable energy sector would require significant investment in the offshore wind energy sector and also significant reinforcement in the onshore girds. [152]. Working with the idea that the wind energy should be unlimited but unsteady, wind industry developers and TSOs are trying to optimise the offshore power acquisition and also improve the quality of the this power. Concerns over the structure of these future offshore renewable sources have arisen and Government or TSO have prioritize to develop offshore grid projects in the North Sea [158], [159, 160].

In general, the OWFs transfer the power produced to onshore through a radial connection. This connection supply power only to local energy consumers. Although, the offshore Supergrid® structure, [19], will incorporate a meshed grid which the power can be

liver to any point into different countries, the existing OWFs will continue to transfer power into a radial power system and when there is an energy surplus, this will be deliver to another point into the meshed grid. In an offshore radial grid, as a consequence of large disturbance, these local customers would most probably lose their energy supply. In a meshed grid, the same disturbance would not interrupt the energy supply and thus the energy can supply to any onshore grids. This Supergrid should have secure parallel paths which can guarantee the energy delivered. Although, the energy can be transferred from different transmission paths, the meshed structure does not guarantee that the power service would continue during a grid fault [160, 161]. Figure A-2 shows how offshore wind capacity could be connected to the onshore grid, giving examples of future offshore design networks for North Sea projects.

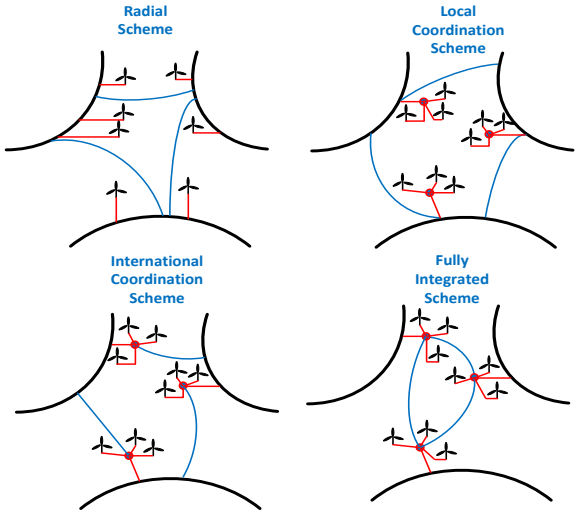

A-2: Future Offshore planning networks for North Sea projects. This plot is taken from: Offshore grid development in the North Seas report, ENTSO-E

The main proposals for the development of this offshore gird connection are based on two different connection strategies, a radial interconnection and a meshed interconnection (multi-terminal interconnection) [162].

A.2 Radial or Point to Point

A radial grid is a single point connection. Due to the length of the connection cable, the cost of this point to point is higher than a meshed grid but the control of the radial scheme is less complex. In this type of connection, OWFs are generally supplying their power to the country in which they are installed, and subsequently the power has to be transferred internationally through an interlinked connection, as shown in the following figure:

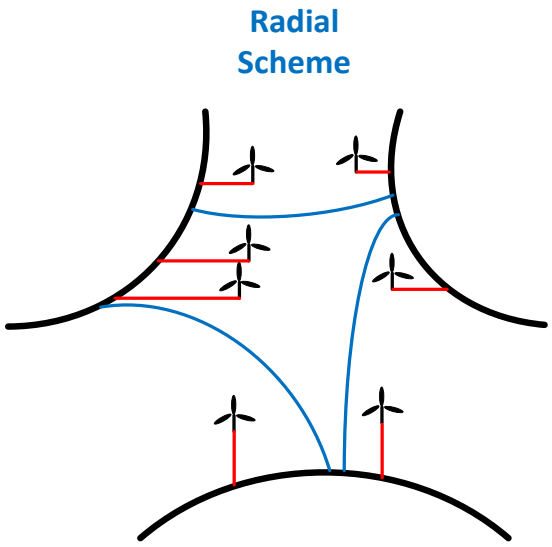

A-3: Radial or point to point Scheme

A.3 Meshed or Multi-Terminal Control

TSOs must improve the adequacy of the offshore transmission system at the same time that they have to maximize its efficiency, as well as the reliability of its layout; thus reducing infrastructure investment in those offshore renewable sources. This should result in a robust and reliable interconnection which will also guarantee the grid security. Furthermore, both types of transmission systems (radial or meshed connections) have to integrate a large amount of wind power, and therefore they must overcome a great variety of challenges and barriers. To connect all the North Sea countries into the same Supergrid; it requires massive wind energy industry development. With the imminent increase in the number of OWFs and the installation of their interconnections, a careful design of the transnational grid is needed in order to efficiently integrate the offshore power and facilitate power exchange and trade.

High numbers of companies and grid associations try to developed interlinkeds or interconnections. Companies and associations such as Eirgrid, EWEA, TradeWind or Offshoregrid, and Statnet) have published number of interesting reports, in which they conclude that the key to transferring the offshore power and to connect in different countries is a meshed grid [18, 158, 161, 163-165]. In order to forecast, the offshore infrastructure and identified capital cost, several proposed topologies have been studied in the report: "*D4.2 – Four Offshore Scenarios for the North and Baltic Sea*". The four design scenarios studied in the report are as follows:

- Trade-Driven
- Wind Driven

- Wind Driven: Special Case
- Mixed Driven

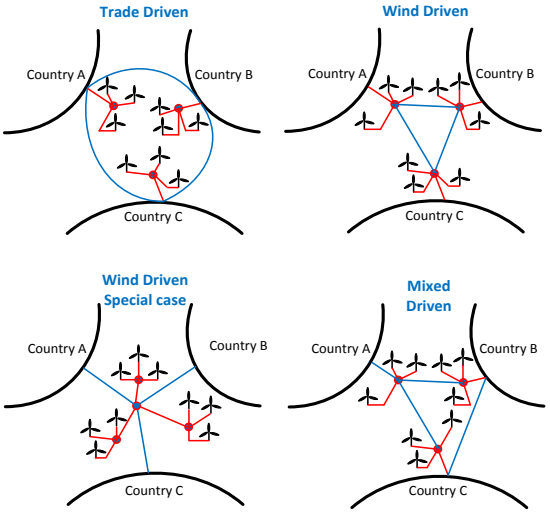

A-4: Topologies for possible offshore connections [163].

Appendix B: Mathematical Approach DFIG Power System

B.1 DFIG Power System

To obtain a reliable control system, the magnitudes of each parameter has to be adapted in per-unit values. To simplify the system, the calculation of the time delay of each component are applied to the system and thus the layout uses to calculate the PI controller is shown Figure B-1:

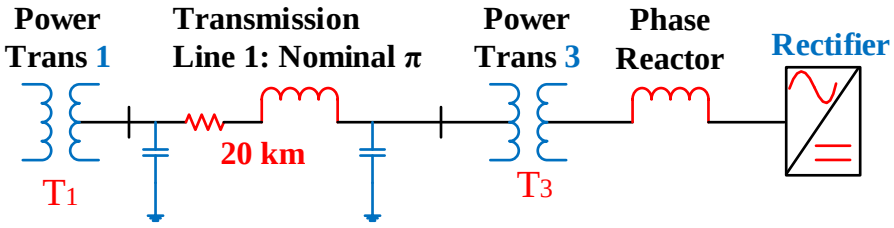

Data

Transmission Line 1	T_1	T_3	S_{base}	V_{base}
r_{l1} 0.0124Ω	300MVA	600MVA	600 MVA	132 kV
l_{l1} 1.05e-3H	33/132kV	132/132kV		
c_{l1} 1.33e-9F	R_{T1} 333.4μ pu	R_{T3} 0.0006 pu		
Ph_{rec} = 0.25H	L_{T1} 0.015 pu	L_{T3} 0.015 pu		

B-1: A block diagram of the examined system

The obtained T_1 values are the per-unit values of the transformer installed in the offshore wind farm substation wind and are calculated as follow:

$$Z_{r_{T_1}-pu.new} = Z_{r_{T_1}-pu.old}\left(\frac{S_{b.new}}{S_{b.old}}\right) * \left(\frac{V_{ac.old}}{V_{ac.new}}\right)^2 = 2.66e^{-3}\left(\frac{600e^6}{300e^6}\right) * \left(\frac{33k}{132k}\right)^2$$

$$= 3.33e^{-4}\ pu$$

$$Z_{l_{T_1}-pu.new} = Z_{l-pu.old}\left(\frac{S_{b.new}}{S_{b.old}}\right) * \left(\frac{V_{ac.old}}{V_{ac.new}}\right)^2 = 0.015\left(\frac{600e^6}{300e^6}\right) * \left(\frac{33k}{132k}\right)^2 = 1.875e^{-3}\ pu$$

The components of the line transmission have to be adapted to their per-unit values too. The system impedances are calculated using the system base values, S_{base} and the V_{base}. Thus, the following calculation steps will lead to obtain the normalized per-unit values:

$$r_{l1} = 0.0124 * 20 = 0.248\Omega$$

$$l_{l1} = 1.05e^{-3} * 20 = 0.021H$$

$$C_{l1} = 11.33e^{-9} * 20 = 2.266e^{-7}F$$

$$r_{l1-pu} = r_{l1} * \frac{\left(V_{ac}^2/S_n\right)}{\omega_b} = 0.248\frac{58.08}{314.16} = 0.248 * 0.184 = 0.04588pu$$

$$l_{l1-pu} = l_{l1} * \frac{\left(V_{ac}^2/S_n\right)}{\omega_b} = 0.021\frac{58.08}{314.16} = 0.021 * 0.184 = 3.885e^{-3}pu$$

$$C_{l1-pu} = \frac{C * \omega_b}{\left(V_{ac}^2/S_n\right)} = 2.266e^{-7}\frac{314.16}{58.08} = 2.266e^{-7} * 5.41 = 1.23e^{-6}pu$$

The transmission lines system per unit base values are calculated as follow:

$$r_{l1-pu.new} = r_{l1-pu.old}\left(\frac{S_{b.new}}{S_{b.old}}\right) * \left(\frac{V_{ac.old}}{V_{ac.new}}\right)^2 = 0.04588\left(\frac{600e^6}{300e^6}\right) * \left(\frac{132k}{132k}\right)^2 = 0.092\ pu$$

$$l_{l1-pu.new} = l_{l1-pu.old}\left(\frac{S_{b.new}}{S_{b.old}}\right) * \left(\frac{V_{ac.old}}{V_{ac.new}}\right)^2 = 3.885e^{-3} * \left(\frac{600e^6}{300e^6}\right) * \left(\frac{132k}{132k}\right)^2$$
$$= 7.77e^{-3}\ pu$$

$$C_{l1-pu.new} = C_{l1-pu.old}\left(\frac{S_{b.new}}{S_{b.old}}\right) * \left(\frac{V_{ac.old}}{V_{ac.new}}\right)^2 = 1.23e^{-6} * \left(\frac{600e^6}{300e^6}\right) * \left(\frac{132k}{132k}\right)^2$$
$$= 2.452e^{-6}pu$$

The T_3 values are calculated as follow:

$$Z_{r_{T3}-pu.new} = Z_{r_{T1}-pu.old}\left(\frac{S_{b.new}}{S_{b.old}}\right) * \left(\frac{V_{ac.old}}{V_{ac.new}}\right)^2 = 0.0006\left(\frac{600e^6}{600e^6}\right) * \left(\frac{132k}{132k}\right)^2$$
$$= 0.0006\ pu$$

$$Z_{l_{T3}-pu.new} = Z_{l-pu.old}\left(\frac{S_{b.new}}{S_{b.old}}\right) * \left(\frac{V_{ac.old}}{V_{ac.new}}\right)^2 = 0.015\left(\frac{600e^6}{600e^6}\right) * \left(\frac{132k}{132k}\right)^2 = 0.015\ pu$$

B.2 Mix Power System

In the Mix power system, the calculated values of the k_p and k_i, of the VSC converter are calculated as the previous section. Figure B-2 shows the schematic of the offshore layout:

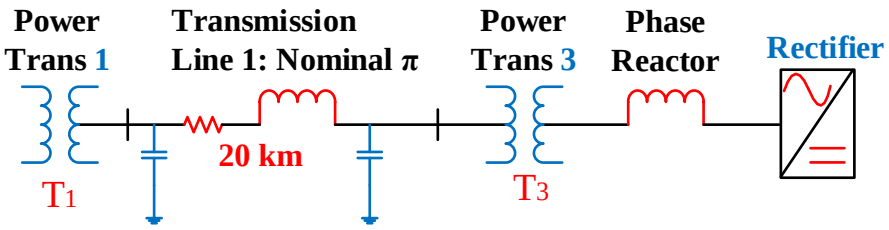

Data

Transmission Line 1	T1	T3	Sbase	Vbase
r_{l1} 0.0124Ω	300MVA	600MVA	600 MVA	
l_{l1} 1.05e-3H	33/132kV	132/132kV		
c_{l1}11.33e-9F	R_{T1} 333.4µ pu	R_{T3} 0.0006 pu		
Ph_{rec} = 0.405H	L_{T1} 0.015 pu	L_{T3} 0.015 pu		

B-2: A block diagram of the examined system

The obtained T_1 values are the per-unit values of the transformer installed in the offshore wind farm substation wind and are calculated as follow:

$$Z_{r_{T_1}-pu.new} = Z_{r_{T_1}-pu.old}\left(\frac{S_{b.new}}{S_{b.old}}\right) * \left(\frac{V_{ac.old}}{V_{ac.new}}\right)^2 = 2.66e^{-3}\left(\frac{600e^6}{300e^6}\right) * \left(\frac{33k}{132k}\right)^2$$

$$= 3.33e^{-4}\ pu$$

$$Z_{l_{T1}-pu.new} = Z_{l-pu.old}\left(\frac{S_{b.new}}{S_{b.old}}\right) * \left(\frac{V_{ac.old}}{V_{ac.new}}\right)^2 = 0.015\left(\frac{600e^6}{300e^6}\right) * \left(\frac{33k}{132k}\right)^2 = 1.875e^{-3}\ pu$$

The components of the line transmission have to be adapted to their per-unit values too. The system impedances are calculated using the system base values, S_{base} and the V_{base}. Thus, the following calculation steps will lead to obtain the normalized per-unit values:

$$r_{l1} = 0.0124 * 20 = 0.248\Omega$$

$$l_{l1} = 1.05e^{-3} * 20 = 0.021H$$

$$C_{l1} = 11.33e^{-9} * 20 = 2.266e^{-7}F$$

$$r_{l1-pu} = r_{l1} * \frac{\left(V_{ac}^2/S_n\right)}{\omega_b} = 0.248\frac{58.08}{314.16} = 0.248 * 0.184 = 0.04588pu$$

$$l_{l1-pu} = l_{l1} * \frac{\left(V_{ac}^2/S_n\right)}{\omega_b} = 0.021\frac{58.08}{314.16} = 0.021 * 0.184 = 3.885e^{-3}pu$$

$$C_{l1-pu} = \frac{C * \omega_b}{\left(V_{ac}^2/S_n\right)} = 2.266e^{-7}\frac{314.16}{58.08} = 2.266e^{-7} * 5.41 = 1.23e^{-6}pu$$

The transmission lines system per unit base values are calculated as follow:

$$r_{l1-pu.new} = r_{l1-pu.old}\left(\frac{S_{b.new}}{S_{b.old}}\right) * \left(\frac{V_{ac.old}}{V_{ac.new}}\right)^2 = 0.04588\left(\frac{600e^6}{300e^6}\right) * \left(\frac{132k}{132k}\right)^2 = 0.092\ pu$$

$$l_{l1-pu.new} = l_{l1-pu.old}\left(\frac{S_{b.new}}{S_{b.old}}\right) * \left(\frac{V_{ac.old}}{V_{ac.new}}\right)^2 = 3.885e^{-3} * \left(\frac{600e^6}{300e^6}\right) * \left(\frac{132k}{132k}\right)^2$$
$$= 7.77e^{-3}\ pu$$

$$C_{l1-pu.new} = C_{l1-pu.old}\left(\frac{S_{b.new}}{S_{b.old}}\right) * \left(\frac{V_{ac.old}}{V_{ac.new}}\right)^2 = 1.23e^{-6} * \left(\frac{600e^6}{300e^6}\right) * \left(\frac{132k}{132k}\right)^2$$
$$= 2.452e^{-6}pu$$

The T_3 values are calculated as follow:

$$Z_{r_{T3}-pu.new} = Z_{r_{T1}-pu.old}\left(\frac{S_{b.new}}{S_{b.old}}\right) * \left(\frac{V_{ac.old}}{V_{ac.new}}\right)^2 = 0.0006\left(\frac{600e^6}{600e^6}\right) * \left(\frac{132k}{132k}\right)^2$$
$$= 0.0006\ pu$$

$$Z_{l_{T3}-pu.new} = Z_{l-pu.old}\left(\frac{S_{b.new}}{S_{b.old}}\right) * \left(\frac{V_{ac.old}}{V_{ac.new}}\right)^2 = 0.015\left(\frac{600e^6}{600e^6}\right) * \left(\frac{132k}{132k}\right)^2 = 0.015\ pu$$

B.3 Multi-Terminal Power System

The proposed multi-terminal scenario has the same characteristic than the mix scenario, presented in the Chapter 5, section 5.4.3 Mix Scenario. There is only one difference in this multi-terminal approach. The phase reactor is again dropped to 0.25mH. Figure B-3 shows the schematic of the offshore layout.

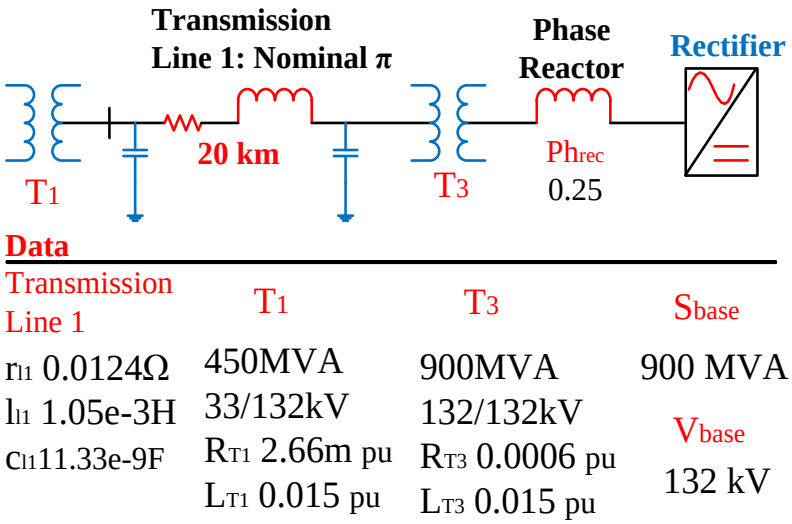

B-3: Diagram of the offshore power system

The obtained T_1 values are the per-unit values of the transformer installed in the offshore wind farm substation wind and are calculated as follow:

$$Z_{r_{T_1}-pu.new} = Z_{r_{T_1}-pu.old}\left(\frac{S_{b.new}}{S_{b.old}}\right) * \left(\frac{V_{ac.old}}{V_{ac.new}}\right)^2 = 2.66e^{-3}\left(\frac{900e^6}{450e^6}\right) * \left(\frac{33k}{132k}\right)^2$$

$$= 0.01655\ pu$$

$$Z_{l_{T_1}-pu.new} = Z_{l-pu.old}\left(\frac{S_{b.new}}{S_{b.old}}\right) * \left(\frac{V_{ac.old}}{V_{ac.new}}\right)^2 = 0.015\left(\frac{900e^6}{450e^6}\right) * \left(\frac{33k}{132k}\right)^2 = 0.001875\ pu$$

The components of the line transmission have to be adapted to their per-unit values too. The system impedances are calculated using the system base values, S_{base} and the V_{base}. Thus, the following calculation steps will lead to obtain the normalized per-unit values:

$$r_{l1} = 0.0124 * 20 = 0.248\Omega$$

$$l_{l1} = 1.05e^{-3} * 20 = 0.021H$$

$$C_{l1} = 11.33e^{-9} * 20 = 2.266e^{-7}F$$

$$r_{l1-pu} = r_{l1} * \frac{\left(V_{ac}^2/S_n\right)}{\omega_b} = 0.248\frac{38.72}{314.16} = 0.031pu$$

$$l_{l1-pu} = l_{l1} * \frac{\left(V_{ac}^2/S_n\right)}{\omega_b} = 0.021\frac{38.78}{314.16} = 2.62e^{-3}pu$$

$$C_{l1-pu} = \frac{C * \omega_b}{\left(V_{ac}^2/S_n\right)} = 2.266e^{-7}\,\frac{314.16}{38.78} = 1.842e^{-6}pu$$

The transmission lines system per unit base values are calculated as follow:

$$r_{l1-pu.new} = r_{l1-pu.old}\left(\frac{S_{b.new}}{S_{b.old}}\right) * \left(\frac{V_{ac.old}}{V_{ac.new}}\right)^2 = 0.031\left(\frac{900e^6}{450e^6}\right) * \left(\frac{132k}{132k}\right)^2 = 0.062\ pu$$

$$l_{l1-pu.new} = l_{l1-pu.old}\left(\frac{S_{b.new}}{S_{b.old}}\right) * \left(\frac{V_{ac.old}}{V_{ac.new}}\right)^2 = 2.62e^{-3} * \left(\frac{900e^6}{450e^6}\right) * \left(\frac{132k}{132k}\right)^2$$

$$= 5.24e^{-3}\ pu$$

$$C_{l1-pu.new} = C_{l1-pu.old}\left(\frac{S_{b.new}}{S_{b.old}}\right) * \left(\frac{V_{ac.old}}{V_{ac.new}}\right)^2 = 1.842e^{-6} * \left(\frac{900e^6}{450e^6}\right) * \left(\frac{132k}{132k}\right)^2$$

$$= 3.684e^{-6}pu$$

The T_3 values are calculated as follow:

$$Z_{r_{T_3}-pu.new} = Z_{r_{T1}-pu.old}\left(\frac{S_{b.new}}{S_{b.old}}\right) * \left(\frac{V_{ac.old}}{V_{ac.new}}\right)^2 = 0.0006\left(\frac{900e^6}{900e^6}\right) * \left(\frac{132k}{132k}\right)^2$$

$$= 0.0006\ pu$$

$$Z_{l_{T3}-pu.new} = Z_{l-pu.old}\left(\frac{S_{b.new}}{S_{b.old}}\right) * \left(\frac{V_{ac.old}}{V_{ac.new}}\right)^2 = 0.015\left(\frac{900e^6}{900e^6}\right) * \left(\frac{132k}{132k}\right)^2 = 0.015\ pu$$

Appendix C: HVDC Light® Converter

The performance of the VSC-HVDC system for the HVDC Light® project is presented in the C-1. The power capacity and total power losses for ±150kV transmission [29].

C-1: Data for ±150 kV symmetric base modules, typical values

Symmetric base Models		**M4**	**M5**	**M6**
DC Voltage	kV_{dc}	±150	±150	±150
Base power	MVA	200	393	600
AC Current	AC	580	1,140	1,740

C-2: Transfer capability for different cable lengths, typical values for ±150kV symmetric base modules

Converter	**DC Voltage**	**DC Current**	**DC Cable**	**Sending Power**	**Receiving Power (MW)**					
Types	kV	A	Cu m_2	MW	Point-t-Point	50 km	100 km	200 km	400 km	800 km
M7	±150	627	300	405.1	395.5	395.1	392.7	388	379.5	-
M8	±150	1,233	1,200	796.6	781.6	777	777	772.4	764.2	746.7
M9	±150	1,881	2,400	1,215.3	1,192.4	1,189.6	1,186.7	1,181.1	1,1698.8	1,147.1